
**Synthesis, characterization, and stability evaluation of novel
hybrid nanoparticles, and their biomedical and chemical
applications**

September 2019

Mahmoud Ibrahiem Mohieeldin Darwish

List of Contents

Chapter 1. General introduction and review of literature

1.1: Introduction	1
1.2: Previous attempts for preparation of metal nanoparticles	2
1.3: Nanoparticles stabilisation in the colloidal solution	7
1.4: General characterising methods for metal nanoparticles	8
1.5: Biofunctionalisation of gold nanoparticles	11
1.6: Application of metal-based nanoparticles	12
1.7: References	17

Chapter 2. Spontaneous Preparation, characterization, stability evaluation of highly stable gold nanoparticle stabilized with ω -sulfonylated alkylsulfanylaniline

2.1: Introduction	35
2.2: Materials and methods	39
2.3: Results and discussion	45
2.4: Conclusion	67
2.5: References	68

Chapter 3. Biomedical application of gold nanoparticles for anti-cancer drug delivery by conjugation with Paclitaxel through DNA-oligonucleotides linker

3.1: Introduction	72
3.2: Materials and methods	76
3.3: Results and discussion	82
3.4: Conclusion	97
3.5: References	98

Chapter 4. Preparation and characterization of platinum nanoparticles stabilized by a polymer modified with sulfonyl aniline and their application as a highly efficient, recyclable, chemo-selective, and broad spectrum nanocatalyst

4.1: Introduction	105
4.2: Materials and methods	109
4.3: Results and discussion	116
4.4: Conclusion	163
4.5: References	164

Chapter 5. Summary of the results

Summary	179
---------	-----

Curriculum Vitae	183
-------------------------	-----

List of abbreviations

Au NP	Gold nanoparticles
1-AuNP	ω -sulfonlated alkylsulfanylaniline gold nanoparticles
UV-vis	Ultra violet visible spectroscopy
TEM	Transmission electron microscope
NaBH ₄	Sodium borohydride
PEG	Polyethylene glycol
PBS	Phosphate-buffered saline
NMR	Nuclear magnetic resonance
DMSO	Dimethyl sulfoxide
FTIR	Fourier transform infrared spectra
SPR	Surface plasmon resonance
ST	Succinyltaxol
LCMS	Liquid chromatography mass spectrometry
EDC	1-Ethyl-3-[3-dimethylaminopropyl] carbodiimide
NHS	<i>N</i> -hydroxysuccinimide
DMEM	Dulbecco's Modified Eagle's Medium

MTT	3-(4,5-Dimethylazol-2-yl)-2,5-diphenyl-tetrazolium Bromide
ST-DNA-Au NPs	Nano-bio-conjugate
SK-BR3	Adenocarcinoma breast cancer cell
Neuro 2a	Brain cancer cells
EPR	Enhanced permeability and retention effect
MDR	Multiple drug resistance
Pgp	P-glycoprotein
PVA-ATB	Polyvinyl alcohol aminothiobenzene
K_{app}	Apparent rate constant
PVA-ATB-Pt NPs	Polymer stabilized platinum nanoparticles
MO	Methyl orange
MB	Methylene blue
GCMS	Gas chromatography mass spectrometry

Acknowledgements

First of all, all deepest thanks and gratitude are for **almighty Allah** who gives me the power and time and health to complete my doctor degree. So, all praises are for Allah.

There are many people I would like to thank for their support and encouragement, without whom, this PhD thesis would not have been possible. My gratitude goes first and foremost to **my parents**, who gave me their time, energy, love and encouragement.

I wish to express my deepest gratitude to my supervisor, Prof. Dr. **Hiroaki Okamura** for teaching me not only chemistry and bioscience but also something about life, for his support, encouragement and obtaining the goals.

I want to express my deepest appreciation and thanks to **the Egyptian ministry of higher education**, mission sector for providing me with the financial support during studying my doctor coarse and giving me this opportunity.

Dedication:

This doctor thesis is dedicated to My Father

Chapter 1

General introduction and review of literature

1.1: Introduction

The nanotechnology is defined as a science, which deals with materials within a size range of 1–100 nm, including synthetic nanoparticles from their precious metal precursors and naturally occurring particles like ash and spray. Examples of biological components, which present in nanoscale size, include cell wall, Golgi apparatus, cell membrane, DNA (about 2.7 nm) and haemoglobin (about 5 nm).¹ Knowledge of metal nanoparticles have a very long history. The colloidal gold nanoparticles (Au NPs) were used historically for decoration purposes and staining of glasses and windows due to its optical properties.² Understanding the synthesis, characterisation and application of the precious metal nanoparticles has been the driving force for the development of nanotechnology research. The unique advantages of nano-sized metals over their bulk materials arise from their large surface area to volume ratio compared to its bulk materials. It was reported that Michael Faraday was

the first to synthesis Au NPs over 150 years ago and he noticed that the nanoscale Au NPs have different properties in addition to its metal precursors.³ The large surface area leads to higher activity when it is used in particular applications.

1.2: Previous attempts for preparation of metal nanoparticles

1.2.1: Gold nanoparticles (Au NP)

During the last decade, the field of nanotechnology has been rapidly growing, in particular Au NPs, owing to its precious biological and medical applications such as drug delivery system,⁴⁻⁷ biological imaging, diagnostics,⁸⁻¹² and sensors.¹²⁻¹⁸ Nanoparticles are generally smaller than 100 nm and contain several metal atoms. Au NPs possess unique physical and chemical properties that make it a superior target for biological and medical applications and this is attributed primarily to their chemical stability, the ability of its modification by many functional molecules and their biocompatibility.

Many methods to synthesize gold nanoparticles have been applied, however the preparation of stable, modifiable with size controlled gold

nanoparticles that are suitable for biological or medicinal applications, is still challenging. The stability of Au NPs are rarely investigated or reported and this remains a challenge (particularly in complex media such as those used for cell bioassay). Frens's method¹⁹ is a well-known method for the synthesis of gold nanoparticles with a simple operation and inexpensive chemicals. It involves the reaction of boiling chloroauric acid solution with warm sodium citrate solution. Citrate ions act as both a reducing agent and capping agent leading to the formation of nearly monodispersed gold nanoparticles with sizes ranging from 10–20 nm. Frens's method uses a weak capping agent, lacking functional branched groups. Therefore, the particles are less stable. The shape of the particles is limited to spherical and they are not stable enough for the biological or medicinal applications. This is attributed to instability of the particles in solutions with high salts concentrations such as phosphate-buffered saline (PBS) or acidic pH that are frequently used in biomedical applications.

Brust's method²⁰ involves the reaction of a chloroauric acid solution in toluene with tetraoctylammonium bromide (TOAB) solution and sodium borohydride as a stabilising and a reducing agent, respectively. The Brust

method uses a weak stabilizing agent and binds weakly to the surface of gold nanoparticles. Therefore, the particles tend to aggregate and precipitate gradually within a maximum of two weeks.

The sodium borohydride reduction method (NaBH_4),²¹⁻²² is a “one-pot” method that involves the reduction of gold precursors (HAuCl_4) by sodium borohydride in the presence of various stabilising agents such as large organic molecules,²³ and peptides.²⁴ NaBH_4 is a strong reducing agent able to produce small Au NPs at room temperature. The particle size is controlled by the amount of stabilising agent used in the reaction. NaBH_4 may have some toxic effect to the cells during biological application of the prepared particles. Thus, a modified polyol synthesis of Au NPs was established. This method depends on the use of small amount of NaBH_4 as a reducing agent that is added to polyethylene glycol (PEG_{600}) solution of PVP under stirring for 1–2 minutes. Then aqueous solution of hot chloroauric acid was added followed by heating of the solution to 125 °C leading to obtaining octahedral Au NPs of varying size from 30–60 nm.²⁵

The use of weak organic acid for the synthesis of Au NPs such as

ascorbic acid has been also investigated.^{26–27} The main interest for this weak acid compared with other reducing agent depends on the fact that the particles can be synthesised at room temperature and at neutral pH, but the particles suffer from lacking of stability. Ma *et al.*²⁸ synthesised Au NPs with trisoctahedral shape and diameter ranged from 100–200 nm. The process included the reaction of an aqueous solution of chloroauric acid with ascorbic acid as a reducing agent at room temperature and cetyltrimethylammonium chloride (CTAC) was used as a capping agent.

Liao *et al.*²⁹ stated the synthesis of star-shaped Au NPs by the reduction of chloroauric acid with ascorbic acid in deep eutectic solvents (DESs) at room temperature. Au NPs with different shapes can be synthesised by controlling the content of water in DESs; if no water is in the DES, snow flake-like Au NPs with a size about 300 nm were obtained. Au NPs have been synthesised by using poly (*o*-phenylenediamine) as a reducing agent and stabiliser for the particles as well as ammonium per sulfate (APS) as an initiator to the reaction system. The size of the prepared Au NPs varied from 3–15 nm by changing the concentration of the Au precursor.³⁰ Au NPs with polygonal shape were synthesised using a

modified citrate reduction, whereas the ferric ammonium citrate (FAC) was used for the reduction of chloroauric solution instead of sodium citrate. The sizes and morphologies of Au NPs can be varied by variation of the mole ratio of FAC to Au salts. The particles were stable for about 6 h and precipitation of the particles completed within 24 h.³¹

1.2.2: Platinum nanoparticles (Pt NP)

Chen *et al* synthesised Pt NPs by the reaction of H_2PtCl_6 with PEG in the presence of poly vinyl pyrrolidone (PVP) at 110 °C.³² Faceted Pt NPs were prepared by the reduction of H_2PtCl_6 in an aqueous solution of PVP with a little amount of FeCl_3 .³³ Wang *et al*³⁴ stated the preparation of dendritic Pt NPs by sonication whereas K_2PtCl_4 and formic acid were sonicated in an aqueous medium in the presence of non-ionic organic compound. Ascorbic acid was used as a reducing agent for a Pt precursor in aqueous medium, assisted by block copolymer to produce Pt nanodendrites.³⁵ Bigall *et al*³⁶ have produced Pt NPs with an average diameter of 10–100 nm by adding aqueous solutions of H_2PtCl_6 , NaBH_4 , and sodium citrate under reflux condition.

1.3: Nanoparticles stabilisation in the colloidal solution

The nanoparticles are in persistent movement in the colloidal solution (Brownian motion). Therefore, there is a need to stabilise the nanoparticles in the solution to prevent them from coming together in close contact and consequently precipitation under gravity.³⁷ The chemical forces used to stabilise the nanoparticles in the colloidal solutions include electrostatic repulsion, steric and electrosteric forces. The first force is the electrostatic repulsion derived from the double electric layer around the particles, which leads to repulsion of the particles from each other and keeps them in a separate state in the aqueous medium.³⁸ The main peculiarity of electrostatic repulsion force is the high sensitivity to high salt concentration where the force is markedly decreased. This is attributed to the suppression of the double electric layer at high salt concentration. This indicates the instability of Frens's particles (citrate-stabilised gold nanoparticles) at high salt concentration.³⁹

The second force of the nanoparticles is steric stabilisation, which originated from the bulky organic materials (stabilising agent or capping agent). This force inhibits the close contact of the nanoparticles in the

colloidal solution provided by the functional branched chains of the organic materials and provides a barrier between the individual particles. The capping agents include polymers such as PVP,⁴⁰⁻⁴² PEG,⁴³⁻⁴⁶ polyvinyl alcohol (PVA),⁴⁷ chitosan,⁴⁸ and polymethyl methacrylate (PMMA).⁴⁹⁻⁵⁰ Surfactants were also used as capping agents.⁵¹ Unlike electrostatic stabilisation, steric stabilisation is less sensitive to high salt concentration and efficient steric power will be achieved by thick and high density polymers with functional branched groups.⁵² This coating reduces the sensitivity of the particles to the salting process. The third force is electro-steric which combines the electrostatic and steric stabilisation as in case of polyoxoanion-coated metal nanoclusters.⁵³⁻⁵⁴

1.4: General characterising methods for metal nanoparticles

Characterisation of the nanoparticles is very important to know the details of the particles such as its formation, morphology, size, stability, charges and surface chemical composition as well as the aggregation state. The commonly used characterisation techniques include UV-visible spectroscopy, transmission electron microscope (TEM), nuclear magnetic

resonance spectroscopy (^1H NMR), and Fourier transform infrared (FTIR). Other techniques are utilised to a lower extent such as atomic force microscopy (AFM), high performance liquid chromatography (HPLC), TEnergy dispersive spectroscopy (EDS) and ion exchange chromatography.

1.4.1: UV-visible spectroscopy

UV-visible spectroscopy is a very useful technique for monitoring nanoparticles formation during the time course of the reaction of metal precursors with the reductive stabilisers. The nanoparticles formation is monitored by the formation of absorbance peaks in the visible wavelength as in case of Au, Ag, Cd, Hg and Cu nanoparticles.⁵⁵ These absorbance peaks originated from the surface plasmon resonance (SPR) due to the oscillation of free excited electrons around the surface of nanoparticles caused by the light from the UV-visible spectroscopy.⁵⁶ In the case of other metals like platinum nanoparticles, the formation of the particles is monitored by the disappearance of the absorbance peak coming from the Pt ions, with an increase in the absorbance towards shorter wavelengths.⁵⁷ SPR gives an indication about the size; as the nanoparticle's size decreases,

blue shift occurs owing to increasing the gap distance of the smaller nanoparticles.⁵⁸ Wilcoxon *et al.*⁵⁹ indicated SPR was also affected by the shape of the nanoclusters, relative distance of the particles to each other (aggregation state), as well as surface chemistry.

1.4.2: Transmission electron microscope (TEM)

TEM is the most useful technique for giving information about morphology, size, and dispersion state of the nanoparticles.⁶⁰ The histogram of the particles could be given by measuring the diameter of each particle in the obtained TEM images. The sample is prepared by sitting a drop of nanoparticles onto a carbon-coated copper grid then the sample is well-dried in desiccators and then exposed to the TEM machine to see the particles. To a limited range Surface Enhanced Raman Spectroscopy (SERS) is used to notify the small particles surfaces by monitoring pyridine absorption on Ag and Au solutions,⁶¹ where pyridine is used to start the agglomeration of nanoclusters.⁶² The limitation of SERS is that it is only utilised for metals with a highly defined plasmon band, which is required to give the desired signal enhancement.⁶³

1.4.3: Nuclear magnetic resonance (NMR)

NMR is another useful technique for probing the interactions between the organic ligands and the nanoparticle surface. The connection of the organic molecules on the nanoparticle surface has an influence on the chemical shifts of the signals originated from these organic molecules in NMR spectroscopy. This connection was confirmed by shifting of the signals to lower chemical shift and its broadening.^{64,65} The samples are prepared by good evaporation and dryness of the colloidal solution in order to get a higher resolution of the NMR spectra. Then a small amount of dried samples (20–50 mg) was dissolved in dimethyl sulfoxide (DMSO_{d6}) or D₂O according to the solubility of the used organic ligand.⁶⁴

1.5: Biofunctionalisation of gold nanoparticles

The nano bio-conjugate can be conducted using different methods including thiol-modified biomolecules and electrostatic interaction.

1.5.1: Biofunctionalisation by thiol-modified biomolecules (covalent approach)

The thiol-modified biomolecules such as DNA, peptides, proteins and organic molecules have strong binding ability to the nanoparticle

surface through its terminal SH group.⁶⁴⁻⁶⁷ It can substitute the weakly attached molecules on the surface of nanoparticles.⁶⁸⁻⁶⁹ For example, the modification of DNA with steroid disulfide derivatives leads to higher stability of the nanoparticles due to a strong attachment process.⁷⁰⁻⁷¹

1.5.2: Biofunctionalisation by electrostatic interaction (ionic approach)

This approach depends on the electrostatic interaction between the oppositely charged nanoparticles and biomolecules. For example, in the case of gold nanoparticles prepared by citrate, when the pH is adjusted slightly higher than the isoelectric point of citrate, this leads to effective binding between negatively charged carboxylic group on the surface of the nanoparticles and positively charged proteins or peptides.^{72,73}

1.6: Application of metal-based nanoparticles

1.6.1: Anti-cancer drug delivery

Cancer is one of the most dangerous diseases facing the world and it is causing many drawbacks on the health and economic status of countries. Chemotherapeutics and surgical interference are the most common current treatment against cancer. These treatments have drawbacks for the patients in terms of the killing of the healthy cells and

causing acute toxicity. Au NPs modified with thiol-PEG effectively delivers doxorubicin (DOX),⁷⁴⁻⁷⁹ anthracycline,⁸⁰ and paclitaxel⁸¹⁻⁸² into the tumour cells. Many efforts are given to improve the peculiarities of the free drugs by using metal nanoparticles, especially Au NPs, for drug delivery systems. These peculiarities include solubility, stability and the efficacy of the anti-cancer drugs as well as protection of the drugs from degradation.⁸² For efficient drug delivery, Au NPs form a complex with the biomolecules, then crosses the cell wall of the tumour cells and unloads the anti-cancer drugs. The use of DNA-Au NPs for drug delivery leads to improvement of cellular uptake of the anticancer drugs in different cell line. This is explained by the loading of oligonucleotides on Au NPs surfaces, which adsorbs a high amount of extracellular proteins on the particle surface and consequently greater uptake by the cells⁸³⁻⁸⁵ and gets rid of toxicity to the normal cells as well as protects the drugs against enzymatic decomposition.^{84,85}

Multiple drug resistance (MDR) can be diminished by using Au NPs as a drug delivery strategy. MDR is a condition where the transporter proteins that release the drugs outside the cells are over-expressed on the

cell membrane of the tumour cells such as P-glycoprotein, leading to lowering the efficacy of the drugs. Overcoming MDR refers to the fact that Pgp may identify the drug only on the cell membrane but not when it is taken up intracellularly after endocytosis.^{86,87} After DOX was conjugated to Au NPs, Au NPs increased intracellular DOX concentrations through endocytic uptake of the Au NPs. Once inside the cell and acidic organelles (i.e., lysosomes), DOX would be released and interfere with the normal cellular processes after its release in acidic environments.⁸⁸ There are two strategies for crossing the cell membrane; passive and active methods. The passive method depends on an enhanced permeability and retention effect and it occurs commonly in diseased tissues via extravasation due to its disrupted permeability and leakage of blood vessels endothelium. The active method relies on specific identification of the bio-ligand by receptors on the cell membrane (cell surface receptor-mediated endocytosis). Additionally, the Au NPs can be used for the transport of highly sensitive biomolecules as RNA, DNA,⁸⁴⁻⁸⁵ peptides, and proteins protecting them from decomposition.

1.6.2: Application of nanoparticles as a nanocatalytic system

Nanotechnology is a very important research field that has attracted interest in the last few years due to its various applications in nanocatalysis.⁹⁹⁻¹⁰¹ The use of nanoparticles as catalysts has been intensively studied; however, the synthesis of nanocatalytic systems possessing high activity and durability remains challenging. Stabiliser-free nanoparticles have been used for catalytic processes,¹⁰² which focus only on the initial catalytic effect and do not consider the durability of the particles. A first issue associated with stabiliser-free nanoparticles is that they can easily agglomerate due to their high surface energy and lack of stabilising agent.¹⁰³ A second drawback is that the recovery of active particles from the reaction medium after catalysis is difficult, thus the particles cannot be recycled, causing limitations to their practical use as well as toxicity to the environment.^{104,105} The main challenge of using metal nanoparticles in catalysts is that such particles should be reusable (recyclability), while remaining active, stable, and dispersed. Therefore, there is a need to design and fabricate highly efficient, stable, and durable metal-based nanocatalysts. The catalytic efficiency of metal nanoparticles

is of great importance for useful using of toxic and less useful compounds such as nitrobenzene or *p*-nitrophenol, which results in contaminants entering the wastewater of industrial factories producing pharmaceutical compounds.¹⁰⁶⁻¹⁰⁷ Different routes of infection can affect the human by *p*-nitrophenol: ingestion, skin contact, and inhalation. Many factors determine the health hazard after the exposure to *p*-nitrophenol like the route of infection, health conditions, dose, and genetics. These hazards include irritation, nausea, vomiting, and headaches. By contrast, *p*-aminophenol, which is produced by the reduction of *p*-nitrophenol, is a very important material in analgesic preparations.¹⁰⁸⁻¹¹⁰ Nanoparticles were found to catalyse a wide range of reactions such as hydrogenations,⁵⁴ selective hydrogenation,¹¹¹ hydrosilylation,¹¹² hydrogenolysis and hydrolysis, oxidative acetoxylation,¹¹³ and oxidation of CO.¹¹⁴

1.7: References

1. S. E. McNeil, Characterization of nanoparticles Intended for Drug Delivery, Humana Press, *Springer Science+Business Media*, LLC, 2011.
2. R. A. Sperling, P. R. Gil, F. Zhang, M. Zanella, W. J. Parak, Biological applications of gold nanoparticles, *Chem. Soc. Rev.*, **37** (2008) 1896–1908.
3. D. A. Giljohann, D. S. Seferos, W. L. Daniel, M. D. Massich, P. C. Patel, C. A. Mirkin, Gold nanoparticles for biology and medicine, *Angewandte Chemie International Edition*, **49** (2010) 3280–3294.
4. R. Shenhar, V. M. Rotello, Nanoparticles: Scaffolds and Building Blocks, *Acc. Chem. Res.*, **36** (2003) 549–561.
5. D. C. Hone, P. I. Walker, P. I., R. R. Evans-Gowing, S. FitzGerald, A. Beeby, I. Chambrier, M. J. Cook, D. A. Russell, Generation of Cytotoxic Singlet Oxygen via Phthalocyanine-Stabilized Gold Nanoparticles: A Potential Delivery Vehicle for Photodynamic Therapy, *Langmuir*, **18** (2002) 2985–2987.
6. M. R. Choi, K. J. Stanton-Maxey, J. K. Stanley, C. S. Levin, R. Bardhan, D. Akin, S. Badve, J. Sturgis, J. P. Robinson, R. Bashir, N. J. Halas, S. E. Clare, A Cellular Trojan Horse for Delivery of Therapeutic Nanoparticles into Tumors, *Nano Lett.*, **7** (2007) 3759–3765.
7. J. M. Bergen, H. A. Von Recum, T. T. Goodman, A. P. Massey, S. H. Pun, Gold nanoparticles as a versatile platform for optimizing physicochemical parameters for targeted drug delivery, *Macromol. Biosci.*, **6** (2006) 506–

516.

8. I. H. El-Sayed, H. Huang, M. A. El-Sayed, Surface Plasmon Resonance Scattering and Absorption of anti-EGFR Antibody Conjugated Gold Nanoparticles in Cancer Diagnostics: Applications in Oral Cancer, *Nano Lett.*, **5** (2005) 829–834.

9. W. Eck, G. Craig, A. Sigdel, G. Ritter, L. J. Old, L. Tang, M. F. Brennan, P. J. Allen, M. D. Mason, PEGylated Gold Nanoparticles Conjugated to Monoclonal F19 Antibodies as Targeted Labeling Agents for Human Pancreatic Carcinoma Tissue, *Acs Nano.*, **2** (2008) 2263–2272.

10. N. L. Rosi, C. A. Mirkin, Nanostructures in Biodiagnostics, *Chem. Rev.*, **105** (2005) 1547–1562.

11. F. Sonvico, C. Dubernet, P. Colombo, P. Couvreur, Metallic colloid nanotechnology, applications in diagnosis and therapeutics, *Curr. Pharm. Des.*, **11** (2005) 2095–2105.

12. J. James, J. J. Storhoff, C. A. Mirkin, Programmed Materials Synthesis with DNA, *Chem. Rev.*, **99** (1999) 1849–1862.

13. H. He, C. Xie, J. Ren, Nonbleaching Fluorescence of Gold Nanoparticles and Its Applications in Cancer Cell Imaging, *Anal. Chem.*, **80** (2008) 5951–5957.

14. R. Popovtzer, A. Agrawal, N. A. Kotov, A. Popovtzer, J. balter, T. E. Carey, R. Kopelman, Targeted Gold Nanoparticles Enable Molecular CT

Imaging of Cancer, *Nano. Lett.*, **8** (2008) 4593–5496.

15. A. Neely, C. Perry, B. Varisli, A. K. Singh, T. Arbneshi, D. Senapati, J. R. Kalluri, P. C. Ray, Ultrasensitive and Highly Selective Detection of Alzheimer's Disease Biomarker Using Two-Photon Rayleigh Scattering Properties of Gold Nanoparticle, *Acs. Nano.*, **3** (2009) 2834–2840.

16. P. Sharma, S. C. Brown, N. Bengtsson, Q. Zhang, G. A. Walter, S. R. Grobmyer, S. Santra, H. Jiang, E. W. Scott, B. M. Moudgil, Gold-Speckled Multimodal Nanoparticles for Noninvasive Bioimaging, *Chem. Mater.*, **20** (2008) 6087–6094.

17. C. A. Mirkin, R. L. Letsinger, R. C. Mucic, J. J. Storhoff, A DNA-based method for rationally assembling nanoparticles into macroscopic materials, *Nature*, **382** (1996) 607–609.

18. A. P. Alivisatos, K. P. Johnsson, X. G. Peng, T. E. Wilson, C. J. Loweth, M. P. Bruchez, P. G. Schultz, Organization of 'nanocrystal molecules' using DNA, *Nature*, **382** (1996) 609–611.

19. G. Frens, G., Controlled Nucleation for the Regulation of the Particle Size in Monodisperse Gold Suspensions, *Nature Phys. Sci.*, **241** (1973) 20–22.

20. M. Brust, M. Walker, D. Bethell, D. J. Schiffrin, R. Whyman, Synthesis of thiol-derivatised gold nanoparticles in a two-phase Liquid–Liquid system, *Chem. Commun.*, **7** (1994) 801–802.

-
21. K. B. Male, J. Li, C. C. Bun, S. C. Ng, J. H. Luong, Synthesis and Stability of Fluorescent Gold Nanoparticles by Sodium Borohydride in the Presence of Mono-6-deoxy-6-pyridinium- β -cyclodextrin Chloride, *J. Phys. Chem. C.*, **112** (2008) 443–451.
22. Y. Liu, K. B. Male, P. Bouvrette, J. H., Luong, Control of the Size and Distribution of Gold Nanoparticles by Unmodified Cyclodextrins, *Chem. Mater.*, **15** (2003) 4172–4180.
23. S. R. Isaacs, E. C. Cutler, J. S. Park, T. R. Lee, Y. S. Shon, Synthesis of tetraoctylammonium-protected gold nanoparticles with improved stability, *Langmuir*, **21** (2005) 5689–5692.
24. G. Scari, F. Porta, U. Fascio, S. Avvakumova, V. Dal Santo, M. De Simone, M. Saviano, M. Leone, A. Del Gatto, C. Pedone and L. Zaccaro, Gold Nanoparticles Capped by a GC-Containing Peptide Functionalized with an RGD Motif for Integrin Targeting, *Bioconjugate Chem.*, **23** (2012) 340–349.
25. C. Li, K. L. Shuford, Q. H. Park, W. Cai, Y. Li, E. J. Lee, S. O. Cho, High-yield synthesis of single-crystalline gold nano- octahedra, *Angew. Chem., Int. Ed.*, **46** (2007) 3264–3268 (modified polyol system)
26. P. K. Vemula, U. Aslam, V. A. Mallia, G. John, In situ synthesis of gold nanoparticles using molecular gels and liquid crystals from vitamin C amphiphiles, *Chem. Mater.*, **19** (2007) 138–140.
27. E. C. Stathis, A. Fabrikanos, preparation of colloidal gold, *Chem. Ind.*,

27 (1958) 860–861

28. Y. Ma, Q. Kuang, Z. Jiang, Z. Xie, R. Huang, L. Zheng, Synthesis of trisoctahedral gold nanocrystals with exposed high-index facets by a facile chemical method, *Angew. Chem. Int.Ed.*, **47** (2008) 8901–8904.

29. H. G. Liao, Y. X. Jiang, Z. Y. Zhou, S. P. Chen, S. G. Sun, Shape-controlled synthesis of gold nanoparticles in deep eutectic solvents for studies of structure-functionality relationships in electrocatalysis, *Angew. Chem., Int. Ed.*, **47** (2008) 9100–9103.

30. J. Han, Y. Liu, R. Guo, Reactive Template Method to Synthesize Gold Nanoparticles with Controllable Size and Morphology Supported on Shells of Polymer Hollow Microspheres and Their Application for Aerobic Alcohol Oxidation in Water, *Adv. Funct. Mater.*, **19** (2009) 1112–1117.

31. M. H. Rashid, T. K. Mandal, Templateless Synthesis of Polygonal Gold Nanoparticles: An Unsupported and Reusable Catalyst with Superior Activity, *Adv. Funct. Mater.*, **18** (2008) 2261–2271.

32. J. Chen, T. Herricks, Y. Xia, Polyol Synthesis of Platinum Nanostructures: Control of Morphology through the Manipulation of Reduction Kinetics, *Angew. Chem. Int. Ed.*, **44** (2005) 2589–2592.

33. B. Lim, X. Lu, M. Jiang, P.H.C. Camargo, E. C. Cho, E. P. Lee, Y. Xia, Facile Synthesis of Highly Faceted Multioctahedral Pt Nanocrystals through Controlled Overgrowth, *Nano Lett.*, **8** (2008) 4043–4047.

-
34. L. Wang, H. Wang, Y. Nemoto, Y. Yamauchi, Rapid and Efficient Synthesis of Platinum Nanodendrites with High Surface Area by Chemical Reduction with Formic Acid, *Chem. Mater.*, **22** (2010) 2835–2841.
35. L. Wang, Y. Yamauchi, Block Copolymer Mediated Synthesis of Dendritic Platinum Nanoparticles, *J. Am. Chem. Soc.*, **131** (2009) 9152–9153.
36. N. C. Bigall, T. Hatling, M. Klose, P. Simon, L. M. Eng, A. Eychmuller, Monodisperse Platinum Nanospheres with Adjustable Diameters from 10 to 100 nm: Synthesis and Distinct Optical Properties, *Nano. Lett.*, **8** (2008) 4588–4592.
37. G. T. Hermanson, Bioconjugate techniques, Second edition, Academic press, 2008.
38. I. Ojea-Jiménez, V. Puentes. Instability of Cationic Gold Nanoparticle Bioconjugates: The Role of Citrate Ions, *J. Am. Chem. Soc.*, **131** (2009) 13320–13327.
39. I. Capek. Dispersions based on noble metal nanoparticles-DNA conjugates, *Adv Colloid Interface Sci.*, **163** (2011) 123–143.
40. K. Meguro, Y. Nakamura, Y. hayashi, M. Torizuka, K. Esumi, The Preparation of Colloidal Precious Metal Particles Using Copolymers of Vinyl Alcohol–N-Vinylpyrrolidone, *Bull. Chem. Soci. Jpn*, **61** (1988) 347–350.
41. G. Carotenuto, Synthesis and characterization of poly(N-vinylpyrrolidone)

filled by monodispersed silver clusters with controlled size, *appl. Organomet. Chem.*, **15** (2001) 344–351.

42. R. Seoudi, A. A. Fouda, D. A. Elmenshawy, Synthesis, characterization and vibrational spectroscopic studies of different particle size of gold nanoparticle capped with polyvinylpyrrolidone, *Phys. B*, **405** (2010) 906–911.

43. M. A. Hayat, *Colloidal Gold, Principles, Methods, and Applications*, Academic Press: New York, 1989.

44. E. Oh, K. Susumu, R. Goswami, H. Mattoussi, One-Phase Synthesis of Water-Soluble Gold Nanoparticles with Control over Size and Surface Functionalities, *Langmuir*, **26** (2010) 7604–7613.

45. K. Susumu, B. C. Mei, H. Mattoussi, Multifunctional ligands based on dihydrolipoic acid and polyethylene glycol to promote biocompatibility of quantum dots, *Nat. Protoc.*, **4** (2009) 424–436.

46. J. B. Tracy, G. Kalyuzhny, M. C. Growe, R. Balasubramanian, J. B. Choi, R.W. Murray, Poly(ethylene glycol) Ligands for High-Resolution Nanoparticle Mass Spectrometry, *J. Am. Chem. Soc.*, **129** (2007) 6706–6707.

47. A. Pucci, M. Bernabo, P. Elvati, L. I. Meza, F. Galembeck, C. A. Leite, N. Tirelli, G. Ruggeri, Photoinduced formation of gold nanoparticles into vinyl alcohol based polymers, *J. Mater. Chem.*, **16** (2006) 1058–1066.

-
48. H. Z. Huang, X. R. Yang, Synthesis of Chitosan-Stabilized Gold Nanoparticles in the Absence/Presence of Tripolyphosphate, *Biomacromolecules*, **5** (2004) 2340–2346.
49. T. K. Mandel, M. S. Fleming, D. R. Walt, Preparation of Polymer Coated Gold Nanoparticles by Surface-Confined Living Radical Polymerization at Ambient Temperature, *Nano lett.*, **2** (2002) 3–7.
50. E. Yilmaz, S. Suzer, Au nanoparticles in PMMA matrix: In situ synthesis and the effect of Au nanoparticles on PMMA conductivity, *Appl. Surf. Sci.*, **256** (2010) 6630–6633.
51. H. Bonnemann, G. Braun, W. Brijoux, R. Brinkmann, A. Schulze, K. Seevogel, K. Siepen, Nanoscale colloidal metals and alloys stabilized by solvents and surfactants Preparation and use as catalyst precursors, *J. Organomet. Chem.*, **520** (1996) 143–162.
52. W. Zhao, M. A. Brook, Y. Li., Design of gold nanoparticle-based colorimetric biosensing assays, *ChemBioChem.*, **9** (2008) 2363–2371.
53. J. D. Aiken 111, Y. Lin, R. G. Finke, A perspective on nanocluster catalysis: polyoxoanion and $(n\text{-C}_4\text{H}_9)_4\text{N}^+$ stabilized $\text{Ir}(0)_{\sim 300}$ nanocluster‘soluble heterogeneous catalysts, *J. Mol. Catal. A: Chem.*, **114** (1996) 29–51.
54. Y. Lin, R. G. Finke, Novel Polyoxoanion- and Bu_4N^+ -Stabilized, Isolable, and Redissolvable, 20-30-.ANG. Ir 300-900 Nanoclusters: The Kinetically Controlled Synthesis, Characterization, and Mechanism of

Formation of Organic Solvent-Soluble, Reproducible Size, and Reproducible Catalytic Activity Metal Nanoclusters, *J. Am. Chem. Soci.*, **116** (1994) 8335–8353.

55. J. A. Creighton, D. G. Eadon, Ultraviolet–visible absorption spectra of the colloidal metallic elements, *J. Chem. Soc. Faraday Trans.*, **87** (1991) 3881–3891.

56. G. Mie, Mie theory: Present developments and Interdisciplinary aspects of light scattering, *Ann. Phy.*, **25** (1908) 377–455.

57. W. Siriwatcharapiboon & N. Tinnarat & P. Supaphol, Preparation and characterization of electrospun poly (vinyl alcohol) nanofibers containing platinum or platinum-ruthenium nanoparticles, *J Polym Res*, **40** (2013) 1–8.

57. J. P. Wilcoxon, R. L. Williamson, R. Baughman, Optical properties of gold colloids formed in inverse micelles, *J. Chem. Phys.*, **98** (1993) 9933–9949.

59. J. P. Wilcoxon, P. P. Newcomer, G. A. Samara, Synthesis and optical properties of MoS₂ and isomorphous nanoclusters in the quantum confinement regime, *J. Appl. Phys.*, **81** (1997) 7934–7944.

60. D. B. Williams, C. B. Carter, Transmission Electron Microscopy, A textbook for materials Science, Plenum, New York, 1996.

61. G. Schmid (Ed.), Clusters and Colloids: From Theory to applications; VCH publishers, New York, 1994, 467.

62. G. Schmid (Ed.), *Clusters and Colloids: From Theory to applications*; VCH publishers, New York, 1994.

63. G. Schmid (Ed.), *Clusters and Colloids: From Theory to applications*; VCH publishers, New York, 1994, 510.

64. A. Badia, L. Demers, L. Dickinson, F. G. Morin, R. B. Lennox, L. Reven. Gold–Sulfur Interactions in Alkylthiol Self-Assembled Monolayers Formed on Gold Nanoparticles Studied by Solid-State NMR, *J. Am. Chem. Soc.*, **119** (1997) 11104–11105.

65. M. I. M. Darwish, Y. Takenoshita, T. Hamada, S. Onitsuka, J. Kurawaki, H. Okamura, Spontaneous Preparation of Highly Stable Gold Nanoparticle Stabilized with ω -Sulfonylated Alkylsulfanylaniline, *J. Oleo Sci.*, **66** (2017) 1349–1354.

66. R. P. Brinãs, A. Sundgren, P. Sahoo, S. Morey, K. Rittenhouse-Olson, G. E. Wilding, W. Deng, J. J. Barchi, Design and Synthesis of Multifunctional Gold Nanoparticles Bearing Tumor-Associated Glycopeptide Antigens as Potential Cancer Vaccines, *Bioconjugate Chem.*, **23** (2012) 1513–1523.

67. L. J. Cruz, F. Rueda, B. Cordobilla, L. Simón, L. Hosta, F. Albericio, and J. Carles Domingo, Targeting Nanosystems to Human DCs via Fc Receptor as an Effective Strategy to Deliver Antigen for Immunotherapy, *Mol. Pharmaceutics*, **8** (2011) 104–116.

68. L. Castaneda, J. Valle, N. Yang, S. Pluskat, K. Slowinska, Collagen

Cross-Linking with Au Nanoparticles, *Biomacromolecules*, **9** (2008) 3383–3388.

69. D. Bartczak, and A. G. Kanaras, Preparation of Peptide-Functionalized Gold Nanoparticles Using One Pot EDC/Sulfo-NHS Coupling, *Langmuir*, **27** (2011) 10119–10123.

70. P. Sandström, M. Boncheva, B. Åkerman, Nonspecific and Thiol-Specific Binding of DNA to Gold Nanoparticles, *Langmuir*, **19** (2003) 7537–7543.

71. N. Bhatt, P. J. Huang, N. Dave, J. Liu, Dissociation and Degradation of Thiol-Modified DNA on Gold Nanoparticles in Aqueous and Organic Solvents, *Langmuir*, **27** (2011) 6132–6137.

72. S. H. Brewer, W. R. Glomm, M. C. Johnson, M. K. Knag, S. Franzen, Probing BSA Binding to Citrate-Coated Gold Nanoparticles and Surfaces, *Langmuir*, **21** (2005) 9303–9307.

73. W. R. Glomm, Ø. Halskau, A-M. D. Hanneseth, S. Volden, Adsorption Behavior of Acidic and Basic Proteins onto Citrate-Coated Au Surfaces Correlated to Their Native Fold, Stability, and pI, *J. Phys., Chem. B*, **111** (2007) 14329–14345.

74. B. Asadishad, M. Vossoughi, I. Alemzadeh, Folate-Receptor-Targeted Delivery of Doxorubicin Using Polyethylene Glycol-Functionalized Gold Nanoparticles, *Ind. Eng. Chem. Res.*, **49** (2010) 1958–1963.

-
75. F. Wang, Y-C. Wang, S. Dou, M-H. Xiong, T.M. Sun, J. Wang, Doxorubicin-Tethered Responsive Gold Nanoparticles Facilitate Intracellular Drug Delivery for Overcoming Multidrug Resistance in Cancer Cells, *ACS Nano*, **5** (2011) 3679–3692.
76. H. Park, J. Yang, J. Lee, S. Haam, I-H. Choi, K-H. Yoo, Multifunctional Nanoparticles for Combined Doxorubicin and Photothermal Treatments, *ACS Nano*, **3** (2009) 2919–2926.
77. X. Zhang, H. Chibli, R. Mielke, J. Nadeau, Ultrasmall Gold–Doxorubicin Conjugates Rapidly Kill Apoptosis-Resistant Cancer Cells, *Bioconjugate Chem.*, **22** (2011) 235–243.
78. C. M. Alexander, J. C. Dabrowiak, M. M. Maye, Investigation of the Drug Binding Properties and Cytotoxicity of DNA-Capped Nanoparticles Designed as Delivery Vehicles for the Anticancer Agents Doxorubicin and Actinomycin D, *Bioconjugate Chem.*, **23** (2012) 2061–2070.
79. Y-L. Luo, Y-S. Shiao, Y-F. Huang, Release of Photoactivatable Drugs from Plasmonic Nanoparticles for Targeted Cancer Therapy, *ACS Nano*, **5** (2011) 7796–7804.
80. J. You, G. Zhang, C. Li, Exceptionally High Payload of Doxorubicin in Hollow Gold Nanospheres for Near-Infrared Light-Triggered Drug Release, *ACS Nano*, **4** (2010) 1033–1041.
81. J. D. Gibson, B. P. Khanal, E. R. Zubarev, Paclitaxel-Functionalized Gold Nanoparticles, *J. Am. Chem. Soc.*, **129** (2007) 11653–11661.

-
82. X-Q. Zhang, X. Xu, R. Lam, D. Giljohann, D. Ho, and C. A. Mirkin., Strategy for Increasing Drug Solubility and Efficacy through Covalent Attachment to Polyvalent DNA–Nanoparticle Conjugates, *ACS Nano*, **5** (2011) 6962–6970.
83. D. A. Giljohann D. S. Seferos, P. C. Patel, J. E. Millstone, N. L. Rosi, C. A. Mirkin, Oligonucleotide Loading Determines Cellular Uptake of DNA-Modified Gold Nanoparticles, *Nano Lett.*, **7** (2007) 3818–3821.
84. N. L. Rosi, D. A. Giljohann, C. S. Thaxton, A. K. R. Lytton-Jean, M. S. Han, C. A. Mirkin, Oligonucleotide-modified gold nanoparticles for intracellular gene regulation, *Science*, **312** (2006) 1027–1030.
85. D. S. Seferos, A. E. Prigodich, D. A. Giljohann, P. C. Patel, C. A. Mirkin, Polyvalent DNA Nanoparticle Conjugates Stabilize Nucleic Acids, *Nano Lett.*, **9** (2009) 308–311.
86. A. K. Larsen, A. E. Escargueil, A. Skladanowski, Resistance mechanisms associated with altered intracellular distribution of anticancer agents, *Pharmacol. Ther.*, **88** (2000) 217–229.
87. S. Bennis, C. Chapey, P. Couvreur, J. Robert, Enhanced cytotoxicity of doxorubicin encapsulated in polyhexylcyanoacrylate nanospheres against multi-drug-resistant tumour cells in culture, *Eur. J. Cancer A*, **30** (1994) 89–93.
88. F. Wang, Y. C. Wang, S. Dou, M. H. Xiong, T. M. Sun, J. Wang, Doxorubicin-tethered responsive gold nanoparticles facilitate intracellular

drug delivery for overcoming multidrug resistance in cancer cells, *ACS Nano*, **5** (2011) 3679–3692.

89. V. K. Gupta, N. Atar, M. L. Yola, Z. Ustundag, L. Uzun, A novel magnetic Fe@Au core-shell nanoparticles anchored graphene oxide recyclable nanocatalyst for the reduction of nitrophenol compounds, *Water Res.*, **48** (2014) 210–217.

90. P. Zhang, C. Shao, Z. Zhang, M. Zhang, J. Mu, Z. Guo and Y. Liu, In situ assembly of well-dispersed Ag nanoparticles (AgNPs) on electrospun carbon nanofibers (CNFs) for catalytic reduction of 4-nitrophenol, *Nanoscale*, **3** (2011) 3357–3363.

91. Y. Lu, Y. Mei, M. Drechsler, M. Ballauff, Thermosensitive Core–Shell Particles as Carriers for Ag Nanoparticles: Modulating the Catalytic Activity by a Phase Transition in Networks, *Angew. Chem., Int. Ed.*, **45** (2006) 813–816.

92. Y. Shin, A. Dohnalkova, Y. Lin, Preparation of Homogeneous Gold–Silver Alloy Nanoparticles Using the Apo ferritin Cavity As a Nanoreactor, *J. Phys. Chem. C*, **114** (2010) 5985–5989.

93. S. Harish, J. Mathiyarasu, K. L. N. Phani, V. Yegnaraman, Synthesis of Conducting Polymer Supported Pd Nanoparticles in Aqueous Medium and Catalytic Activity Towards 4-Nitrophenol Reduction, *Catal. Lett.*, **128** (2009) 197–202.

94. H. Liu, Q. Yang, Facile fabrication of nanoporous Au–Pd bimetallic

foams with high catalytic activity for 2-nitrophenol reduction and SERS property, *J. Mater. Chem.*, **21** (2011) 11961–11967.

95. S-D. Oh, M-R. Kim, S-H. Choi, J-H. Chun, K-P. Lee, A. Gopalan, C-G. Hwang, K. Sang-Ho, O. J. Hoon, Radiolytic synthesis of Pd–M (M = Ag, Au, Cu, Ni and Pt) alloy nanoparticles and their use in reduction of 4-nitrophenol, *J. Ind. Eng. Chem.*, **14** (2008) 687–692.

96. T. Yao, T. Cui, X. Fang, F. Cui, J. Wu, Preparation of yolk–shell $\text{Fe}_x\text{O}_y/\text{Pd}@$ mesoporous SiO_2 composites with high stability and their application in catalytic reduction of 4-nitrophenol, *Nanoscale*, **5** (2013) 5896–5904.

97. S. Tang, S. Vongehr, X. Meng, Controllable incorporation of Ag and Ag–Au nanoparticles in carbon spheres for tunable optical and catalytic properties, *J. Mater. Chem.*, **20** (2010) 5436–5445.

98. J. Li, C.Y. Liu, Y. Liu, Au/graphene hydrogel: synthesis, characterization and its use for catalytic reduction of 4-nitrophenol, *J. Mater. Chem.*, **22** (2012) 8426–8430.

99. H. Hu, J. H. Xin, H. Hu, PAM/graphene/Ag ternary hydrogel: synthesis, characterization and catalytic application, *J. Mater. Chem. A*, **2** (2014) 11319–11333.

100. M. Tang, S. Zhang, X. Li, X. Pang, H. Qiu, Fabrication of magnetically recyclable $\text{Fe}_3\text{O}_4@\text{Cu}$ nanocomposites with high catalytic performance for the reduction of organic dyes and 4-nitrophenol, *Mater.*

Chem. Phys., **148** (2014) 639–647.

101. Y. Zhang, P. Zhu, L. Chen, G. Li, F. Zhou, D. Lu, R. Sun, F. Zhou, C-P. Wong, Hierarchical architectures of monodisperse porous Cu microspheres: synthesis, growth mechanism, high-efficiency and recyclable catalytic performance, *J. Mater. Chem. A*, **2** (2014) 11966–11973.

102. Y. Du, H. Chen, R. Chen, N. Xu, Synthesis of p-aminophenol from p-nitrophenol over nano-sized nickel catalysts, *Appl. Catal., A*, **277** (2004) 259–264.

103. H. Hu, J. H. Xin, H. Hu, X. Wang, D. Miao, Y. Liu,(2015), Synthesis and stabilization of metal nanocatalysts for reduction reactions—a review, *J. Mater. Chem. A*, **3** (2015) 11157–11182.

104. H. Li, J. Liao, Y. Du, T. You, W. Liao, L. Wen, Magnetic-field-induced deposition to fabricate multifunctional nanostructured Co, Ni, and CoNi alloy films as catalysts, ferromagnetic and superhydrophobic materials, *Chem. Commun.*, **49** (2013) 1768–1770.

105. N. B. Golovina, L. M. Kustov, Toxicity of metal nanoparticles with a focus on silver, *Mendeleev commun.*, **23** (2013) 59–65.

106. Y. P. Li, H. B. Cao, C. M. Liu, Y. Zhang, Electrochemical reduction of nitrobenzene at carbon nanotube electrode. *J. Hazard Mater.*, **148** (2007) 158–163.

107. V. K. Gupta, N. Atar, M. L. Yola, Z. Ustundag, L. Uzun, A novel

magnetic Fe@Au core-shell nanoparticles anchored graphene oxide recyclable nanocatalyst for the reduction of nitrophenol compounds, *Water Res.*, **48** (2014) 210–217.

108. Y. T. Woo, D. Y. Lai, Aromatic amino and nitro-amino compounds and their halogenated derivatives, in: *Patty's toxicology*. Wiley, New York (2001).

109. S. C. Mitchell, R. H. Waring, Aminophenols, in: *Ullmann's encyclopedia of industrial chemistry*, Weinheim (2002).

110. S. Panigrahi, S. Basu, S. Praharaj, S. Pande, S. Jana, A. Pal, S. K. Ghosh, T. Pal, Synthesis and size-selective catalysis by supported gold nanoparticles: study of heterogeneous and homogeneous catalytic process, *J. Phys. Chem. C*, **111** (2007) 4596–4605.

111. H. Bonneman, G. A. Braun, Enantioselective Hydrogenations on Platinum Colloids, *Angew. Chem. Int. Ed. Engl.*, **35** (1996) 1992–1995.

112. L. N. Lewis, N. Lewis, Platinum-catalyzed hydrosilylation-colloid formation as the essential step, *J. Am. Chem. Soc.*, **108** (1986) 7228–7231.

113. M. N. Vargaftik, V. P. Zagorodnikov, I. P. Stolarov, I. I. Moiseev, D. I. Kochubey, V. A. Likholobov, A. L. Chuvilin, K. I. Zamaraev, Giant palladium clusters as catalysts of oxidative reactions of olefins and alcohols, *J. Mol. Catal.*, **53** (1989) 315–348.

114. T. J. Schmidt, M. Noeske, H. A. Gasteiger, R. J. Behm, P. Britz, W.

Brijoux, H. Bönemann, Electrocatalytic Activity of PtRu Alloy Colloids for CO and CO/H₂Electrooxidation: Stripping Voltammetry and Rotating Disk Measurements, *Langmuir*, **13** (1997) 2591–2595.

Chapter 2

Spontaneous Preparation, characterisation, and stability evaluation of highly stable gold nanoparticle stabilized with ω -sulfonylated alkylsulfanylaniline

2.1: Introduction

Au NP have been recognised as one of the most common and popular nanomaterials, because they are easily modified by using various functionalised molecules such as DNAs, proteins, or fluorescent molecules. Functionalised Au NP have found many applications in various fields; their biological and medicinal applications in particular have been studied most intensively.¹⁻¹² Functionalised Au NP are usually obtained by a ligand exchange reaction of thiol-terminated molecules with desired functional groups and pre-prepared nanoparticles. In most cases, citrate-¹³ or ascorbate-¹⁴ stabilised Au NP were used as raw materials because they are easily prepared from inexpensive chemicals such as citric acid or ascorbic acid, and they readily undergo ligand exchange reactions. However, the citrate- or ascorbate-stabilized Au NP must be stored as diluted basic

solutions, as they are unstable in acidic or neutral media and in saline solutions, which are the common conditions in biological and medicinal experiments. Many methods were adopted to synthesise Au NP, however the preparation of a stable, modifiable with size-controlled Au NP that are suitable for biological or medicinal applications, is still challenging. The stability of Au NP are rarely investigated or evaluated and this remains a challenge (particularly in complex media such as those used for cell bioassay). Therefore, much attention should be paid for designing and constructing a biocompatible, aggregation-free Au NP in order to meet the demand call for its application in nanomedicine.

In this study, the preparation and properties of ω -sulfonylated alkylsulfanylaniline-stabilized Au NP, which can be an attractive alternative for citrate- or ascorbate stabilised Au NP, is described. It includes a novel method to synthesise stable Au NP by the chemical reduction method, which provides a new approach to construct well-defined hybrid organic-inorganic nanomaterials. ω -Sulfonylated alkylsulfanylaniline **1** is a newly developed reductive stabiliser (RS) in this research for preparation of Au NP. It is a mild reducing reagent, similar to citric acid or ascorbic

acid, and was reacted with HAuCl_4 and coordinated with Au NP by its amino group to form highly stable Au NP spontaneously. It is well known that the size and shape of the Au NP can be controlled by the rate of reduction of Au^{3+} and the specific coordination of stabilising agents on the surface of the seed crystals (nuclei), respectively. In this research, the effect of pH and different ratios of reducing stabilisers to Au^{3+} during their reactions were examined, which may change the rate of the reduction and the direction of coordination to give highly stable Au NP by using *ω*-sulfonylated alkylsulfanylaniline **1** as a reductive stabilizer.

The optical and physical properties of resulting Au NP were characterised by ^1H NMR, UV-visible spectroscopy, TEM analysis, and FTIR spectra.

The surface modification of the resulting Au NP was examined with a thiol-terminated dye through ligand exchange with thiol molecules. This study allows for improving the stability of Au NPs in biologically relevant media, including PBS and extremes of pH (3–13) and can be stored in powdered form and re-dissolved without aggregation, leading to long term

chemical and physical stability, so that it can be applied in biology and nanomedicine as a drug delivery system.

2.2: Materials and methods

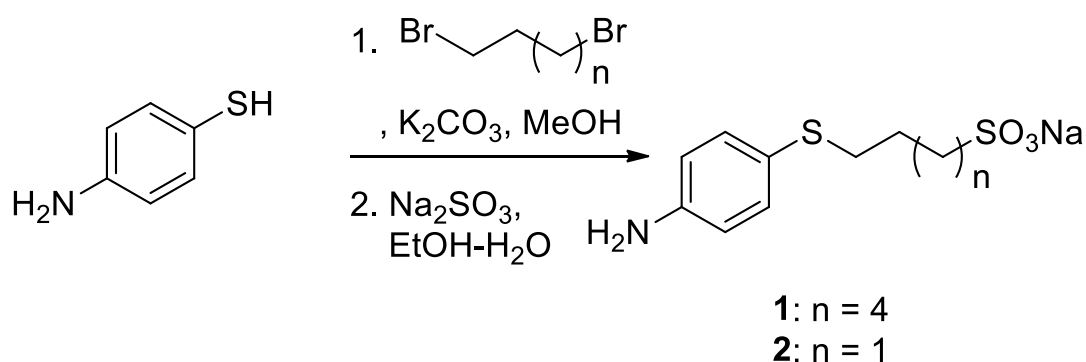
2.2.1: Materials

All starting materials were of analytical grade, commercially available and used without further purifications. Double distilled water has been used in all experiments. UV-visible spectroscopy and FTIR spectra were measured using a Hitachi U-2900 spectrophotometer and a Perkin Elmer Multiscope FTIR spectrophotometer in a transmission mode, as a KBr pellet in a spectral range from 1000-4000 cm^{-1} , respectively. ^1H and ^{13}C NMR charts were measured by a JEOL GSX-400 spectrophotometer at room temperature. TEM images were obtained by JEOL JEM-3010 VII operating at 300 kV. The samples for TEM measurements were prepared by putting a drop of the diluted colloidal solution of the nanoparticles on a carbon-coated copper grid. The solvent was dried by placing the copper grid in a desiccator at room temperature for 2 days until the solvent was completely evaporated.

2.2.2: Preparation of ω -sulfonylated alkylsulfanylanilines **1** and **2**

Two ω -sulfonylated alkylsulfanylanilines **1** and **2** were prepared as shown in Scheme 1. Detailed protocol to prepare **1** was as follows: To a solution of 4-aminobenzenethiol (10 mmol in 100 mL of methanol (MeOH)), K₂CO₃ (10 mmol) and 1,6-dibromohexane (20 mmol) was added, and the mixture was stirred at room temperature for 12 h. After usual extraction procedure (extraction by ethyl acetate (AcOEt) 10 ml/NaOH) aqueous 3 mL, evaporation and then silica gel column chromatography for the extracted materials was performed using hexane and AcOEt as growing solvent 4:1 respectively. The liquids in the tubes containing the target material were collected in a large flask, evaporated, and then the product (pale yellow oil) was collected in a small flask. This unstable ω -bromoalkylsulfanylanilin was obtained as a pale yellow oil, which was immediately treated with excess Na₂SO₃ (15 mmol) in aqueous ethanol (EtOH) (20 mL of EtOH and 20 mL of H₂O) under reflux conditions. After 4 h, the reaction mixture was concentrated, the product was frozen for 15 min to get it as solid material and the resulting white solid was washed with AcOEt (2 mL for two times) and H₂O (2 mL for two times) to remove

excess unreacted *p*-aminothiobenzene and Na₂SO₃. The product was dried using desiccator overnight at 60 °C to remove the remaining water and finally to give **1** (yield 87%). Compound **2** was also prepared by the same method to give 93% yield.



Scheme 1. Preparation of compounds **1** and **2**.

2.2.3: Preparation of Au NPs stabilized with ω -sulfonated alkylsulfanylaniline (1-Au NP)

The typical preparation method for stabilised Au NP using **1** is as follows: Freshly prepared aqueous solution of H₂AuCl₄ (1.0 mM, 10 mL) was added to an aqueous solution of disodium succinate (10 mM, 10 mL). The pH of the solution was controlled by adding a few drops of aqueous NaOH (1.0 M) or HCl (1.0×10⁻² M). The volume of the solution was adjusted to 50 mL by adding distilled water, and the solution was heated

until boiling. An aqueous solution of **1** (2.0 mM, 10 mL) was added drop wise to the boiled solution, and the whole mixture was left for 48 h at 90 °C. The final molar concentration was 0.16 and 0.33 mM for H₂AuCl₄ and **1**, respectively (1:2 molar ratio). After cooling to room temperature, the resulting red solution was used as **1-Au NP** solution (0.17 mM based on Au).

Powdered **1-Au NP** was obtained by concentrating the solution in a rotary evaporator, followed by drying using a vacuum pump. The powdered **1-Au NP** was re-dispersed in water (60 mL) or PBS (pH 7.4, 60 mL). The ¹H NMR spectrum of **1-Au NP** was measured after purification. Freshly prepared aqueous solution of **1-Au NP** (60 mL) was concentrated to approximately 10 mL that was dialysed using dialysis tube (Spectra/Por 3). The dialysis tube was placed in a beaker containing 500 mL of water and stirred at room temperature. The water was replaced every 8 hours for a total period of 24 h to remove inorganic salts and free ligands. The purified solution was concentrated to dryness with a vacuum pump, and the resulting **1-Au NP** was dissolved in DMSO-d₆ (0.7 mL) to measure ¹H NMR.

2.2.4: Stability evaluation

For pH dependent stability, 3 samples were prepared by dilution 1:4 (**1-Au NP** and water respectively). The first sample was used as control **1-Au NP**, in the second sample, the pH of the **1-Au NP** solution was changed to pH 3 by using 1.5 M HCL and, in the third sample, the pH of Au NPs solution was changed to pH 13 by using 1 M Na OH. For examination of the stability in PBS, the samples were prepared by dilution 2:2 (**1-Au NP** and PBS (154 mmol/L NaCl, pH 7.4) respectively).

Dryness-redispersion stability was evaluated as following: Two samples were prepared; the first one was 10 mL of **1-Au NP** where it was completely dried by evaporator, then re-dispersed immediately and monitored by the UV-visible spectra. The second sample was 10 mL of **1-Au NP** where it was completely dried and lyophilised in a freezer for 2 weeks, then reconstituted and monitored by the UV-visible spectra.

2.2.5: Ligand exchange reaction with thiol molecules

An aqueous solution of sodium 2-(3-mercaptopropanamido) naphthalene-1-sulfonate (**3**, 0 to 0.80 mM, 2.0 mL) and aqueous NaOH

(1.0×10^{-2} M, 2.0 mL) were added to an aqueous solution of **1-Au NP** (0.40 mM based on Au, 4.0 mL, pH 8.0) at 50 °C, and the mixture was stirred for 1 h at the same temperature. The reaction mixture was cooled to room temperature, and poured into a dialysis tube (Spectra/ Por 3) that was put in a beaker filled with water (500 mL) at room temperature. The water was slowly stirred, and was replaced every 8 h. After 24 h, excess **3** and the free ligand were removed, and the resulting solution was diluted with water to 16 mL to measure its absorption spectrum.

2.3: Results and discussion

2.3.1: Characterization of ω -sulfonylated alkylsulfanylanilines 1 and 2

Compound 1: ^1H NMR (DMSO- d_6) δ 7.02 (d, $J=8.5$ Hz, 2H, 6.49 (d, $J=8.5$ Hz, 2H, 5.06 (s, 1H), 2.62 (t, $J=7.8$ Hz, 2H, 2.38 (t, $J=7.8$ Hz, 2H), 1.35 (m, 8H); ^{13}C NMR (Fig. 1) (DMSO- d_6) δ 148.7, 133.9, 115.1, 87.2, 51.5, 29.1, 28.9, 28.7, 28.3; IR (KBr pellet) 3360, 2941, 2855, 1686, 1604, 1495, 1427, 1257, 1136, 1107, 1041, 979, 621 cm^{-1} ; HRFABMS m/z 311.0624, calcd for M^+ : 311.0626.

Compound 2: ^1H NMR (DMSO- d_6) δ 7.02 (d, $J=8.5$ Hz, 2H), 6.49 (d, $J=8.5$ Hz, 2H), 3.33 (s, 1H), 2.70 (t, $J=7.8$ Hz, 2H), 2.50 (t, $J=7.8$ Hz, 2H), 1.70 (tt, $J=7.8$ Hz, 7.8 Hz, 2H; ^{13}C NMR (Fig. 2) (DMSO- d_6) δ 148.7, 133.9, 115.2, 87.2, 50.5, 25.4; IR (KBr pellet) 3360, 1604, 1495, 1427, 1191, 1066, 978, 814, 629 cm^{-1} ; HRFABMS m/z 292.0054, calcd for M^+ Na^+ : 292.0049.

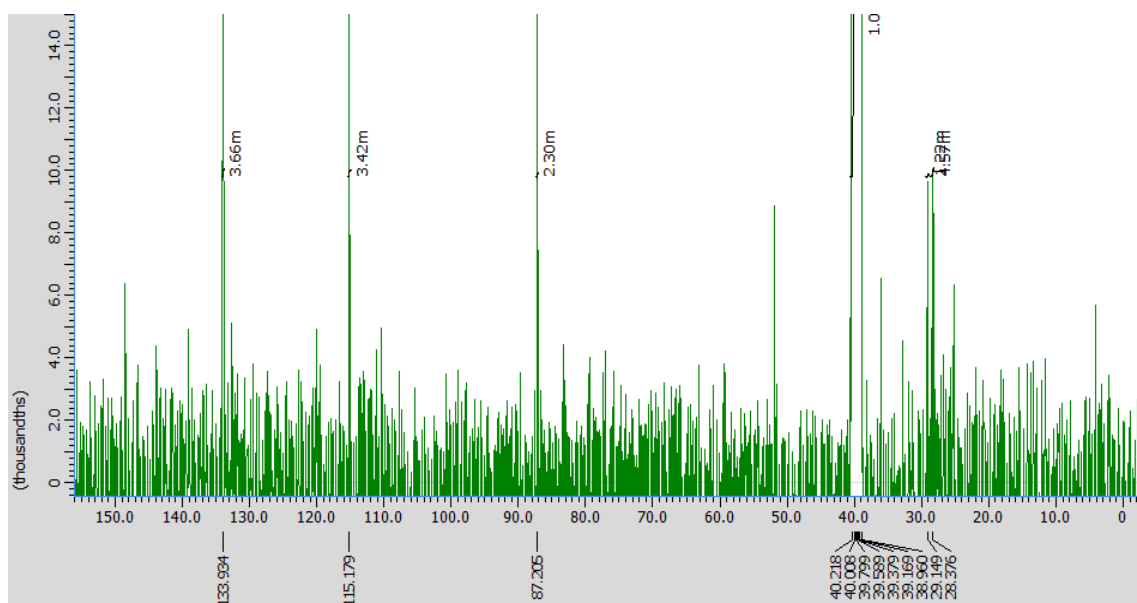


Figure 1. ^{13}C NMR of compound **1**. (400 MHz in DMSO- d_6).

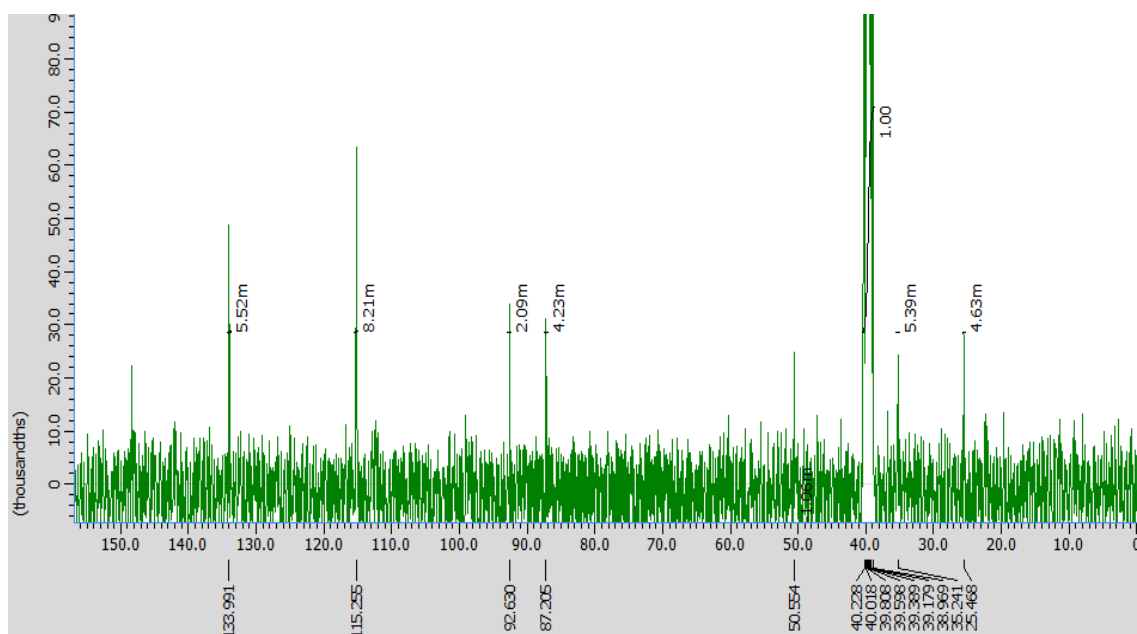


Figure 2. ^{13}C NMR (DMSO) of compound **2**. (400 MHz in DMSO- d_6).

2.3.2: pH effect on preparation and peculiarities of stabilized gold nanoparticles (1-Au NP)

Preparation of Au NP in nearly neutral media is favourable, particularly in biological applications. The reaction of **1** and HAuCl₄ successfully proceeded in a weak basic solution (pH 8) that is acceptable for most of the biological applications, to give a stable **1-Au NP** solution in 48 h. The pH effect (4.5, 6.5, and 8) was checked with different ratios of RS to Au³⁺ in order to establish the most suitable conditions for preparation of highly stable Au NPs and size assessment of the as-prepared **1-Au NP**. The pH of the aqueous solution during preparation of **1-Au NP** affected on the surface plasmon resonance (SPR) of the particles. The maximum absorbance (λ_{max}) of **1-Au NP** appeared at a longer wavelength (red shift) when the pH values were decreased from 8 to 4.5 together with decreasing the intensity of the absorbance peak due to the fact large sized-particles were obtained in acidic pH. The λ_{max} of **1-Au NP** appeared at 537, 531, 526 nm at pH 4.5, 6.5, 8, respectively. These changes were monitored using UV-visible spectroscopy (Fig. 3) and TEM (Fig. 4).

TEM has been utilised to evaluate the morphology and size distribution of the nanoparticles. The TEM image showed the majority of the particles were spherical with a diameter of 10–15 nm with an average particle size of 11.2 ± 5.9 nm and size distribution of the particles (histogram) was performed by systematic analysis of 257 particles from the TEM images (Fig. 4A and B). The reaction also proceeded in a neutral solution (pH 6.5) or in a weakly acidic solution (pH 4.5), and completed much faster (24 h and 8 h, respectively). It is well known that the reaction of Au^{3+} to Au^0 accelerates in a weakly acidic solution.¹⁵ The reactivity of Au^{3+} decreases and Au^{3+} solutions changed from the predominance of $[\text{AuCl}_4]^-$ to $[\text{Au}(\text{OH})_4]^-$ with increasing the pH value^{16–20} and our results have supported the pH effect. The resulting Au NPs from these reactions at pH 6.5 and pH 4.5 were much larger and their shapes were ununiformed (Fig. 4C and D). This can be explained by the protonation of the aniline moiety in **1**. As shown in Scheme 2, the Au^{3+} ion is easily reduced by **1** to form Au^0 . The resulting Au^0 starts growing into nanoparticles. Since an excess of **1** is used for this reaction, the unreacted **1**, which is more coordinative than the oxidised **1**, coordinates to the surface of the

nanoparticles. This stops the growth of the gold nanoparticles, thereby forming stable **1-Au NP** in an alkaline solution. In the acidic or neutral medium, a considerable amount of **1** is protonated and is less coordinative; thus, the nanoparticles grow to become larger and uneven particles. The ^1H NMR spectra of **1** and **1-Au NP** are shown in Fig. 5. The signals corresponding to the aromatic protons (H_a and H_b) and aniline protons ($-\text{NH}_2$) in **1** shifted toward the lower magnetic field by the formation of **1-Au NP**, whereas the shifting difference in H_a is 0.16, in H_b is 0.23, and in aniline protons ($-\text{NH}_2$) is 0.60. It is noteworthy that the signals corresponding to the protons of $-\text{SCH}_2-$ (H_c), $\text{NaO}_3\text{SCH}_2-$ (H_d), and other methylene groups were almost unchanged. This observation strongly indicated that **1** binds to the surface of Au NP with its $-\text{NH}_2$ group.

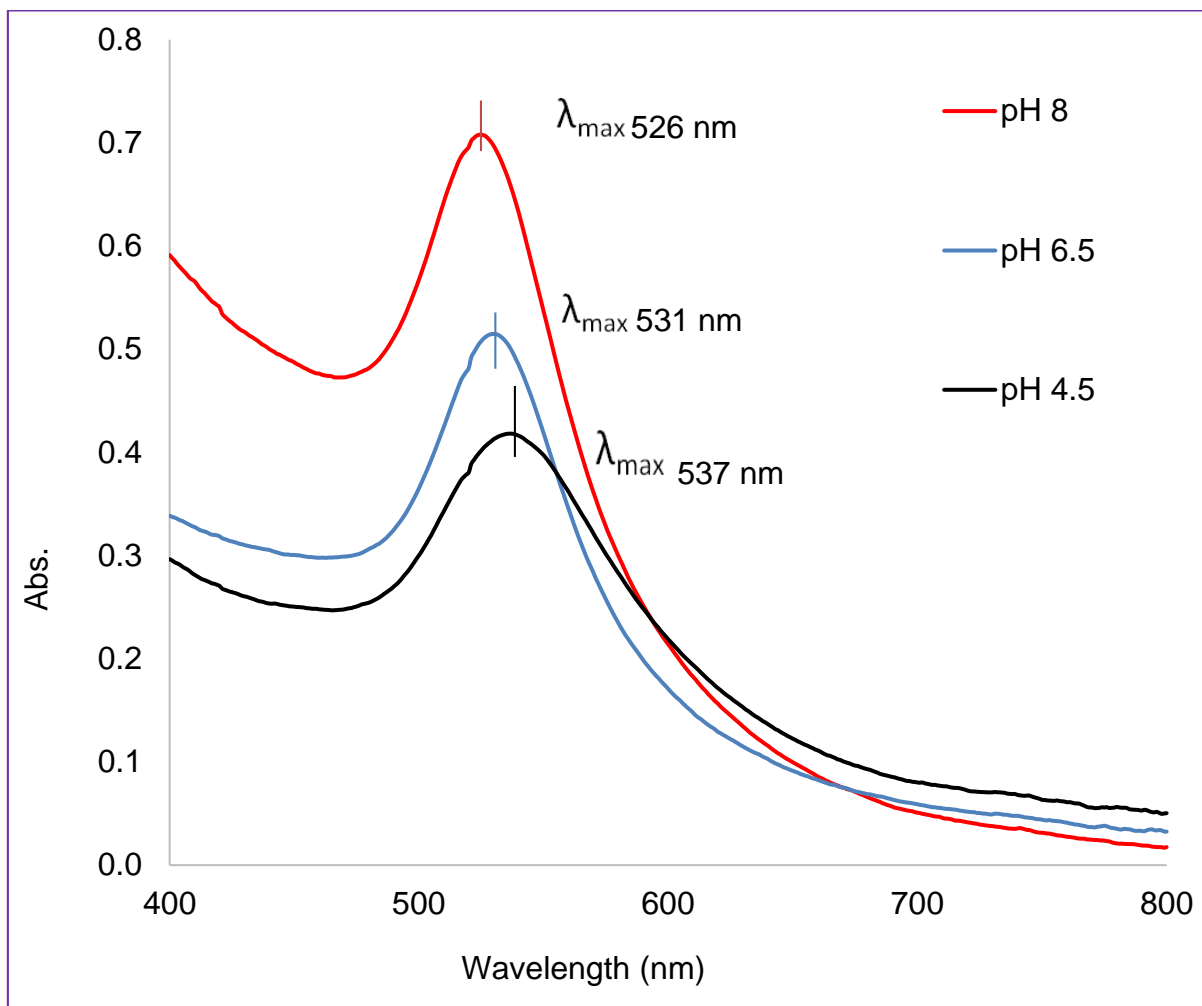


Figure 3. Absorption spectra of aqueous solutions of **1-Au NP** prepared at different pH.

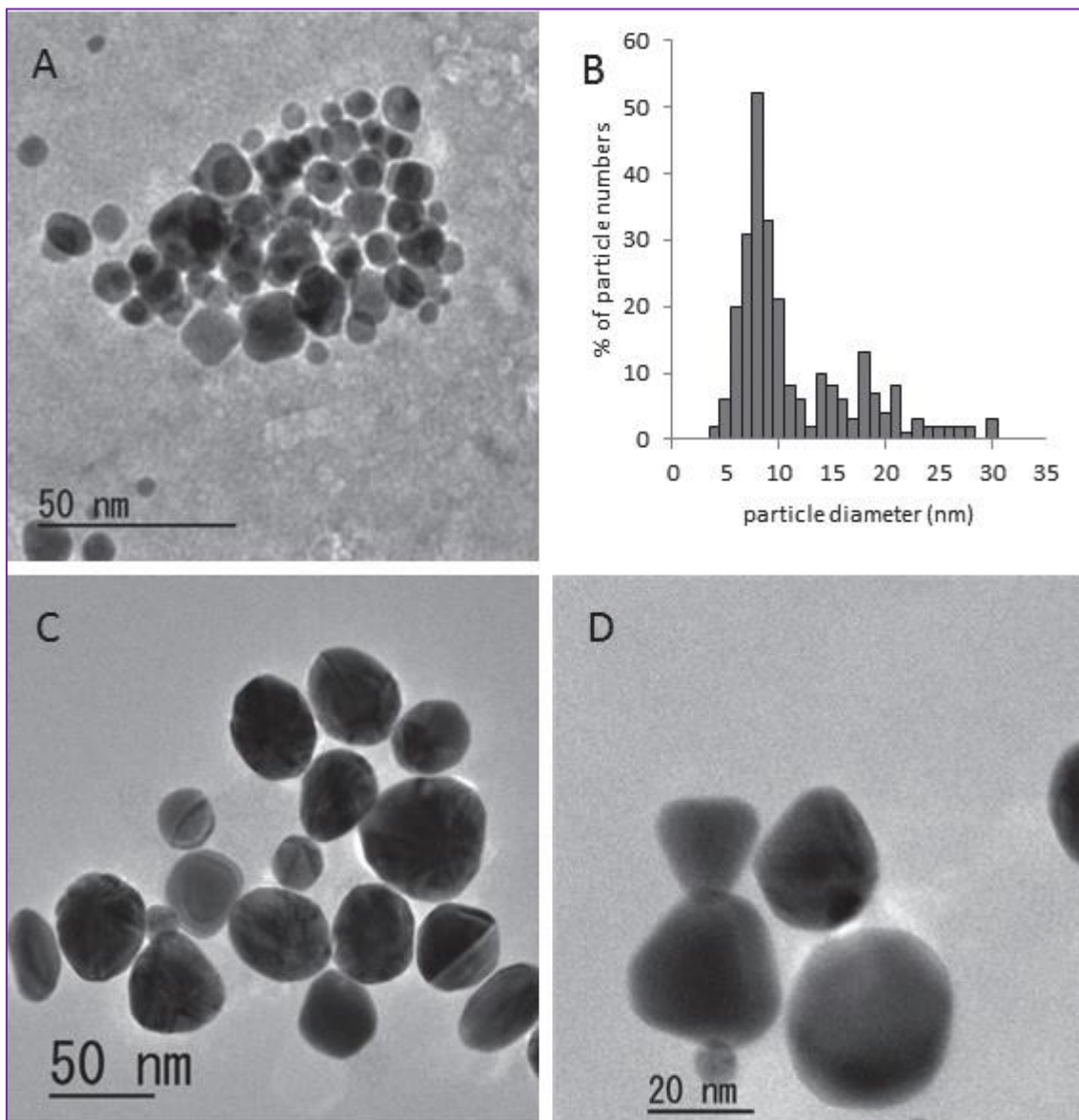
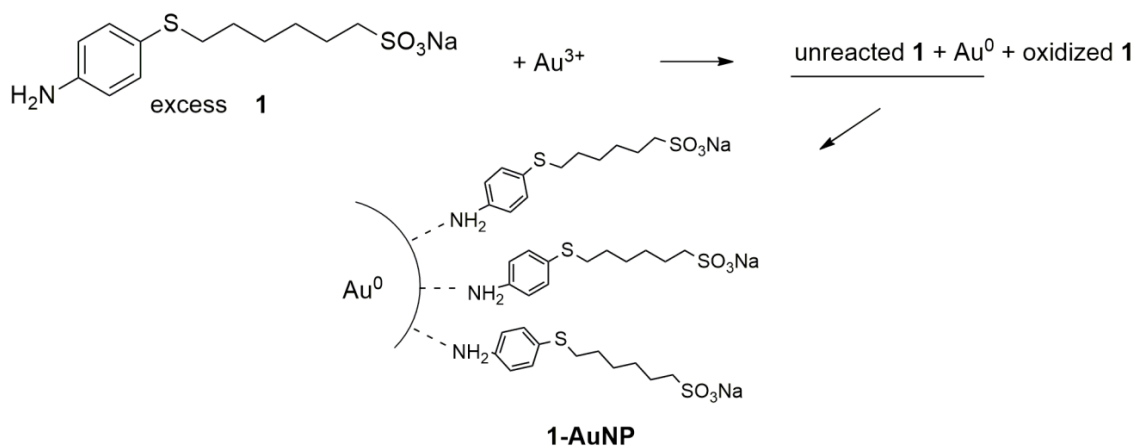


Figure 4 (A) TEM image of the particles prepared in a solution of pH 8.0. (B) Distribution of particle diameters in a solution of pH 8.0. (C) TEM image of the particles prepared in a solution of pH 6.5. (D) TEM image of the particles prepared in a solution of pH 4.5.



Scheme 2. Plausible pathway to form **1-Au NP**.

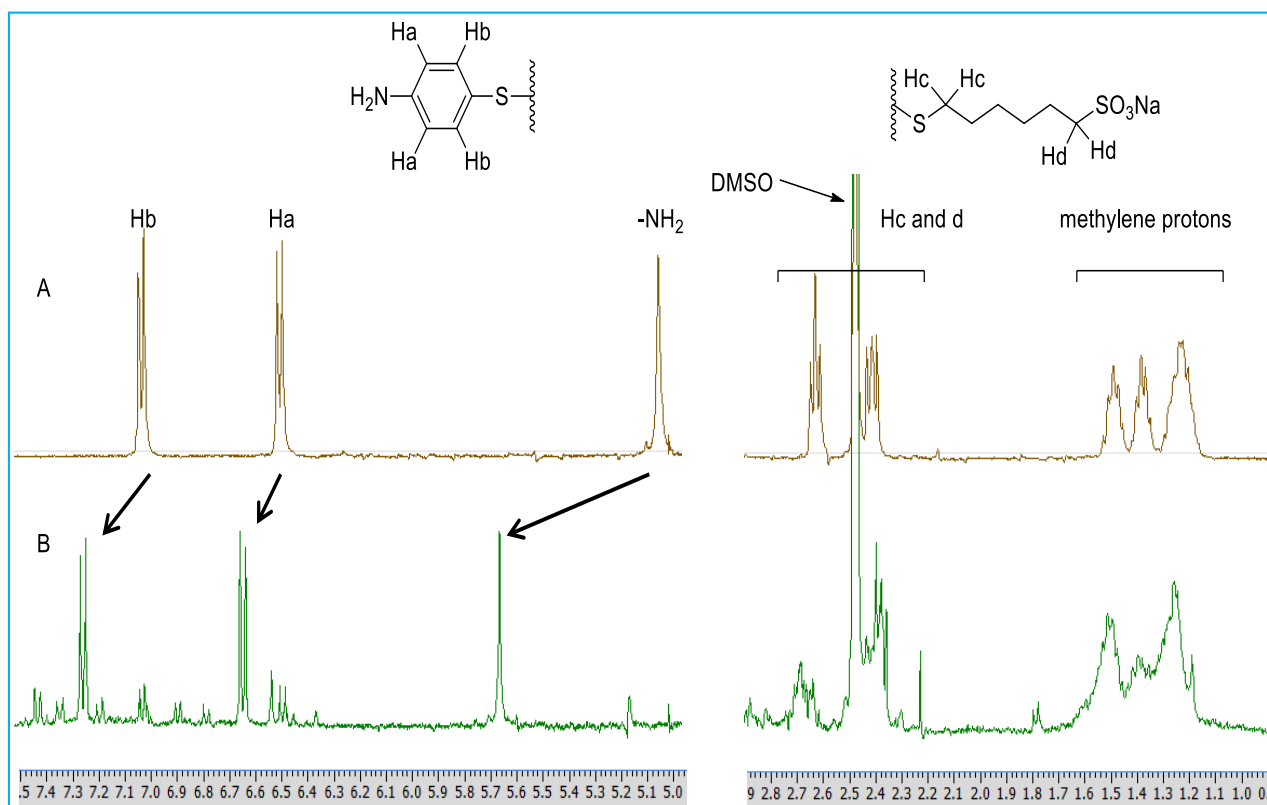


Figure 5. (A) ¹H NMR spectrum of **1**. (B) ¹H NMR spectrum of **1-Au NP**.

(400 MHz in DMSO-d₆).

2.3.3: Stability evaluation of 1- and 2-Au NP

2.3.3.1: Dryness-redispersion stability

Stability of Au NP plays a vital role in their subsequent potential applications. Dry storage condition is most prominent for long term stability and robustness of Au NP as compared to aqueous based conditions; therefore, the possibility of the dryness-redispersion cycles was investigated. The solution of **1-Au NP** was stable for a very long time. The absorption spectrum showed λ_{\max} at 526 nm, which did not change for at least six months (Fig. 6A (a)). It is noteworthy that **1-Au NP** was stable even in its powdered form, and was re-dispersible in water or PBS (pH 7.4), and gave an absorption spectra almost identical to that of its freshly prepared solution (Fig. 6A (b)). The powdered **1-Au NP** could be stored in air at room temperature for at least two weeks, and its solution showed the same λ_{\max} at 526 nm with the freshly prepared solution, although the absorbance was slightly smaller (Fig. 6A (c)). TEM images obtained for the redispersed solution clearly showed that the size and shape of the nanoparticles were almost unchanged by the drying-redispersion process, and the average particle size of the redispersed **1-Au NP** was 11.6 ± 7.0 nm

(Fig. 6C and D).

The solution of **2-Au NP**, prepared by the same method as the **1-Au NP** solution, was also stable for a long time. Its absorption spectrum showed λ_{\max} at 523 nm with Abs 0.77, and it did not change for six months (Fig. 6B (a)). However, the absorption spectra of the redispersed solutions of powdered **2-Au NP** were much smaller and broader (Fig. 6B (b)), λ_{\max} at 523 nm with Abs 0.62, and (c), λ_{\max} at 552 nm with Abs 0.42) than those of the **1-Au NP** solutions, indicating that a considerable amount of **2-Au NP** aggregated during the drying-redispersion process and storage. Therefore, only **1-Au NP** was studied in detail. On the other hand, Frens's particles completely crashed, precipitated, and loss of SPR either immediately or 2 weeks after dryness (Fig. 7).

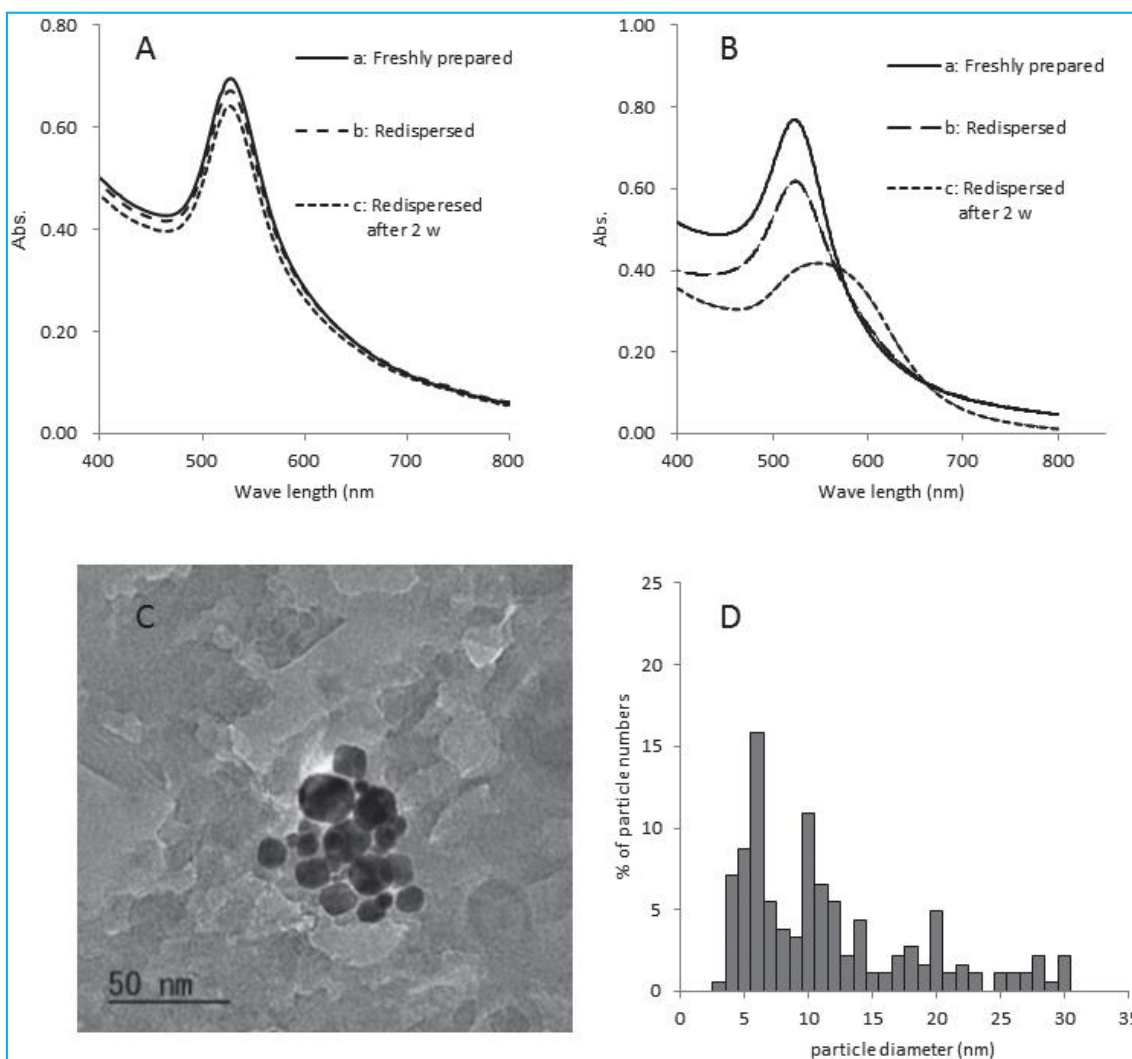


Figure 6 (A) Absorption spectra of **1-Au NP**; a: freshly prepared solution, b: redispersed solution of **1-Au NP** powder in water, and c: redispersed solution of **1-Au NP** powder (stored for two weeks) in water. (B) Absorption spectra of **2-Au NP**; a: freshly prepared solution, b: redispersed solution of **2-Au NP** powder in water, and c: redispersed solution of **2-Au NP** powder (stored for two weeks) in water. (C) TEM image obtained for the redispersed solution of **1-Au NP** powder in water. (D) Distribution of particle diameters of the redispersed **1-Au NP** powder in water.

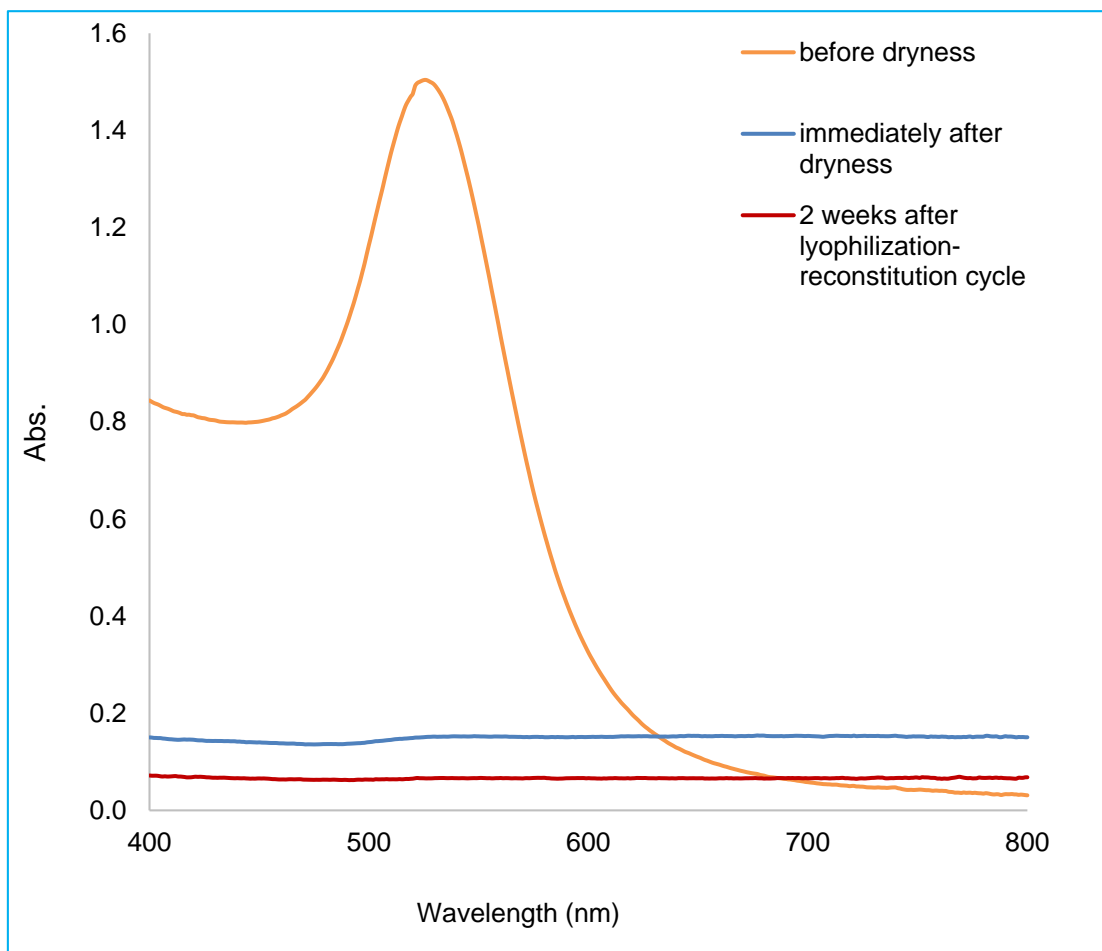


Figure 7. Absorption spectra after dryness-redispersion of Frens's particles.

2.3.3.2: The pH dependent stability

The pH dependent stability is very crucial factor for therapeutic applications and biomedical uses of Au NP.²¹ The solution of **1-Au NP** was tolerant to a wide range of pH and the particles maintained their robustness. The absorption spectrum of a solution of pH 13, prepared by adding 1.0 M aqueous NaOH to the freshly prepared **1-Au NP** solution, showed the same λ_{\max} (526 nm) as the original **1-Au NP** solution of pH 8 (Fig. 8). In the acidic condition of pH 3, achieved by adding 1.0 M aqueous HCl, the spectrum was slightly broader and λ_{\max} shifted to 531 nm (Fig. 8), although the profile did not change for several weeks (Fig. 9). **1-Au NP** is protected against aggregation by both the electrostatic repulsion force and stable steric protection provided by the ligand. The amino group (NH₂) is coordinated on the surface of **1-Au NP** and possibly the aliphatic chain of sulfanyl aniline acts as a barrier against intrusion of acidified solution to the **1-Au NP** core. Therefore, the particles were still viable and did not aggregate or precipitate. In the case of Fren's particles (native citrate method), the particles were crashed out, aggregated, did not redissolve at all with a subsequent loss of SPR, and a black precipitate was observed

immediately at pH 3 (Fig. 10). Citrate primarily provides stability for Fren's particles by electrostatic repulsion derived from deprotonated carboxyl groups. In acidic pH, concurrent protonation of the carboxyl terminal coating on the surface of the Au NP occurred, diminishing the electrostatic repulsive force between the particles and consequently resulted in a loss of stability, aggregation and precipitation.²²

A highly acidic condition was detrimental to the nanoparticles. The absorption spectrum of the **1-Au NP** solution of pH 2 showed a weak and broad signal (Fig. 8), and a black precipitate was formed within a few hours. The pH dependent stability can be explained by the pKa of compound **1**. Since the pKa of protonated anilinium ion is known as 5.2,²³ most of the –NH₂ groups are supposed to be protonated at pH 3 or lower. The protonated **1** is released from the Au NP surface, and the resulting naked Au NP aggregate to form larger particles or precipitates. On the other hand, in alkali condition the particles are stable where Au³⁺ become less reactive and this is due to the formation of stable hydroxylated complexes, which cause neutralisation of H⁺, leading to an absence of hydrogen bonding with –NH₂,^{24,25} which occurred in the highly acidic conditions. Therefore, all of

the -NH_2 groups are not protonated, and **1-Au NP** has not been changed at all in alkali condition.

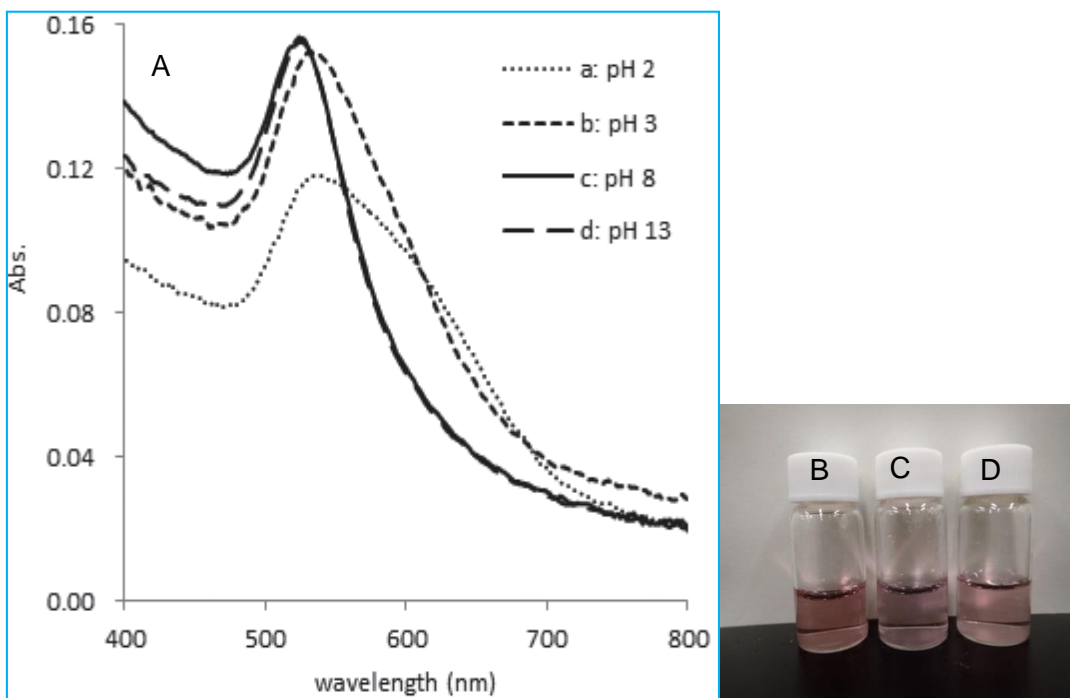


Figure 8. (A) Absorption spectra of **1-Au NP** solutions in different pH. (B) Control **1-Au NP** sample, (C) **1-Au NP** at pH 3 and (D) **1-Au NP** at pH 13.

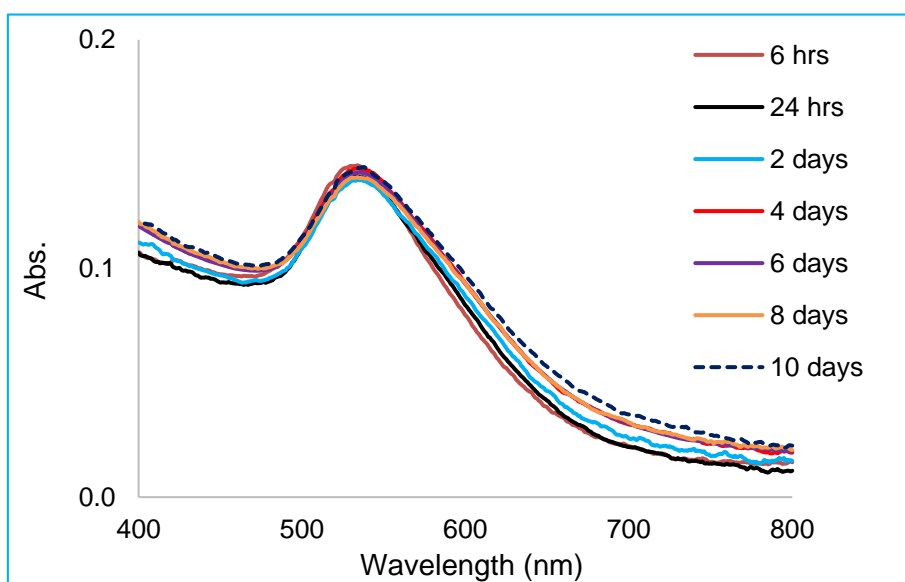


Figure 9. Absorption spectra profile of a solution of **1-Au NPs** at pH 3 with time.

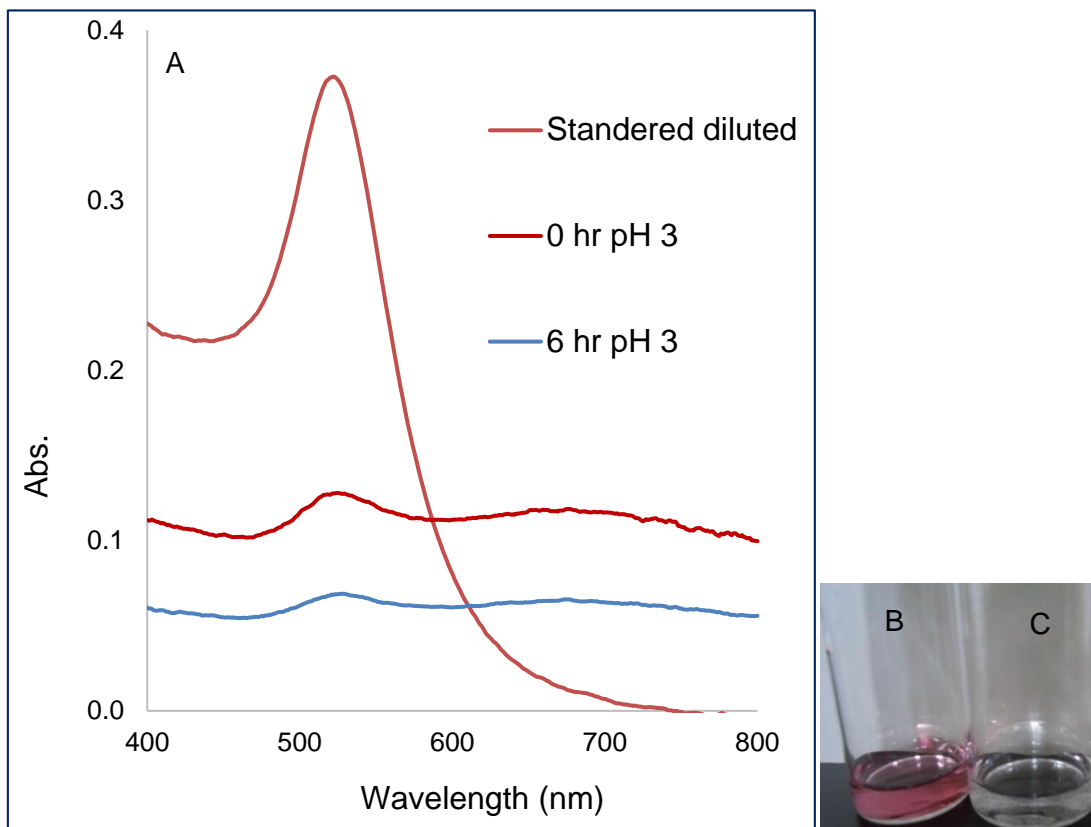


Figure 10. (A) UV-visible spectra of Frens's particles at pH 3, (B) Frens's Au NP (control), and (C) Black precipitate of Frens's particles (pH 3).

2.3.3.3: Salinity stability (stability in physiological saline, PBS):

Stability of **1-Au NP** in physiological saline (PBS, pH 7.4) was evaluated over a period of 3 days suitable to many cell lines bioassays. The **1-Au NP** have been found to be highly stable in PBS (Fig. 11) and no concurrent aggregation of the particles has occurred. This is attributed to the ligand steric repulsive forces between the particles, which reduces the sensitivity to salt; minimises the effect of the salt on the particles, owing to the ligand branched molecular structure.²⁶ In contrast, the Frens's particles crashed out, aggregated and precipitated just after addition of the PBS (Fig. 12). This is owing to using a weak stabilizing agent in the case of Frens's particles, which makes it highly sensitive to the salts. The electrostatic repulsion, which is the only force, stabilizes Frens's particles, decreases significantly at high salt concentrations whereas electric double layers around the Au NPs were highly suppressed.²⁷

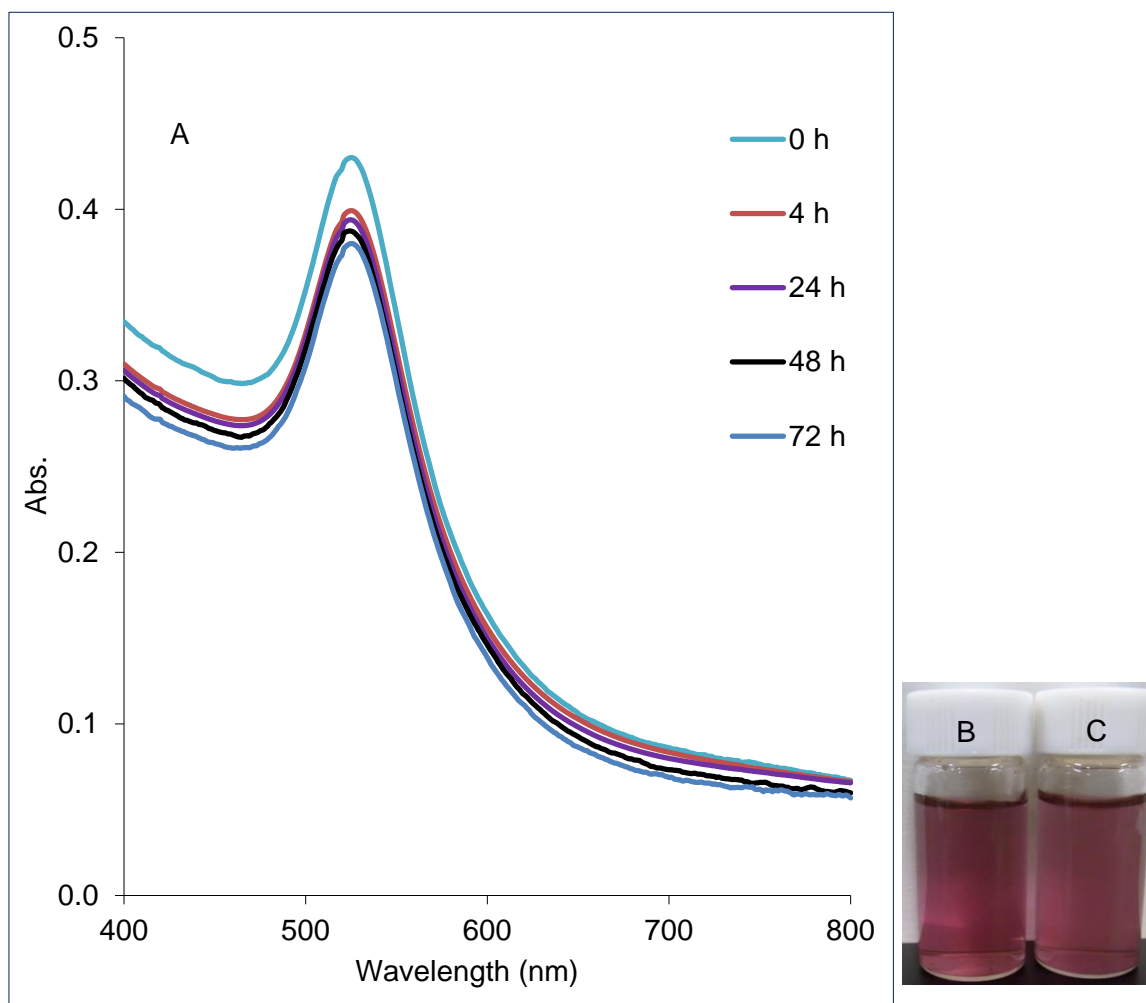


Figure 11. (A) Absorption spectra profile of **1-Au NP** in PBS. (B) **1-Au NP** solution (control). (C) **1-Au NP** in PBS.

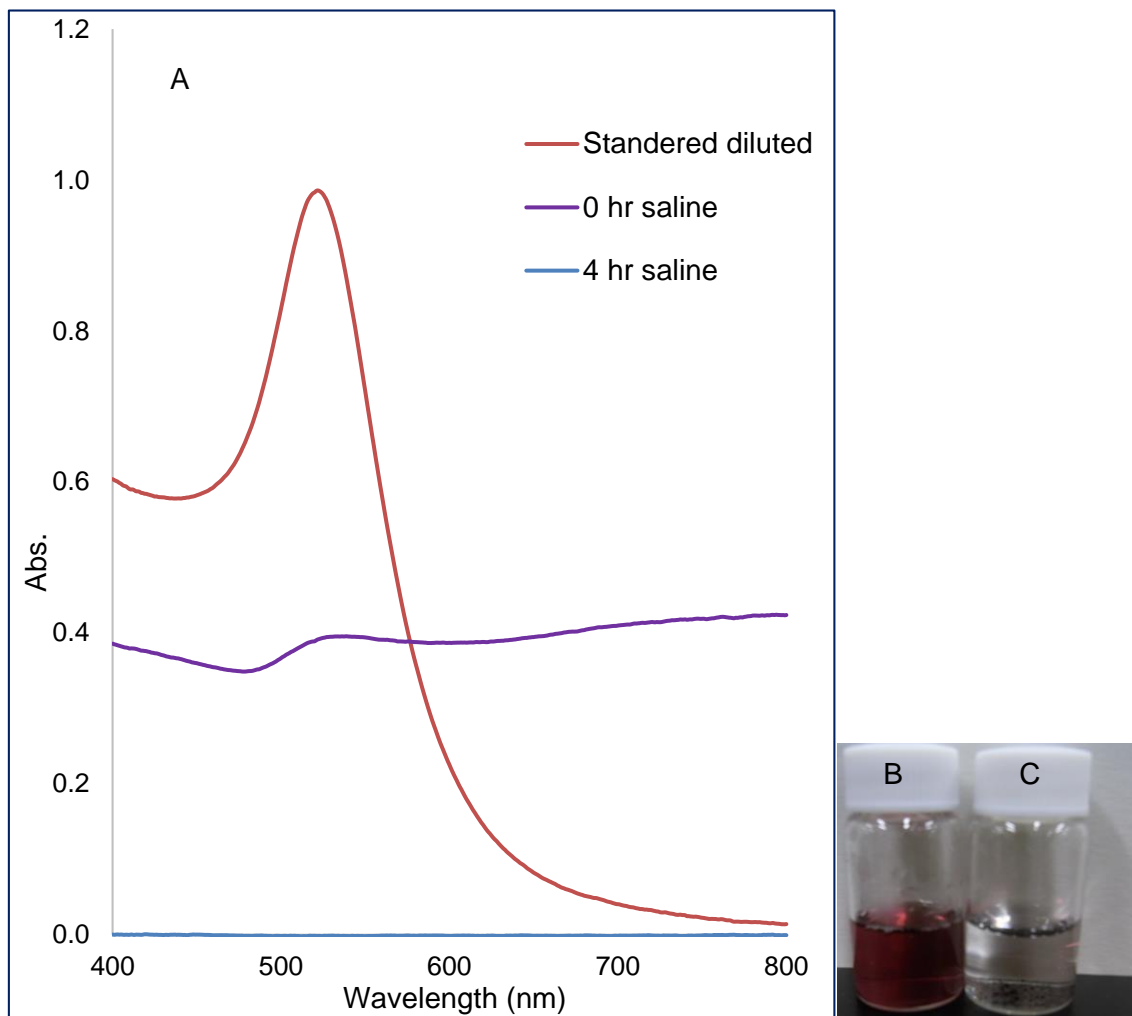


Figure 12. (A) UV-visible spectra of Frens's particles in PBS. (B) Standard diluted Au NP, and (C) Precipitated Au NP in PBS.

2.3.4: Ligand exchange with thiol molecule

Since **1-Au NP** was formed by coordination between the Au NP and aniline's $-\text{NH}_2$ group, it can be modified by the ligand exchange reaction with a thiol that can firmly bind to the Au NP. A given concentrations of thiol **3** (0.050, 0.10, and 0.20 mM) and **1-Au NP** were stirred for 1 h at 50 °C, and the resulting solution was dialysed to remove excess **3**. The absorption spectra of the resulting solutions are shown in Fig. 13. Because the molar absorption coefficient of **3** is much higher than that of **1** (compound **3**: λ_{max} at 246 nm, ϵ $3.4 \times 10^4 \text{ M}^{-1} \text{ cm}^{-1}$, compound **1**: λ_{max} at 260 nm, ϵ $1.2 \times 10^4 \text{ M}^{-1} \text{ cm}^{-1}$), a dose-dependent increase of the characteristic absorption peak of **3** has been clearly observed at λ_{max} of 246 nm (Fig. 14), which suggests that the expected ligand exchange reaction proceeded well.

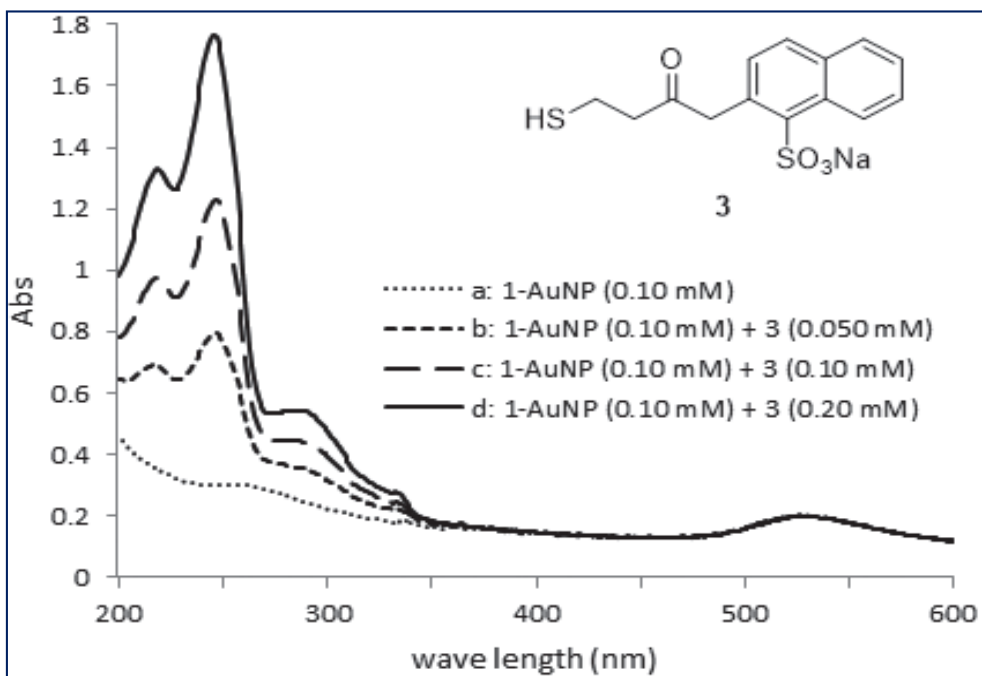


Figure 13. Absorption spectra of the ligand exchange reaction of **1-Au NP** and **3**.

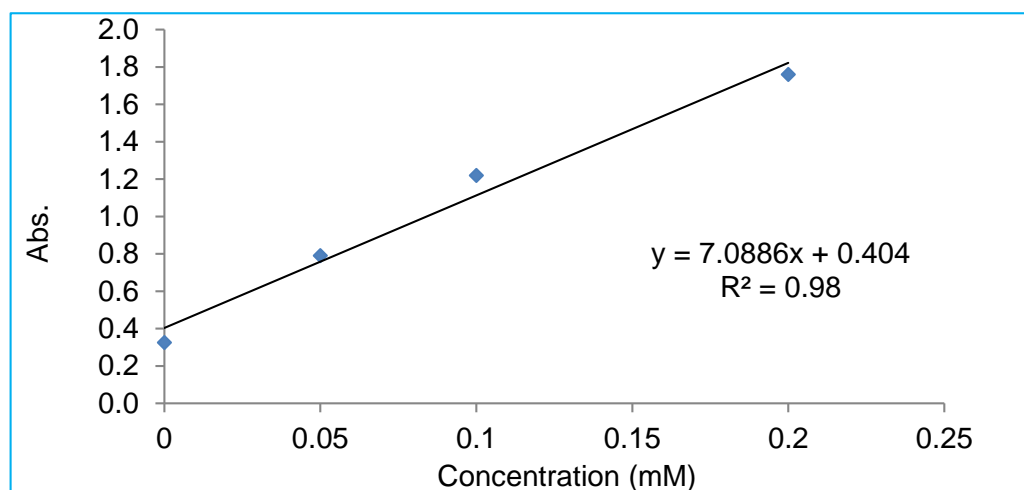


Figure 14. A Dose-dependent increase of characteristic absorption of **3** at 246 nm.

2.4: Conclusion

Highly stable, long-time storable and modifiable gold nanoparticles were obtained by one-pot spontaneous reaction of HAuCl_4 and ω -sulfonylated alkylsulfanylanilines **1** and **2** in boiling water under stirring. The colour of the solution changed from colourless to deep red originated from the surface plasmon resonance of the resulting gold nanoparticles. The rate of particle formation and its size were pH dependent. Different pH values were attempted and pH 8 was found to be the most suitable condition, which gives a highly stable Au NPs. Characterisation of **1-Au NP** has been performed by UV-visible spectroscopy, TEM, ^1H NMR, and FTIR spectra. Stability evaluation of **1-Au NP** under different dispersing media, various pH conditions, and after dryness-redispersion cycle has been evaluated. Modification of the particle's surface was achieved by adding thiol-terminated molecules to the particle solution.

2.5: References

1. R. Shenhar, V. M. Rotello, Nanoparticles: scaffolds and building blocks, *Acc. Chem. Res.*, **36** (2003) 549–561.
2. M. R. Choi, K. J. Stanton-Maxey, J. K. Stanley, C. S. Levin, R. Bardhan, D. Akin, S. Badve, J. Sturgis, J. P. Robinson, R. Bashir, N. J. Halas, S. E. Clare, A cellular trojan horse for delivery of therapeutic, *Nano Lett.*, **7** (2007) 3759–3765.
3. J. M. Bergen, H. A. Von Recum, T. T. Goodman, A. P. Massey, S. H. Pun, S.H. Gold nanoparticles as a versatile platform for optimizing physicochemical parameters for targeted drug delivery, *Macromol. Biosci.*, **6** (2006) 506–516.
4. I. H. El-Sayed, H. Huang, M. A. El-Sayed, Surface plasmon resonance scattering and absorption of anti-EGFR antibody conjugated gold nanoparticles in cancer diagnostics: applications in oral cancer, *Nano Lett.*, **5** (2005) 829–834.
5. W. Eck, G. Craig, A. Sigdel, G. Ritter, L. J. Old, L. Tang, M. F. Brennan, P. J. Allen, M. D. Mason, PEGylated gold nanoparticles conjugated to monoclonal F19 antibodies as targeted labeling agents for human pancreatic carcinoma tissue, *ACS Nano.*, **2** (2008) 2263–2272.
6. N. L. Rosi, C. A. Mirkin, Nanostructures in biodiagnostics, *Chem. Rev.*, **105** (2005) 1547–1562.

-
7. F. Sonvico, C. Dubernet, P. Colombo, P. Couvreur, Metallic colloid nanotechnology, applications in diagnosis and therapeutics, *Curr. Pharm. Des.*, **11** (2005) 2095–2105.
 8. S. Li, L. Xu, W. Ma, X. Wu, M. Sun, H. Kuang, L. Wang, N. A. Kotov, C. Xu, Dual-mode ultrasensitive quantification of microRNA in living cells by chiroplasmonic nanopyramids self-assembled from gold and upconversion nanoparticles, *J. Am. Chem. Soc.*, **138** (2016) 306–312.
 9. H. He, C. Xie, J. Ren, Nonbleaching fluorescence of gold nanoparticles and its applications in cancer cell Imaging, *Anal. Chem.*, **80** (2008) 5951–5957.
 10. R. Popovtzer, A. Agrawal, N. A. Kotov, A. Popovtzer, J. balter, T. E. Carey, R. Kopelman, Targeted gold nanoparticles enable molecular CT imaging of cancer, *Nano Lett.*, **8** (2008) 4593–4596.
 11. P. Sharma, S. C. Brown, N. Bengtsson, Q. Zhang, G. A. Walter, S. R. Grobmyer, S. Santra, H. Jiang, E. W. Scott, B. M. Moudgil, Gold-speckled multimodal nanoparticles for noninvasive bioimaging, *Chem. Mater.*, **20** (2008) 6087–6094.
 12. A. Shinoharaand, H. Shinmori, Controlled generation of singlet oxygen by porphyrin-appended gold nanoparticles, *Bull. Chem. Soc. Jp.*, **89** (2016) 1341–1343.
 13. G. Frens, Controlled nucleation for the regulation of the particle size in monodisperse gold suspensions, *Nature Phys. Sci.*, **241** (1973) 20–22.

-
14. P. K. Vemula, U. Aslam, V. A. Mallia, G. John, In situ synthesis of gold nanoparticles using molecular gels and liquid crystals from vitamin-C amphiphiles, *Chem. Mater.*, **19** (2007) 138–140.
15. X. Ji, X. Song, J. Li, Y. Bai, W. Yang, X. Peng, Size control of gold nanocrystals in citrate reduction: The third role of citrate, *J. Am. Chem. Soc.*, **129** (2007) 13939–13948.
16. D. V. Goia, E. Matijevic, Tailoring the particle size of monodispersed colloidal gold, *Colloids Surf. A*, **146** (1999) 139–152.
17. L. Pei, K. Mori, M. Adachi, Formation process of two-dimensional networked gold nanowires by citrate reduction of AuCl₄⁻ and the shape stabilization, *Langmuir*, **20** (2004) 7837–7843.
18. Y. Y. Yu, S. S. Chang, C. L. Lee, C. R. Wang, Gold Nanorods: Electrochemical Synthesis and Optical Properties, *J. phy. Chem. B*, **101** (1997) 6661–6664.
19. U. Krebig, M. Vollmer, Optical Properties of Metal Clusters, Springer series in Material Science 25, springer, Berlin, 1995.
20. J. A. Peck, C. D. Tait, B. I. Swanson, G. E. Brown, Speciation of aqueous gold(III) chlorides from ultraviolet/visible absorption and Raman/resonance Raman spectroscopies, *Jr. Geochem. Cosmochem.*, **55** (1991) 671–676.
21. R. H. Garrett, C. M. Grisham, Biochemistry, Saunders College publishing, Fort Worth, 1995.
22. T. Zhu, K. Vasilev, M. Kreiter, S. Mittler, W. Knoll, Surface

Modification of Citrate-Reduced Colloidal Gold Nanoparticles with 2-Mercaptosuccinic Acid, *Langmuir*, **19** (2003) 9518–9525.

23. J. J. Elliott, S. F. Mason, The heats and entropies of ionisation of some aromatic and N-heteroaromatic amines, *J. Chem. Soc.*, (1959) 2352–2359.

24. M. Zhou, B. X. Wang, Z. Rozynek, Z. H. Xie, J. O. Fossum, X. F. Yu, S. Raaen, Minute synthesis of extremely stable gold nanoparticles, *Nanotechnology*, **20** (2009) 505606–505616.

25. F. Schulz, T. Homolka, N. G. Bastus, V. Puentes, H. Weller, T. Vossmeier, Little adjustments significantly improve the Turkevich synthesis of gold nanoparticles, *Langmuir*, **30** (2014) 10779–10784.

26. B. C. Mei, E. Oh, K. Susumu, D. Farrell, T. J. Mountziaris, H. Mattoussi, Effects of ligand coordination number and surface curvature on the stability of gold nanoparticles in aqueous solutions, *Langmuir*, **25** (2009) 10604–10611.

27. I. Capek, Dispersions based on noble metal nanoparticles-DNA conjugates, *Adv. Colloid Interface Sci.*, **163** (2011) 123–143.

Chapter 3

Biomedical application of gold nanoparticles for anti-cancer drug delivery by conjugation with Paclitaxel through DNA-oligonucleotides linker

3.1: Introduction

Cancer is considered one of the prominent causes of all deaths globally. The term 'cancer' refers to unlimited abnormal growths and multiplications of the cells causing pressure and impairment to the surrounding normal tissues, due to the strain on the nutrient support to the healthy tissues.¹

The current methods for cancer treatment principally include surgical intervention, radiation and utilisation of chemotherapeutic drugs, including paclitaxel, that destroy not only the cancer cells but also the normal cells and have limited effectiveness due to low aqueous solubility and chemoresistance, which may be developed by the cancer cells.¹

Therefore, an anti-cancer drug delivery system (DDS) is a hopeful and promising method for efficient and safe treatment against oncological

diseases. Through the drug delivery vehicle, the drug will be directed and targeted only to the cancerous cells, thus minimising the toxicity caused by the conventional therapy towards the normal cells. As well as enhancing the pharmacological aspects of the antineoplastic drugs, such as water solubility, stability and effectivity.² DDS enables many of the biologically active compounds, including macromolecular drugs, to be efficiently introduced intracellularly to express their therapeutic effect inside the cells. The size of nanoparticles is very small (1–100 nm) compared with large biomolecules such as antibodies, enzymes, and cell receptors. Therefore, it gives a chance for the nanoparticles to integrate with biomolecules either on the cell surface or inside the cell, which, in turn, causes a revolution in nanomedicine.

Recently, the applications of oligonucleotides loaded-Au NPs (DNA-Au NPs) in biology and medicine have received much attention.³ The bio-conjugate of DNA-Au NPs composed of Au NPs in the centre, and covalently loaded DNA-oligonucleotides on the surface of Au NPs.^{4,5} The unique characteristics of DNA-Au NPs make it a highly promising candidates for therapeutic and biomedical uses.^{6–11} These peculiarities

involve the uptake of DNA-Au NPs by different cell types after addition directly to the cell culture media and are subsequently up-taken by the cells in high numbers without the need for transfection reagents.^{12,13} The stability and biocompatibility of Au NPs before and after loading of the biomolecules make it highly applicable in a drug delivery system and as diagnostics at the molecular level.^{13,14} Moreover, Au NPs are chemically inert with reliable surface biofunctionalisation by a variety of biomolecules.^{15,16} Furthermore, Au NPs have been found to be less or non-toxic compared to other inorganic nanoparticles.¹⁷ The DDS includes drug targeting of difficult, unstable molecules (proteins, siRNA, DNA), delivery to the difficult sites (brain, retina, tumours, intracellular organelles) and drugs with serious side effects (e.g. anti-cancer agents). Another critical feature of DNA-Au NPs is resistance to enzymatic degradation as DNase.¹⁸ This resistance is attributed to the steric inhibition of enzymatic cleavage owing to the dense packing of DNA on the nanoparticle surface, thereby hindering the enzymatic attack. Another hypothesis is that the high concentration of Na⁺ ions together with densely loaded DNA hinders the enzymatic activity of DNase.^{19,20} This

withstanding ability of DNA-Au NPs against nuclease degradation is of great importance for entrance of nucleic acids into the cells, protecting oligonucleotides from enzymatic degradation.

3.2: Materials and Methods

3.2.1: Synthesis of anticancer-Au NPs bioconjugate using DNA oligonucleotides as a linker (nano bio-conjugate)

3.2.1.1: Preparation of succinyltaxol (ST)

Succinic anhydride (0.75 mmol) was added to a paclitaxel solution (0.049 mmol in 1mL pyridine) and the reaction was carried out at room temperature for 3 h under magnetic stirring. Then the reaction mixture was evaporated and the resulting residues were stirred in 1.6 mL water for 20 min, and then filtered. The precipitate was dissolved in acetone (2 mL), water was slowly added (total 2 mL) and the final crystals (ST) were collected. The product was characterised by liquid chromatography mass spectrometry (LCMS).

3.2.1.2: Preparation of succinyltaxol-DNA (thymine oligonucleotides, 5' NH₂-TTTTT-SH-3')

ST was reacted with 1-ethyl-3-[3-dimethylaminopropyl] carbodiimide (EDC) and *N*-hydroxysuccinimide (NHS) in HEPES buffer for 15 min under gentle stirring at room temperature as an activator, and then DNA

oligonucleotides were added to the solution. The reaction mixture was shaken gently at room temperature for 3 days. Table 1 shows the different concentrations and solvents used for every biomolecule. The ST-DNA oligonucleotides conjugate was characterised by LCMS.

Table 1. The different reactants used for preparation of succinyl taxol-DNA oligonucleotides.

The reactant	Amount (nmol)	Final concentration (mM)
Succinyltaxol	30.0 nmol/ 48.5 μ L (acetonitrile)	0.176 mM
EDC/NHS	300 nmol/ 120 μ L (HEPES buffer, 0.1 M, pH 7)	1.76 mM
DNA oligonucleotides (5'- NH ₂ -TTTTT-SH-3')	15 nmol/ 1.5 μ L (TE buffer)	0.088 mM

3.2.1.3: Preparation of ST-DNA-Au NPs (nano bio-conjugate)

The nano bio-conjugates were prepared as follows: ST-DNA (0.176 mM, 20.0 μ L) was added to ω -sulfonylated alkylsulfanylaniline Au NPs (**1-Au NP**) (see chapter 2) (0.500 mL) after its purification by centrifugation to remove excess reductive stabilisers. The reaction was carried out at room temperature under gentle shaking for 20 h. Then sodium dodecyl sulfate (10.0% SDS, 1.00 μ L) was added to reach the final concentration of 0.010% and the reaction mixture was incubated at room temperature for 30 min. NaCl was added gradually using 1.0 M NaCl to reach the final concentration of 0.70 M and, after this salting process, the reaction mixture was incubated overnight at room temperature under gentle shaking. The final nano bio-conjugate was centrifuged at 18000 rpm for 15 min to remove excess, unbound ST-DNA until there was no DNA detected by UV- visible spectroscopy in the supernatant. The nano bio-conjugate was stored at 4 °C in a solution state.

3.2.2: Cancerous cell line bioassay

The cancer cells were incubated in a 96-well tissue culture plate for 48 h before the assay in a density of 3.2×10^4 cells/well. Cell density was

calculated using a haemocytometer and it was carried out before the experiments. During the experimental work, the cells were kept in ice at 4 °C. Dulbecco's Modified Eagle's Medium (DMEM) supplemented with 10% foetal bovine serum, l-glutamine and sodium bicarbonate, was used for growth of the cells. Cells were cultured at 37 °C in a humidified atmosphere containing 5% CO₂ in air for 48 h to form cell sheets. The cancerous cells were divided into 4 groups as follows:

- a. Control group, the cancerous cells were treated with sterile distilled water (SDW) as a control.
- b. The SK-BR3 cells were treated with anti-cancer drug (paclitaxel only).
- c. The SK-BR3 cells were treated with modified anti-cancer drug (succinyl taxol, ST).
- d. The SK-BR3 cells were treated with Au NPs conjugated with the anticancer drug for drug delivery (nano bio-conjugate, ST-DNA-Au NPs).

The following steps were then performed:

1. The SK-BR3 cells were seeded in six wells for each group and incubated with different agents regarding the previous groups for 48 h. The estimation of the cell viability of each group was carried out in comparison with the

control group.

2. At the end of each exposure, the evaluation of cell viability % was assessed by 3-(4,5-dimethylazol-2-yl)-2,5-diphenyl-tetrazolium bromide (MTT) assay (10 µL) for 4 h. The MTT assay helps in cell-viability assessment by measuring the enzymatic reduction of yellow tetrazolium MTT to a purple formazan product. The formazan was dissolved by formazan solubilising solution 100 µl in each well and incubation for 4 h until the crystal dissolved completely, following the manufacture's protocol. The absorbance was measured at 570 nm using UV–vis micro plate reader.²¹⁻²²

3. All experiments were performed in sex replicate, and the average of all of the experiments has been shown as cell-viability percentage in comparison with the control experiment, which was considered as 100% viable. The same steps previously identified were carried out for the neuro 2a brain cancer cells.

Statistical analysis

Statistical analysis was done using Student's *t* test with $p \leq 0.05$ was considered as significantly different. The results were expressed in the format of mean \pm SD with $*p \leq 0.05$, $**p \leq 0.04\sim 0.009$, and $***p \leq 0.008$ or less.

3.2.3: Liquid chromatograph mass spectrometry (LCMS) measuring conditions

LCMS analysis was performed using a Polymer-based reverse-phase chromatography column (ODP column (2.0 mm x 150 mm)). The gradient solvent was (A: 0.01M TEAA/H₂O (pH 6.0), B: acetonitrile (100%), gradient 0 \rightarrow 7 min, and %B 2% \rightarrow 100%). The flow rate was 200 μ L /min and the column temperature was 50 °C. The wave length was 250 nm.

3.3: Results and discussion

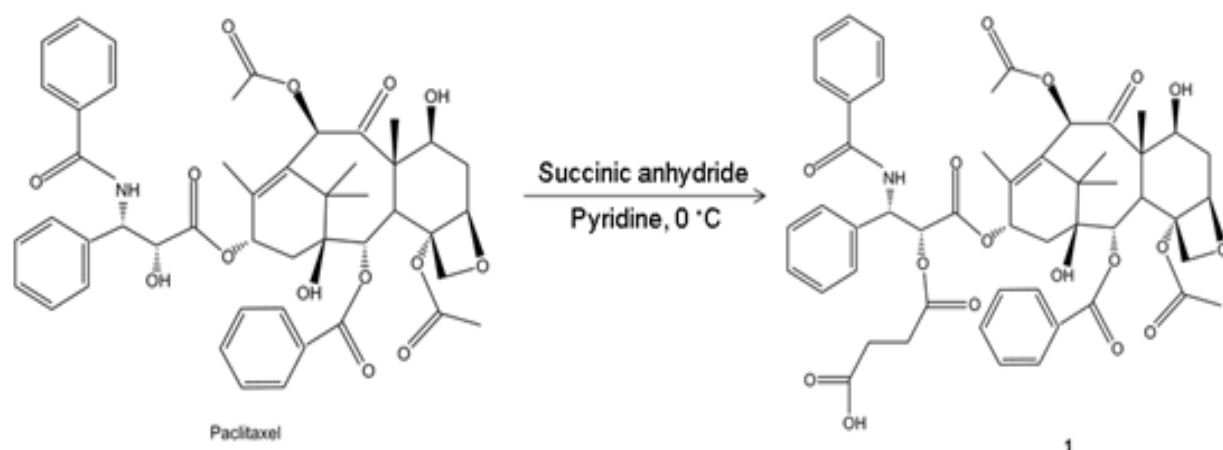
3.3.1: Synthesis of anticancer-oligonucleotide Au NPs bioconjugate (nano-bioconjugate)

As shown in scheme 1, Paclitaxel was modified by succinic anhydride to give ST terminated with carboxylic group. The successful formation of succinyltaxol was confirmed by LCMS (Fig. 1); where the signals from succinic acid and paclitaxel disappeared and a new signal appeared at a retention time of 26 min, which is attributed to the formation of ST (**1**). Fig. 2 displays the mass spectrometry results, which confirmed the formation of succinyltaxol (calcd 953.97, found 954.2).

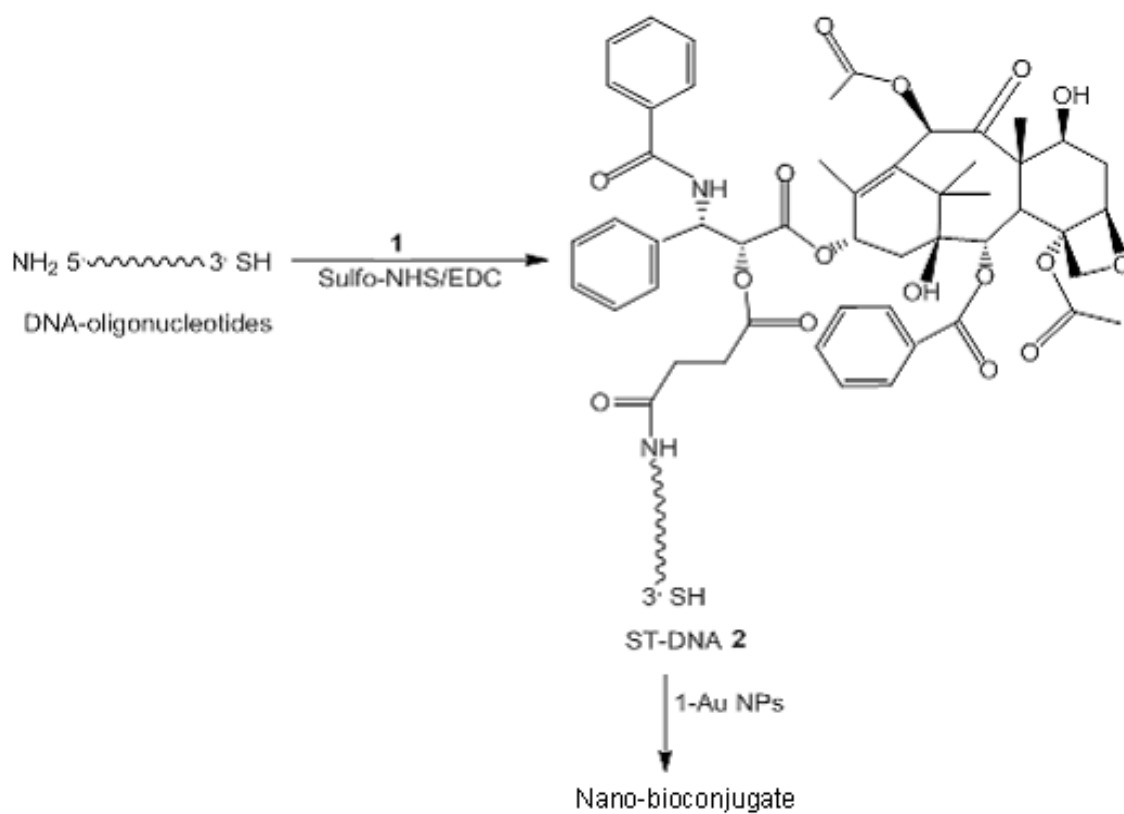
As shown in scheme 2, the DNA oligonucleotides (5'-NH₂-TTTTT-SH-3') terminated with amino group at 5' terminal and ST terminated with carboxylic group were coupled together via amide linkage using sulfo-NHS/EDC coupling chemistry as an activator. This reaction gives an unstable ester bond (active ester) by reaction with carboxyl terminal of succinylaxol. Then this active ester reacts with amino terminated DNA forming amide bond to give ST-DNA (**2**). ST-DNA was

characterised by LCMS, where the signals coming from ST and oligonucleotides depleted with the appearance of a new signal at a retention time of 27 min, which was attributed to ST-DNA (Fig. 3). In Fig. 4, mass spectrometry indicated the formation of ST-DNA (calcd trimer 940.78, found 941.7). Then ST-DNA reacted with **1-Au NP**, where thiolated DNA substituted the NH₂-terminal of the reductive stabiliser of **1-Au NP**. The SH group strongly coordinates on the nanoparticle surfaces more than on NH₂ through the ligand exchange reaction with thiol-terminated molecules,¹⁶ yielding the nano bio-conjugate. The product was purified by centrifugation (18000 rpm, 15 min) to remove excess, free ST-DNA. The product was characterised by UV-visible spectroscopy through the characteristic absorbance peak of DNA oligonucleotides at 260 nm (Fig. 5). It is noteworthy that, the SPR of Au NPs remained almost unchanged after loading of the bio conjugate, which indicates no aggregation of the particles has occurred. The use of surfactant molecules as SDS is essential before loading of DNA on the surface of Au NPs. These molecules hinder the possibility of Au NPs to aggregate and prevent their close contact, as well as maintain their stability, especially at high salt concentrations.⁴ The

DNA loading on the surface of Au NPs was enhanced by the salting process; higher salt concentration in between 0.7 to 1.0 M as a final concentration resulted in higher DNA loading on Au NPs surfaces. This is attributed to the inhibition of the repulsive forces between DNA strands by the salting process,^{4, 23} and thereby, large amount of DNA oligonucleotides will be adsorbed on the Au NPs surface.



Scheme1. Preparation of succinyltaxol (**1**).



Scheme 2. Preparation of ST-DNA (2) and nano bioconjugate.

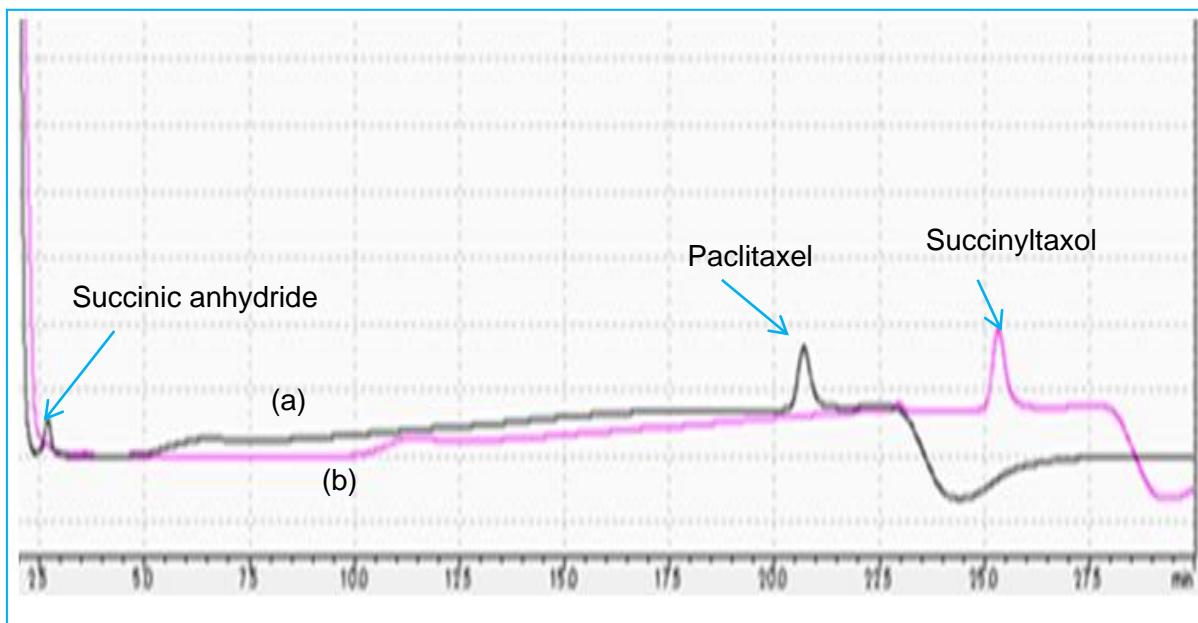


Figure 1. Chromatograph of paclitaxel and succinic anhydride (a) 0 min after the reaction and (b) 3 h after the reaction, ST formation.

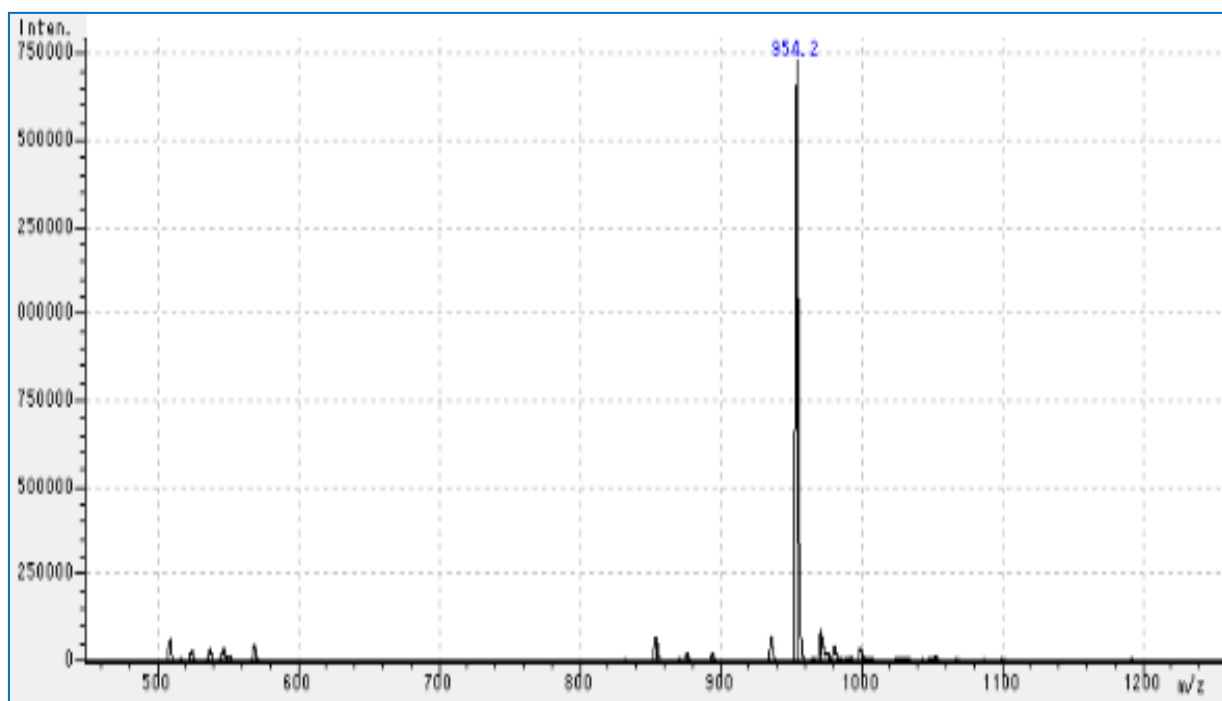


Figure 2. Mass spectrometry results confirmed the formation of ST.

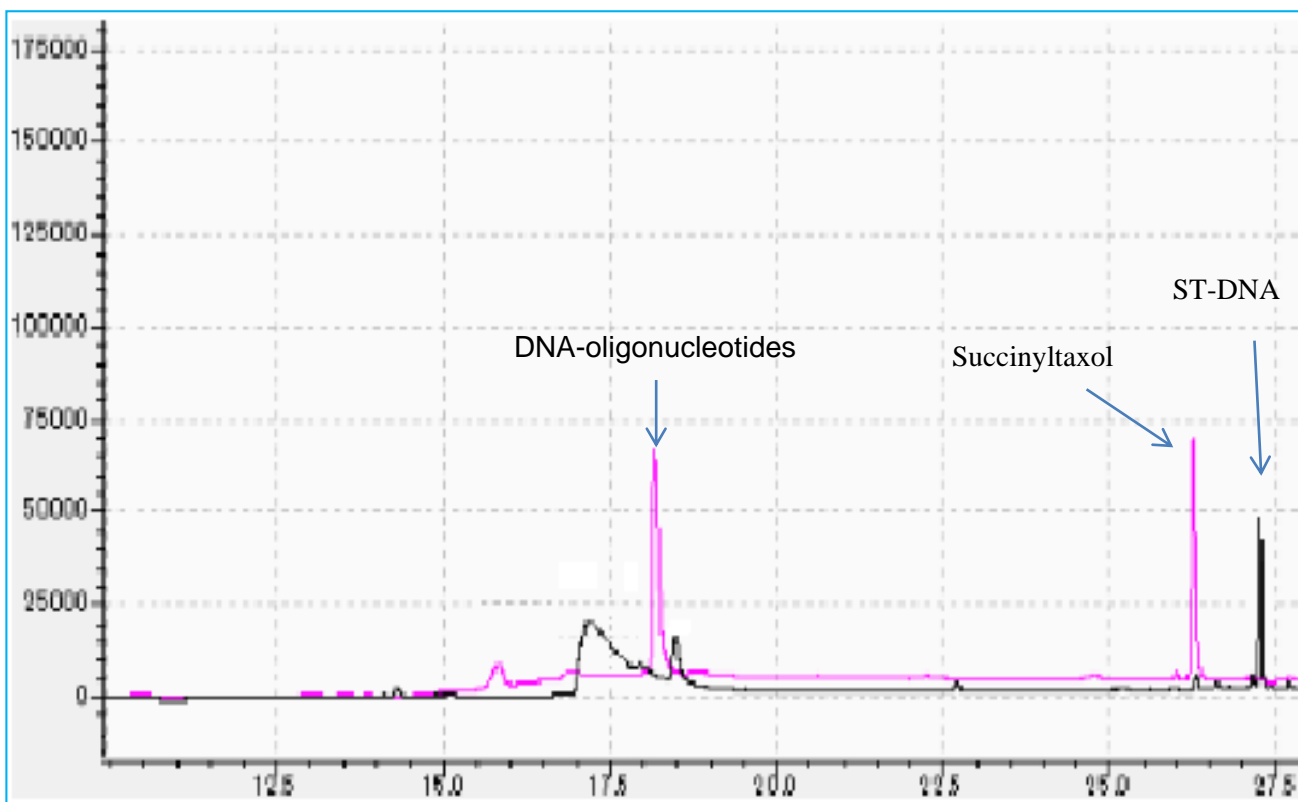


Figure 3. Chromatograph of ST-DNA formation, the peak of ST-DNA appeared with retention time of 27.25 min (black color) together with the disappearance of the peaks (red color) from ST and DNA oligonucleotides.

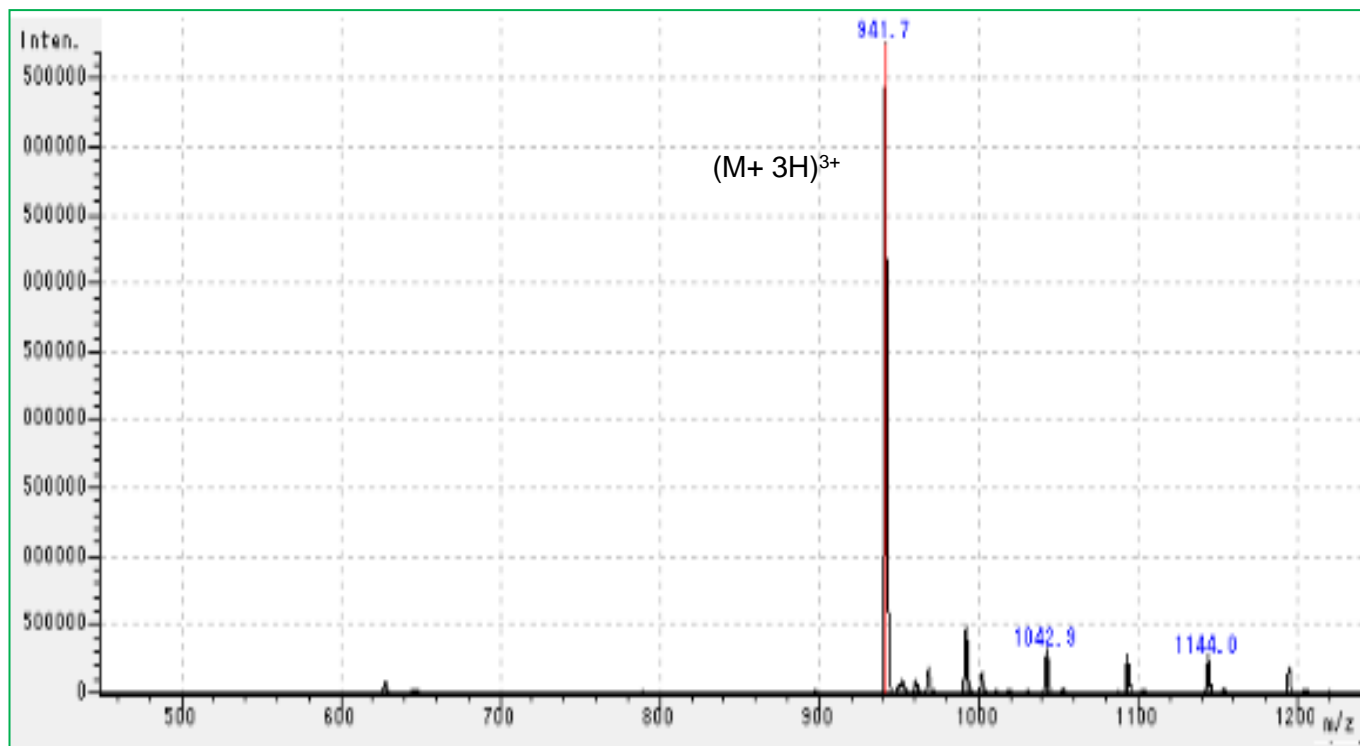


Figure 4. Mass spectrometry of ST-DNA.

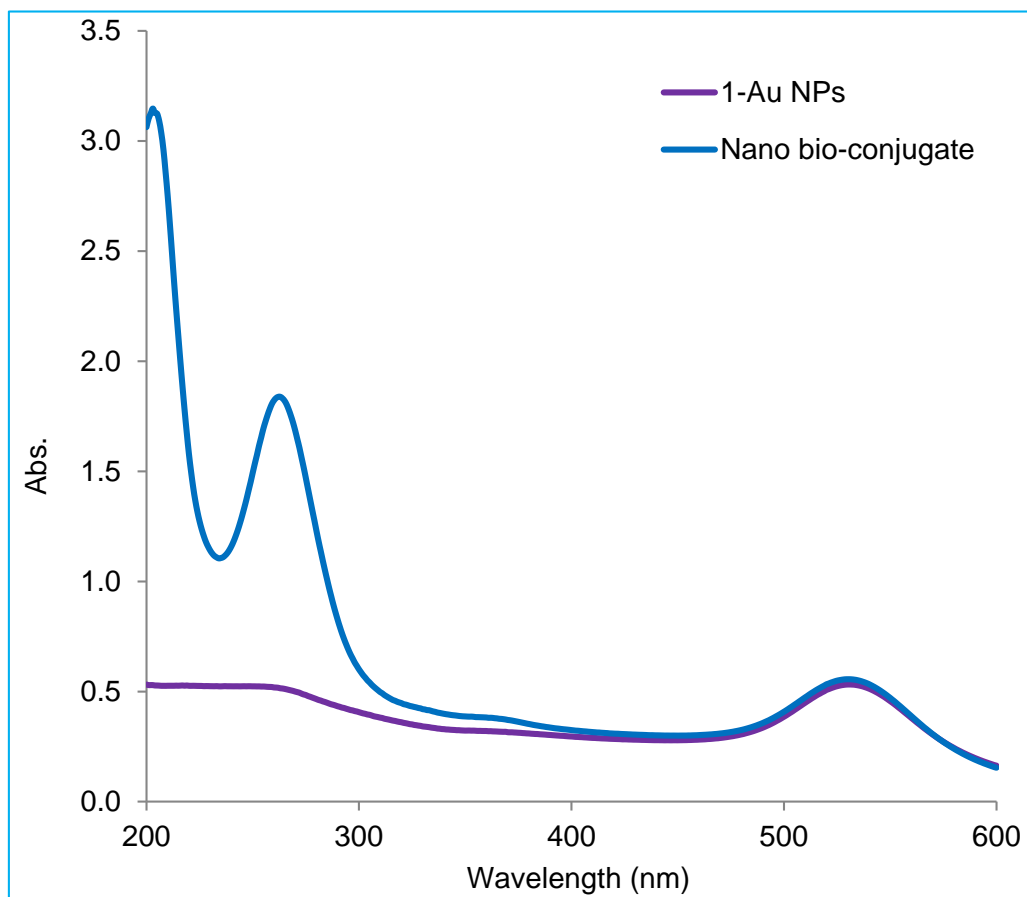


Figure 5. Absorption spectra of ligand exchange reaction of **1-Au NPs** and nano bio-conjugate, displaying the strong absorbance peak of oligonucleotides at 260 nm.

3.3.2: Cytotoxicity evaluation

The efficacy of the nano bio-conjugate over the free drugs was evaluated. The cytotoxic effect of the nano bio-conjugate was tested against cancer cells of various origins and the activity was compared with that of the free drugs. The adenocarcinoma breast cancer cell, SK-BR3 was cultured with Paclitaxel, ST, and nano bio-conjugate at various concentrations ($5, 50, 500, 5000 \times 10^{-9}$ M based on paclitaxel concentration). The absorbance was measured at 570 nm for different reagents using UV-vis micro plate reader. After a 48 h treatment with different concentrations of paclitaxel, ST and nano bio-conjugate under the same experimental conditions, the anticancer activity of paclitaxel against SK-BR3 cancer cells was more enhanced than that of the free drugs when conjugated on the surface of Au NPs through DNA linker as shown in Fig. 6. This was ascertained by decreasing the viability of the SK-BR3 cells significantly to $12 \pm 4.2\%$ in case of nano bio-conjugate at 5000×10^{-9} M comparing to $23 \pm 5.9\%$, and $26 \pm 6.5\%$ in the case of free paclitaxel, and ST respectively at the same concentration.

In the case of brain cancer cells, neuro 2a, the absorbance was measured at 570 nm for different reagents using a UV-vis micro plate reader. The anticancer activity of free paclitaxel is insignificant at its various concentrations compared with the control experiments except at 5000×10^{-9} M whereas the cell viability significantly decreased to $61 \pm 12\%$. A similar trend was found with ST but the cell viability significantly decreased to $59 \pm 13\%$ at $\times 10^{-9}$ M. On the other side, the nano bio-conjugate displayed a significant anticancer activity at concentrations of 500 and 5000×10^{-9} M where the cell viability significantly decreased to $54 \pm 10\%$ and $38 \pm 7.4\%$, respectively (Fig. 7). The IC_{50} values of the free paclitaxel, ST and the nano bio-conjugate were shown in Table 2 for both of the SK-BR3 and neuro 2a. Paclitaxel is acting by stabilising and polymerization of tubulin through binding to N-terminal of β -tubulin, disrupting the cell division, and thus causing cell death.²⁴⁻²⁵

These findings magnify the importance of using Au NPs-mediated drug delivery of paclitaxel to fight the cancer cells. The use of DNA-Au NPs for drug delivery is due to the ability of DNA-Au NPs to enter the cells efficiently, compared to other types of Au NPs without other

reagents.²⁶ For example, HeLa cells uptake few thousands of citrate-stabilized Au NPs,²⁷ compared to more than 1 million of DNA-Au NPs under almost the same experimental conditions.¹² The cellular internalisation of DNA-Au NPs was 3 folds higher than that of PEG functionalised Au NPs.¹² The uptake of Au NPs by cancer cells could be done by either a passive or active strategy or a combination of both strategies for tumour- targeting drug delivery. The passive strategy depends on the enhanced permeability and retention effect (EPR),²⁸⁻³⁰ In this strategy, due to the leaky, defective and irregular vasculatures of the tumour cells, the cell membrane permeability for Au NPs is enhanced which, in turn, allows for the entrance and accumulation of Au NPs inside the cancer cells (extravasation). Moreover, Au NPs is retained inside the cells due to impaired lymphatic drainage of the tumour cells. Principally, this attributed to defective vascular formation owing to the higher growth rate and the collapse of blood and lymph vessels of the tumour tissues. The active strategy (cell surface receptor-mediated endocytosis) depends on the biofunctionalisation of the surface of Au NPs with biomolecules such as aptamers (DNA oligonucleotides),³¹ peptides,³² polysaccharides,³³

antibodies,³⁴ and vitamins.³⁵ These biomolecules have a high affinity and engage to the receptors on the surface of the tumour cells. DNA-Au NPs have been successively taken up by more than 40 various cell lines involving neuron cells and primary cells after direct addition of DNA-Au NPs to the cell culture medium.²⁶ This is attributed to the dense loading of DNA oligonucleotides on the surface of Au NPs, which resulted in adsorption of a large amount of the extracellular protein on the particles surfaces which, in turn, enhances recognition and endocytosis.³⁶ The acidic pH inside the cancerous cells especially in endosomes (pH 5.5–6) and lysosomes (pH 4.5–5.0)³⁷ caused the release of the drug from the nanoparticles surface.^{38–40} Besides pH, the intracellular glutathione (GSH) plays a role in drug release as a reducing agent for thiol linkage due to the higher intracellular GSH (thiol-containing peptides) concentration and thereby, passive drug release.^{40,41}

Our results are in agreement with a study performed by Lippard and co-workers, where they used cisplatin tethered to DNA-Au NPs with amino terminal.⁴² They found that this nano conjugate exerted a significant improvement in cytotoxicity of cisplatin against neoplastic cells more than

free cisplatin. Their results were indicative of the crucial role of DNA-Au NPs in the drug delivery system where the efficiency of the antineoplastic agent was much improved than the free one.

In multiple drug resistance (MDR), P-glycoprotein (Pgp) is overexpressed on the cell surface of the cancer cells, which causes efflux of the drugs from the cells. Au NPs could minimise the chemoresistance of many antitumor drugs including paclitaxel by enhancing the internalisation of the drug, protecting the drugs from P-glycoprotein recognition^{43, 44} and thereby hindering its efflux from the cells caused by P-glycoprotein.⁴⁵ Therefore, the anti-cancer activity of paclitaxel was enhanced in the case of nano bio-conjugate. Consequently, this approach provides a biomolecules-inorganic hybrid complex, which is a possible strategy for curing of the neoplastic diseases such as breast adenocarcinoma and brain cancer. These results suggest that Paclitaxel-loaded Au NPs could minimise the effective dose of paclitaxel given to the patients during treatment of breast and brain neoplasms.

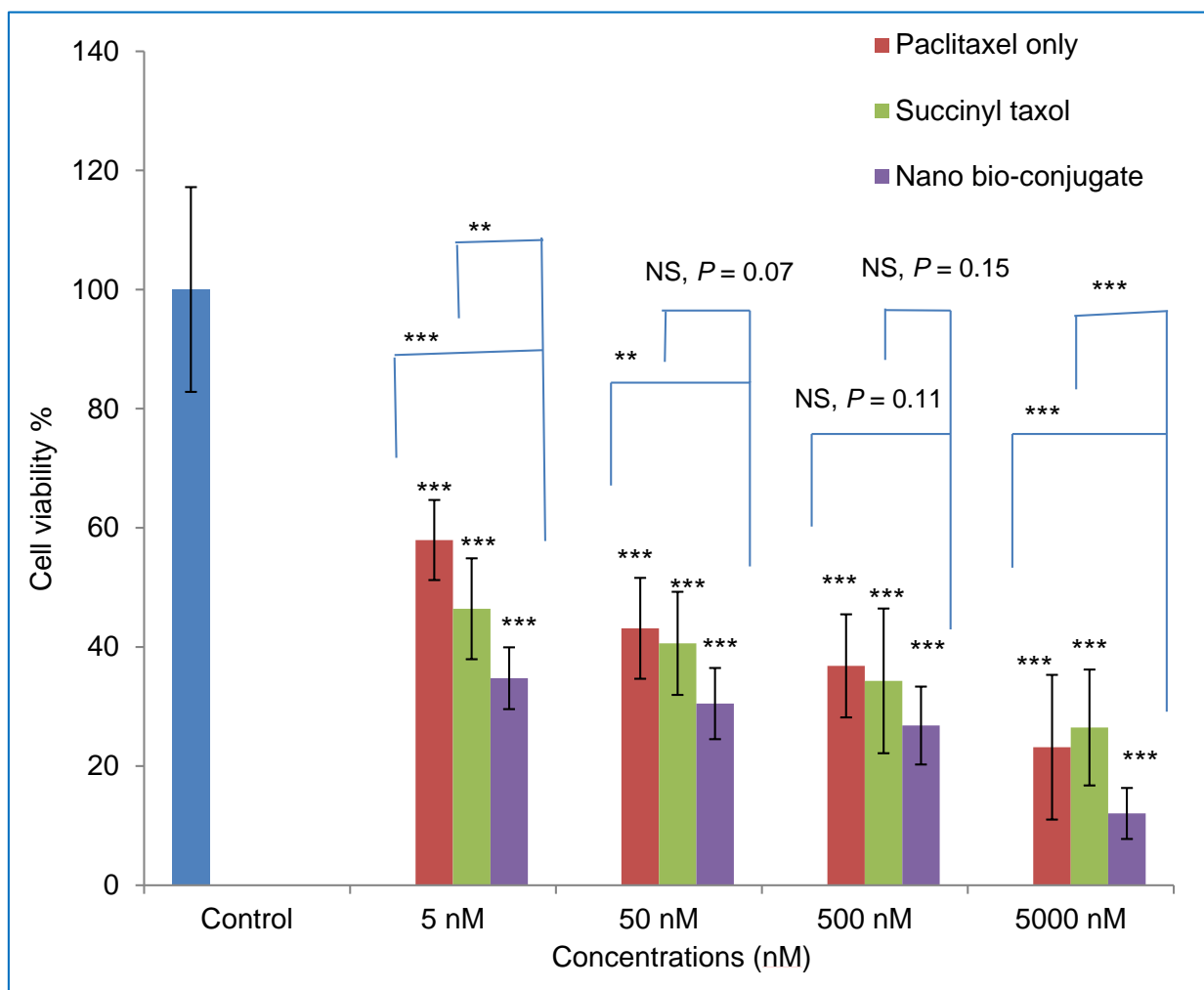


Figure 6. Cytotoxicity profiles of paclitaxel, ST and nanoconjugate against SK-BR3, breast cancer cells (n = 6). Cytotoxicity was evaluated by MTT assay. * $p \leq 0.05$, ** $p \leq 0.04\sim 0.009$, and *** $p \leq 0.008$ or less.

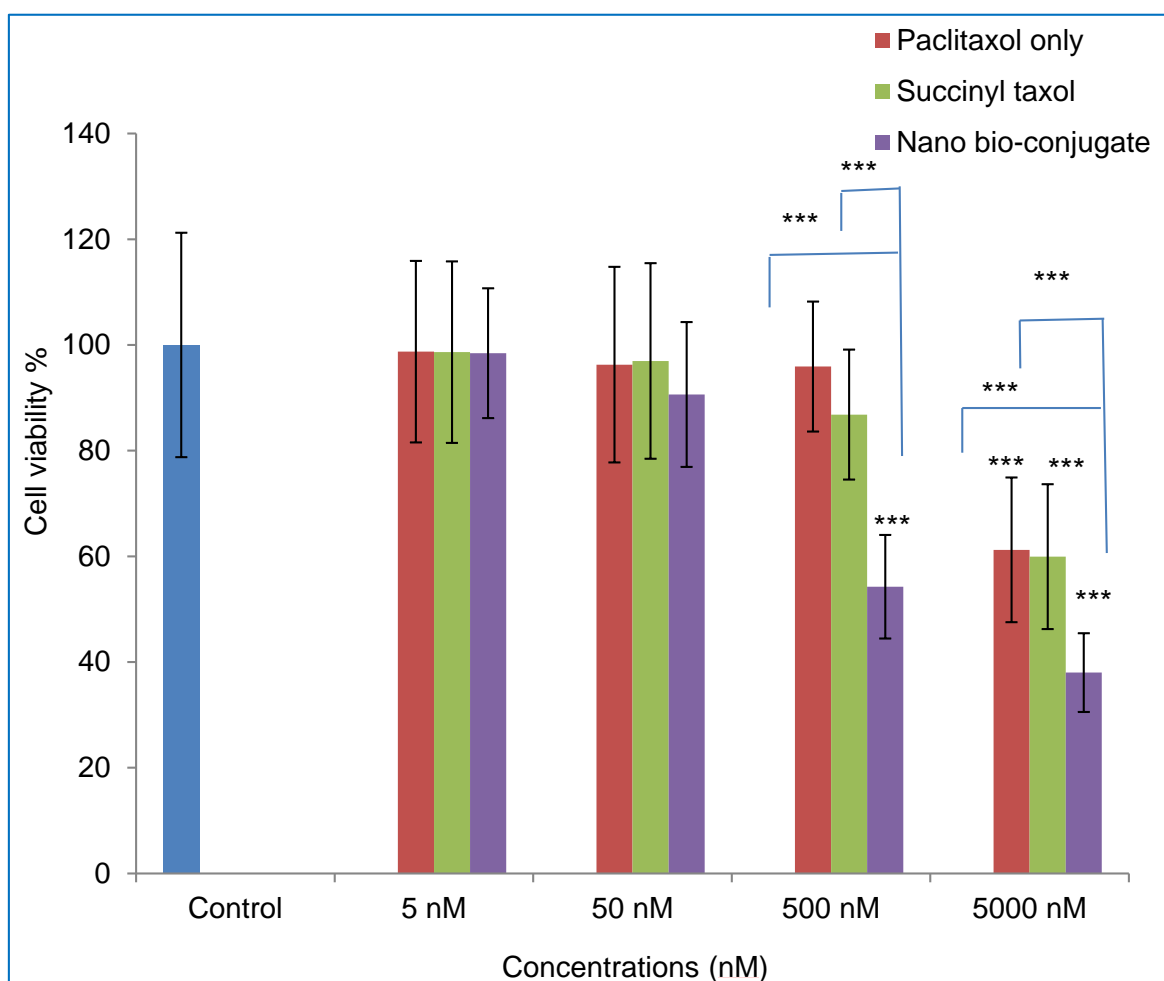


Figure 7. Cytotoxicity profiles of free paclitaxel, ST, and nanoconjugate against neuro 2a, brain cancer cells (n = 6). Cytotoxicity was evaluated by MTT assay. * $P \leq 0.05$, ** $p \leq 0.04 \sim 0.009$, and *** $p \leq 0.008$ or less.

Table 2. Displaying IC_{50} of nano-bioconjugate, Paclitaxel, and succinylaxol.

Entry	Cancer cells	Nano bio-conjugae	Paclitaxel	Succinyltaxol
1	SK-BR3	<0.005 μ M	0.028 μ M	< 0.005 μ M
2	Neuro2a	1.750 μ M	>5 μ M	>5 μ M

3.4: Conclusion

In this study, we synthesised and characterised a novel paclitaxel-DNA-Au NPs bio-conjugate for targeted drug delivery of paclitaxel. The drug-loaded NPs have significant anti-cancer effects against SK-BR3 breast cancer cells and neuro 2a brain tumour cells, which resulted in higher cancer cell cytotoxicity suggesting enhanced cellular uptake in comparison with the free drug. Our results imply that the paclitaxel-DNA-Au NPs bio-conjugate could have high potentials to be used for targeted chemotherapy for treating neoplastic diseases.

3.5: References

1. R. Panchagnula, Pharmaceutical aspects of Paclitaxel, *Int. J. Pharm.*, **172** (1998) 1–15.
2. J. R. Heath, M. E. Davis, Nanotechnology and Cancer, *Annu Rev Med.*, **59** (2008) 251–265.
3. C. A. Mirkin, R. L. Letsinger, R. C. Mucic, J. J. Storhoff, A DNA-based method for rationally assembling nanoparticles into macroscopic materials, *Nature*, **382** (1996) 607–609.
4. S. J. Hurst, A. K. R. Lytton-Jean, C. A. Mirkin, Maximizing DNA Loading on a Range of Gold Nanoparticle Sizes, *Anal. Chem.*, **78** (2006) 8313–8318.
5. J-S. Lee, D. S. Seferos, D. A. Giljohann, C. A. Mirkin, Thermodynamically controlled separation of polyvalent 2-nm gold nanoparticle-oligonucleotide conjugates, *J. Am. Chem. Soc.*, **130** (2008) 5430–5431.
6. R. Elghanian, J. J. Storhoff, R. C. Mucic, R. L. Letsinger, C. A. Mirkin, Selective colorimetric detection of polynucleotides based on the distance-dependent optical properties of gold nanoparticles, *Science*, **277** (1997) 1078–1081.

-
7. J. Liu, Y. Lu, A colorimetric Lead Biosensor Using DNAzyme-Directed Assembly of Gold nanoparticles, *J. Am. Chem. Soc.*, **125** (2003) 6642–6643.
 8. C. D. Medley, J. E. Smith, Z. Tang, Y. Wu, S. Bamrungsap, W. Tan, Gold Nanoparticle-Based Colorimetric Assay for the Direct Detection of Cancerous Cells, *Anal. Chem.*, **80** (2008) 1067–1072.
 9. L. He, M. D. Musick, S. R. Nicewarner, F. G. Salinas, S. J. Benkovic, M. J. Natan, C. D. Keating, Colloidal Au-Enhanced Surface Plasmon Resonance for Ultrasensitive Detection of DNA Hybridization, *J. Am. Chem. Soc.*, **122** (2000) 9071–9077.
 10. J-M. Nam, C. S. Thaxton, C. A. Mirkin, Nanoparticle-based bio-bar codes for the ultrasensitive detection of proteins, *Science*, **301** (2003) 1884–1886.
 11. D. G. Thompson, A. Enright, K. Faulds, W. E. Smith, D. Graham, Ultrasensitive DNA Detection Using Oligonucleotide–Silver Nanoparticle Conjugates, *Anal. Chem.*, **80** (2008) 2805–2810.
 12. D. A. Giljohann, D. S. Seferos, P. C. Patel, J. E. Millstone, N. L. Rosi, C. A. Mirkin, Oligonucleotide Loading Determines Cellular Uptake of DNA-Modified Gold Nanoparticles, *Nano Lett.*, **7** (2007) 3818–3821.
 13. D. S. Seferos, D. A. Giljohann, H. D Hill, A. E. Prigodich, C. A. Mirkin, Nano-Flares: Probes for Transfection and mRNA Detection in Living Cells, *J. Am. Chem. Soc.*, **129** (2007) 15477–15479.
 14. D. S. Seferos, D. A. Giljohann, N. L. Rosi, C. A. Mirkin, Locked nucleic acid-nanoparticle conjugates, *Chembiochem.*, **8** (2007) 1230–1232.

-
15. X. Li, M. Takashima, E. Yuba, A. Harada, K. Kono, PEGylated PAMAM dendrimer–doxorubicin conjugate-hybridized gold nanorod for combined photothermal-chemotherapy, *Biomaterials*, **35** (2014) 6576–6584.
16. I. M. D. Mahmoud , Y. Takenoshita , T. Hamada , S. Onitsuka , J. Kurawaki , H. Okamura, Spontaneous Preparation of Highly Stable Gold Nanoparticle Stabilized with ω - Sulfylated Alkylsulfanylaniline, *j. of oleo science*, **66** (2017) 1349–1354.
17. V. L. Calvin, The potential environmental impact of engineered nanomaterials, *Nat. Biotechnol.*, **21** (2003) 1166–1170.
18. N. L. Rosi, D. A. Giljohann, C. S. Thaxton, A. K. R. Lytton-Jean, M. S. Han, C. A. Mirkin, Oligonucleotide-modified gold nanoparticles for intracellular gene regulation, *Science*, **312** (2006) 1027–1030.
19. C. Q. Pan, and R. A. Lazarus, Engineering Hyperactive Variants of Human Deoxyribonuclease I by Altering Its Functional Mechanism, *Biochemisry*, **36** (1997) 6624–6632.
20. J. Shack, The Influence of Sodium and Magnesium Ions on the Action of Deoxyribonuclease II, *J. Biol. Chem.*, **234** (1959) 3003–3006.
21. Z. Zhang, S. H. Lee, S-S. Feng, Folate-decorated poly (lactide-*co*-glycolide)-vitamin E TPGS nanoparticles for targeted drug delivery, *Biomaterials*, **28** (2007) 1889–1899.

-
22. T. Mosmann, Rapid Colorimetric Assay for Cellular Growth and Survival: Application to Proliferation and Cytotoxicity Assays, *Journal of Immunological Methods*, **65** (1983) 55–63.
23. L. M. Demers, C. A. Mirkin, R. C. Mucic, A. Robert, I. Reynolds, R. L. Letsinger, R. Elghanian, G. Viswanadham, A Fluorescence-Based Method for Determining the Surface Coverage and Hybridization Efficiency of Thiol-Capped Oligonucleotides Bound to Gold Thin Films and Nanoparticles, *Anal. Chem.*, **72** (2000) 5535–5541.
24. M. A. Jordan, L. Wilson, Microtubules as a target for anticancer drugs. *Nat. Rev. Cancer*, **4** (2004) 253–265.
25. D. G. I. Kingston, Tubulin-interactive natural products as anticancer agents (1), *J. Nat. Prod.*, **72** (2009) 507–515.
26. D. A. Giljohann, D. S. Seferos, W. L. Daniel, M. W. Massich, P. C. Patel, C. A. Mirkin, Gold Nanoparticles for Biology and Medicine, *Angew. Chem., Int. Ed.*, **49** (2010) 3280–3294.
27. B. D. Chithrani, A. A. Ghazani, C. W. Chan, Determining the Size and Shape Dependence of Gold Nanoparticle Uptake into Mammalian Cells, *Nano Lett.*, **6** (2006) 662–668.
28. J. W. Y. H. Bae, EPR: Evidence and fallacy, *J Control Release*, **190** (2014) 451–464.
29. Y. Matsumura, H. Maeda, A new concept for macromolecular therapeutics in cancer chemotherapy: Mechanism of tumorotropic

accumulation of proteins and the antitumor agent SMANCS, *Cancer Res.*, **46** (1986) 6387–6392.

30. M. R. Dreher, W. Liu, C. R. Michelich, M. W. Dewhirst, F. Yuan, A. Chilkoti, Tumor vascular permeability, accumulation, and penetration of macromolecular drug carriers, *J Natl Cancer Inst.*, **98** (2006) 335–344.

31. O. C. Farokhzad, S. Jon, A. Khademhosseini, T. N. Tran, D. A. Lavan, R. Langer, Nanoparticle-aptamer bioconjugates: A new approach for targeting prostate cancer cells, *Cancer Res.*, **64** (2004) 7668–7672.

32. X. Montet, M. Funovics, K. Montet-Abou, R. Weissleder, L. Josephson, Multivalent effects of RGD peptides obtained by nanoparticle display, *J. Med. Chem.*, **49** (2006) 6087–6093.

33. S. R. Popielarski, S. H. Pun, M. E. Davis, A nanoparticle-based model delivery system to guide the rational design of gene delivery to the liver. 1. Synthesis and characterization, *Bioconjugate Chem.*, **16** (2005) 1063–1070.

34. D. E. Lopes de Menezes, L. M. Pilarski, T. M. Allen, In vitro and in vivo targeting of immunoliposomal doxorubicin to human B-cell lymphoma, *Cancer Res.*, **58** (1998) 3320–3330.

35. R. Bhattacharya, C. R. Patra, A. Earl, S. Wang, A. Katarya, L. Lu, J. N. Kizhakkedathu, M. J. Yaszemski, P. R. Greipp, D. Mukhopadhyay, P. Mukherjee, Attaching folic acid on gold nanoparticles using noncovalent

interaction via different polyethylene glycol backbones and targeting of cancer cells, *Nanomed Nanotechnol Biol. Med.*, **3** (2007) 224–238.

36. N. L. Rosi, D. A. Giljohann, C. S. Thaxton, A. K. R. Lytton-Jean, M. S. Han, C. A. Mirkin, Oligonucleotide-modified gold nanoparticles for intracellular gene regulation, *Science*, **312** (2006) 1027–1030.

37. Q. Yang, S. H. Wang, P. W. Fan, L. F. Wang, Y. Di, K. F. Lin, F. S. Xiao, PH-Responsive Carrier System Based on Carboxylic Acid Modified Mesoporous Silica and Polyelectrolyte for Drug Delivery, *Chem. Mater.*, **17** (2005) 5999–6003.

38. K. Yang, H. Luo, M. Zeng, Y. Jiang, J. Li, X. Fu, Intracellular pH-triggered, targeted drug delivery to cancer cells by multifunctional envelope-type mesoporous silica nanocontainers, *ACS Appl Mater Interfaces*, **7** (2015) 17399–17407.

39. J. Z. Du, X. J. Du, C. Q. Mao, J. Wang, Tailor-made dual pH-sensitive polymerdoxorubicin nanoparticles for efficient anticancer drug delivery, *J. Am. Chem. Soc.*, **133** (2011) 17560–17563.

40. J. Huang, Y. Xue, N. Cai, H. Zhang, K. Wen, X. Luo, S. Long, F. Yu, Efficient reduction and pH co-triggered DOX-loaded magnetic nanogel carrier using disulfide crosslinking, *Mater Sci Eng C Mater Biol Appl.*, **46** (2015) 41–51.

41. Z. Xu, D. Wang, S. Xu, X. Liu, X. Zhang, H. Zhang, Preparation of a camptothecin prodrug with glutathione-responsive disulfide linker for anticancer drug delivery, *Chem Asian J.*, **9** (2014) 199–205.

-
42. S. Dhar, W. L. Daniel, D. A. Giljohann, C. A. Mirkin, S. J. Lippard, Polyvalent oligonucleotide gold nanoparticle conjugates as delivery vehicles for platinum (IV) warheads, *J. Am. Chem. Soc.*, **131** (2009) 14652–14653.
43. Y. Zhang, L. Tang, L. Sun, J. Bao, C. Song, L. Huang, K. Liu, Y. Tian, G. Tian, Z. Li, H. Sun, L. Mei, A novel paclitaxel-loaded poly(ϵ -caprolactone)/Poloxamer 188 blend nanoparticle overcoming multidrug resistance for cancer treatment, *Acta Biomater.*, **6** (2010) 2045–2052.
44. D. B. Buxton, Nanomedicine for the management of lung and blood diseases, *Nanomedicine*, **4** (2009) 331–339.
45. I. Brigger, C. Duberne, P. Couvreur, Nanoparticles in cancer therapy and diagnosis, *Adv. Drug Delivery Rev.*, **54** (2002) 631–651.

Chapter 4

Preparation and characterization of platinum nanoparticles stabilised by a polymer modified with sulfonyl aniline and their application as a highly efficient, recyclable, chemo-selective, and broad spectrum nanocatalyst

4.1: Introduction

Different metal nanoparticles have been utilised in the catalytic reduction of nitrobenzene derivatives. In principal, catalyst recovery and re-using are very crucial issues when noble, precious and costly metal-based nanocatalysts are used, but these issues remain challenging. Silver nanoparticles were previously used as catalyst in the reduction of *p*-nitrophenol to *p*-aminophenol.¹ The catalytic efficiency of different metal nanoparticles can be affected not only by their size, but also their stability as well as the preparation method.^{2,3} Gold and copper nanoparticles were also utilised for the catalytic hydrogenation of *p*-nitrophenol.⁴⁻⁶ Platinum nanoparticles are generally prepared by a chemical reduction method. This method depends on the reduction of metallic ions to metal atoms

(nucleation phase), which act as a nucleation centre for other metal atoms to form the nanoparticles (growth phase). These nanoparticles are coated with a support or stabilising agent to prevent further aggregation and provide their easy isolation.⁷ Platinum nanoparticles were utilised in the catalytic reduction of *p*-nitrophenol and aromatic ketones with various activities and apparent rate constants.^{5,8} These metals are precious with high production costs, and thus it is desirable to decrease their consumption by developing durable metal-based nanocatalysts; active, recyclable with chemo-selective properties.

Principally, small-sized nanoparticles have good catalytic properties, however these particles easily agglomerate together owing to their high surface energy, leading to significant reduction of their catalytic efficiency.^{9,10} To get rid of this drawback, it is desirable to use suitable coating agents as organic molecules, surfactants and polymers to adjust the nucleation/growth phases and prevent the aggregation of the nanoparticles together during their preparation, without blocking most of the active sites on the surfaces of the metal nanoparticles.⁹⁻²⁰

p-Nitrophenol is commonly used as model compound for hydrogenation reactions to evaluate the catalytic efficiency of metal based-nanocatalysts as the reduction can be easily monitored by UV-visible spectroscopy. Considerable interest has also focused on the chemo-selective reduction of halonitrobenzenes to haloanilines, and indeed an effective catalytic process has been achieved for the reduction of *p*-chloronitrobenzene to *p*-chloroaniline,²¹⁻²⁸ however not *p*-bromonitrobenzene, which remains challenging owing to the concurrent occurrence of hydrodebromination reaction.

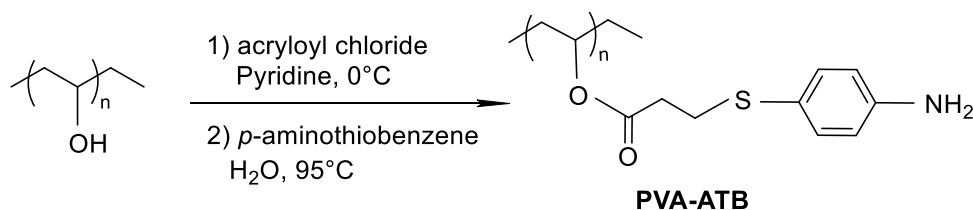
In this study, we described a new chemical method for the preparation of an efficient, stable, and recyclable platinum-based nanocatalyst stabilised with a polymer acting as a reductive stabiliser. The polymer (**PVA-ATB**) was prepared from acrylated polyvinyl alcohol modified with 4-aminothiobenzene. The method was simple, safe, and used inexpensive chemicals. The nanoparticles were spontaneously prepared by addition of the polymer solution into a boiling fresh solution of H₂PtCl₆ under stirring. The resulting particles were coordinated by the amino terminals of the polymer and coated with the polymer chains leading to an

improvement of stability, recyclability, and dispersion. The characterisation of the prepared Pt NPs was carried out by UV-visible spectroscopy and TEM. The average particle size of the prepared Pt NPs was 12.6 ± 5.7 nm. The resulting platinum nanoparticles have a broad spectrum nanocatalytic activity for various reactions. The prepared platinum-based nanocatalyst exhibited a high catalytic efficiency with a high apparent rate constant (k_{app}) in the reduction of *p*-nitrophenol at a concentration higher than were those reported in the literature.^{1-4,29} Furthermore, the active particles could be recovered from the reaction media and reused for at least six successive catalytic cycles owing to their stability. Moreover, the prepared Pt NPs could catalyse the reduction of *p*-bromonitrobenzene to *p*-bromoaniline successively without any additives and no concurrent hydrodebromination reaction occurred.

4.2: Materials and Methods

4.2.1: Preparation of the PVA–ATB polymer

The polymer used in this study was prepared as shown in Scheme 1. Polyvinyl alcohol (PVA, average MW 1500, 0.36 g) was dissolved in 20 mL of pyridine and reacted with acryloyl chloride (1.35 g) under magnetic stirring at 0 °C for 1 h. The reaction mixture was filtered to remove the excess of acryloyl chloride, and the resulting residue was washed with ethyl acetate (2×10 mL). In the second step, an aqueous solution of the resulting residue (0.27 g in 20 mL of water) was heated at 95 °C for 2 h, and then it was treated with a *p*-aminothiobenzene solution (0.23 g in 5 mL of ethyl acetate) under magnetic stirring at room temperature for 12 h to give the desired **PVA–ATB** polymer. The product was purified by extraction using water and ethyl acetate; the aqueous layer was collected and evaporated to obtain the pure polymer. Such polymer was dried under vacuum and its structure was confirmed by ¹H NMR. The yield of the product was 87%.



Scheme 1. Preparation of **PVA-ATB**.

4.2.2: Preparation of polymer-stabilised Pt NPs (PVA-ATB-Pt NPs, nanocatalyst)

The typical method for the preparation of **PVA-ATB-Pt NPs** is described below. An aqueous solution of disodium succinate (10 mM, 10 mL) was added to a freshly prepared aqueous solution of H₂PtCl₆ (1.0 mM, 10 mL). The pH of the solution was controlled by adding a few drops of aqueous NaOH (1.0 M) to pH 8 or HCl (10 mM) to pH 4.5. The volume of the solution was adjusted to 50 mL by adding water, and the mixture was then heated to reflux. An aqueous solution of the polymer (10 mM based on acrylated polymer unit (83% modified), 4.43 mg in 2 mL of H₂O) was added dropwise to the boiling solution under stirring. The colour of the solution started to change from faint yellow to dark brown within 4 h, and the reaction was completed within 48 h. The final molar concentration was 0.19 mM and 0.38 mM for H₂PtCl₆ and the polymer respectively (1:2 molar

ratio). After the synthesis of **PVA–ATB–Pt NPs**, the colloidal solution was purified using a dialysis tube (Spectra/Por 3), which was placed in a beaker containing 500 mL of water and stirred at room temperature. The water was replaced every 8 h for a total period of 24 h in order to remove the unreacted free Pt⁴⁺ ions and polymer. The characterisation of the prepared **PVA–ATB–Pt NPs** was carried out by UV-visible spectroscopy and TEM. The particle solution was stored at room temperature.

4.2.3: Application of the prepared nanocatalyst in nanocatalysis and its broad spectrum activity

4.2.3.1: Nanocatalytic reduction of *p*-nitrophenol and chemo-selective reduction of *p*-bromonitrobenzene to *p*-bromoaniline

The catalytic reduction activity of **PVA–ATB–Pt NPs** was studied using the standard hydrogenation reaction of *p*-nitrophenol. The reaction involved the sequential addition of aqueous NaOH (10 mM, 1.0 mL) and NaBH₄ (3.0 mg, 8.0 × 10⁻⁵ mol) to *p*-nitrophenol (30 mM, 1.0 mL). Then, **PVA–ATB–Pt NPs** (0.19 mM, 0.50 mL) were added as a catalyst to start the reaction at approximately pH 9. The reaction was carried out under

magnetic stirring at room temperature. The concentration of *p*-nitrophenol used in this reaction was higher than the concentration range commonly reported in the literature.^{1-4,29} Pure Pt black was also used as a catalyst under the same reaction conditions of the **PVA-ATB-Pt NPs** nanocatalyst. The catalytic reduction of *p*-nitrophenol to *p*-aminophenol was monitored by the UV-visible spectroscopy.

The recyclability of the **PVA-ATB-Pt NPs** was also evaluated. After completion of the reaction, the mixture was evaporated to dryness. Then, ethyl acetate was added to dissolve *p*-aminophenol and separate it from the nanoparticle catalyst. The residue, containing **PVA-ATB-Pt NPs**, was washed with ethyl acetate (2 mL). The purified nanoparticles were re-dispersed in water (0.5 mL) and reused for at least six successive catalytic cycles. The same reaction conditions were used in all catalytic cycles. Moreover, the catalytic reduction activity of the prepared Pt NPs was examined for the reduction of *p*-bromonitrobenzene to *p*-bromoaniline under the same reaction conditions as *p*-nitrophenol, but the *p*-bromonitrobenzene was dissolved in MeOH.

4.2.3.2: Reduction potassium hexacyanoferrate reaction (redox reaction)

In this reaction, aqueous solution of sodium thiosulphate $\text{Na}_2\text{S}_2\text{O}_3 \cdot 5\text{H}_2\text{O}$ (2 mL, 1 mM) was added to aqueous solution potassium hexacyanoferrate $\text{K}_3[\text{Fe}(\text{CN})_6]$ (2 mL, 10 mM) at approximately pH 8. Then Pt NPs were added as a nanocatalyst to the mixed reactants (1 mL). The reaction was carried out under stirring at 45 °C. The reaction was monitored by UV-visible spectroscopy.

4.2.3.3: Carbon-carbon double bond reduction

a. Reduction of cinnamyl alcohol to hydrocinnamyl alcohol

The typical reaction conditions include the addition of NaBH_4 (3 mg) to an aqueous solution of cinnamyl alcohol (0.1 mmol, 1.5 mL) followed by the addition of **PVA-ATB-Pt NPs** (2 mL) as a nanocatalyst. The reaction was carried out at approximately pH 8 under stirring at room temperature. The experiment was monitored by GCMS.

b. Reduction of polyaromatic hydrocarbons (anthracene)

The reaction includes NaBH_4 (3 mg) was added to anthracene solution in MeOH (1.5 mM, 1.5 mL), and then the nanocatalyst was added (6.0 mL). The reaction was carried out at approximately pH 8 at 50 °C under magnetic stirring. The purity of anthracene used in the reaction was 94%. The experiment was monitored by UV-visible spectroscopy.

4.2.3.4: Nanocatalytic reduction of organic dyes

a. Methyl orange (MO)

The catalytic reaction was performed by sequential addition of NaBH_4 (5.0 mg) and **PVA-ATB-Pt NPs** as a catalyst (1.0 mL) to an aqueous solution of MO (3.0 mM, 1.0 mL). The pH was adjusted to pH 8 by the addition of 10 μL of 1.0 mM of NaOH and the experiment was carried out at room temperature under magnetic stirring. The experiment was monitored by the UV-visible spectroscopy.

b. Methylene blue (MB)

The catalytic reaction was performed through the addition of NaBH_4 (5.0 mg) to a freshly prepared aqueous solution of MB (10 mM, 1.0

mL), then the **PVA-ATB-Pt NPs** was added (0.8 mL) to the mixture. The experiment was carried out at 40 °C under magnetic stirring at approximately pH 8. The experiment was monitored using the UV-visible spectroscopy.

4.2.4: Gas chromatography mass spectrometry (GCMS) conditions

GCMS analysis was performed using a capillary column (Agilent Technologies, HP-5MS, 60 m length, 0.25 mm diameter, and 0.25 µm film thicknesses); the initial temperature was 40 °C for 2 min, then it was increased at a rate of 20 °C/min up to 110 °C. Then, the temperature was further increased at a rate of 25 °C/min to reach the final temperature of 250 °C and the injection volume was 1 µL.

4.3: Results and discussion

4.3.1: Characterisation of the PVA-ATB polymer

The ^1H NMR spectrum shown in Fig. 1 indicates the successive coupling of the acrylated PVA with 4-aminothiobenzene to form **PVA-ATB**. The assignment of the signals originating from the aromatic protons (Ha and Hb) and methylene (Hc) protons of PVA is also displayed. The percentage of coupling of the acrylated PVA unit with 4-aminothiobenzene was found to be 83%.

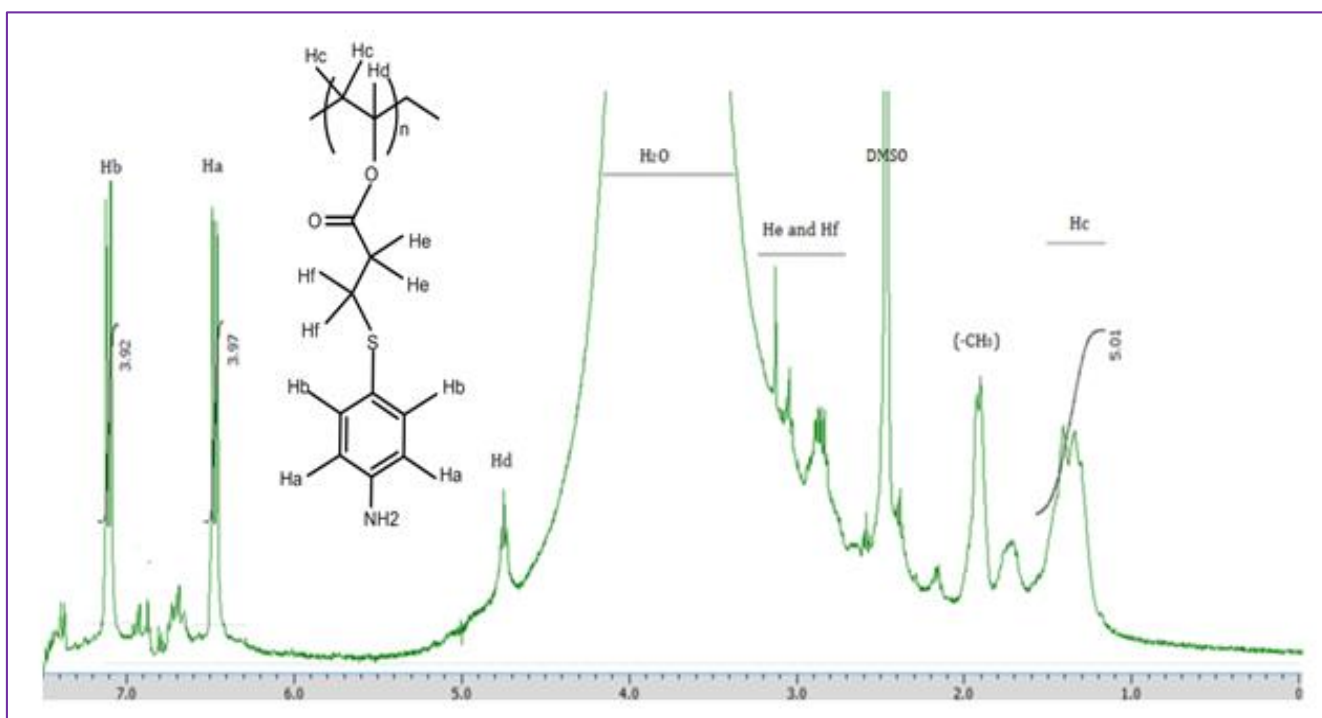
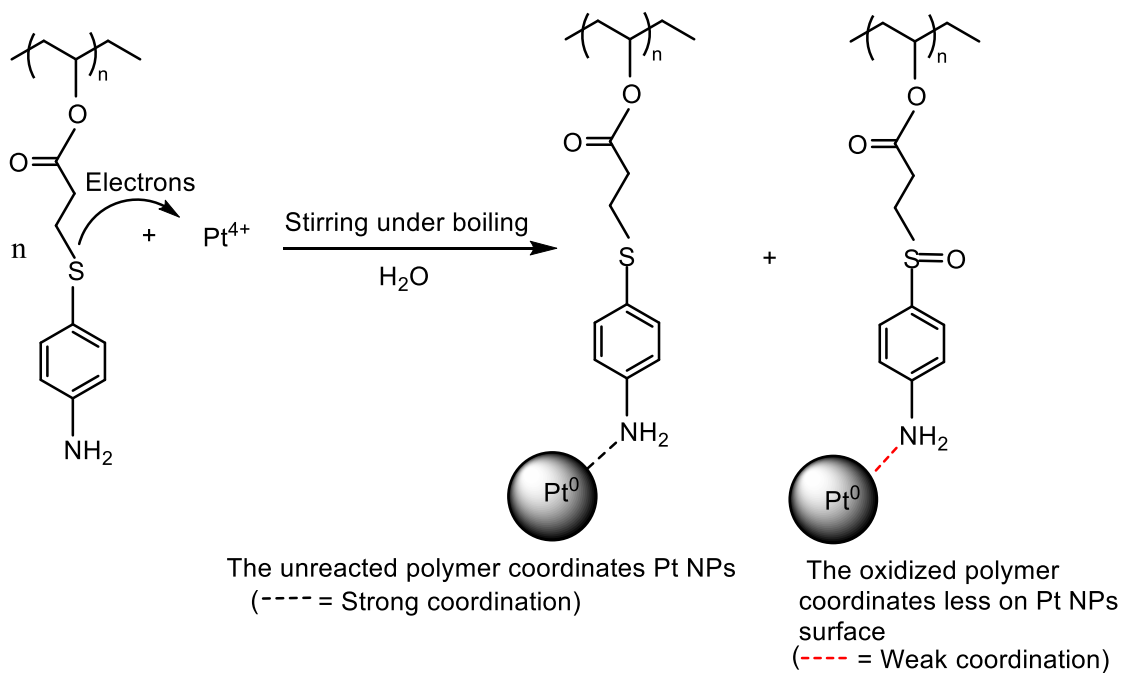


Figure 1. ^1H NMR spectrum of **PVA-ATB** (400 MHz in DMSO-d_6).

4.3.2: Characterisation and peculiarities of PVA–ATB–Pt NPs

4.3.2.1: Preparation and properties of PVA–ATB–Pt NPs

As shown in Scheme 2, the **PVA–ATB** polymer easily reduced the Pt^{4+} ions to Pt^0 by receiving the electrons provided by the sulphur atoms. The resulting Pt^0 (nucleation phase) started the growth phase to generate the nanoparticles. The polymer that did not participate in the reduction of Pt^{4+} to Pt^0 was more strongly coordinated to the surface of the Pt NPs than the oxidized polymer. This is because the amino groups of the oxidised polymer possess a lower electron density than those of the unreacted polymer owing to an electron withdrawing effect of the oxidised sulphur.



Scheme 2. Plausible pathway to form PVA-ATB-Pt NPs

4.3.2.1.1: UV- visible spectroscopy

UV-visible spectroscopy was used to monitor the reduction of the Pt^{4+} ions to Pt^0 by PVA-ATB. An aqueous solution of Pt^{4+} showed a characteristic absorbance peak at 265 nm. Fig. 2 shows the decrease of the intensity of this peak over time, suggesting the reduction of Pt^{4+} to Pt^0 and the formation of platinum nanoparticles (PVA-ATB-Pt NPs).³⁰ The complete disappearance of this peak together with an increase in the absorbance towards shorter wavelengths implied the completion of the platinum nanoparticle synthesis.³¹⁻³⁴

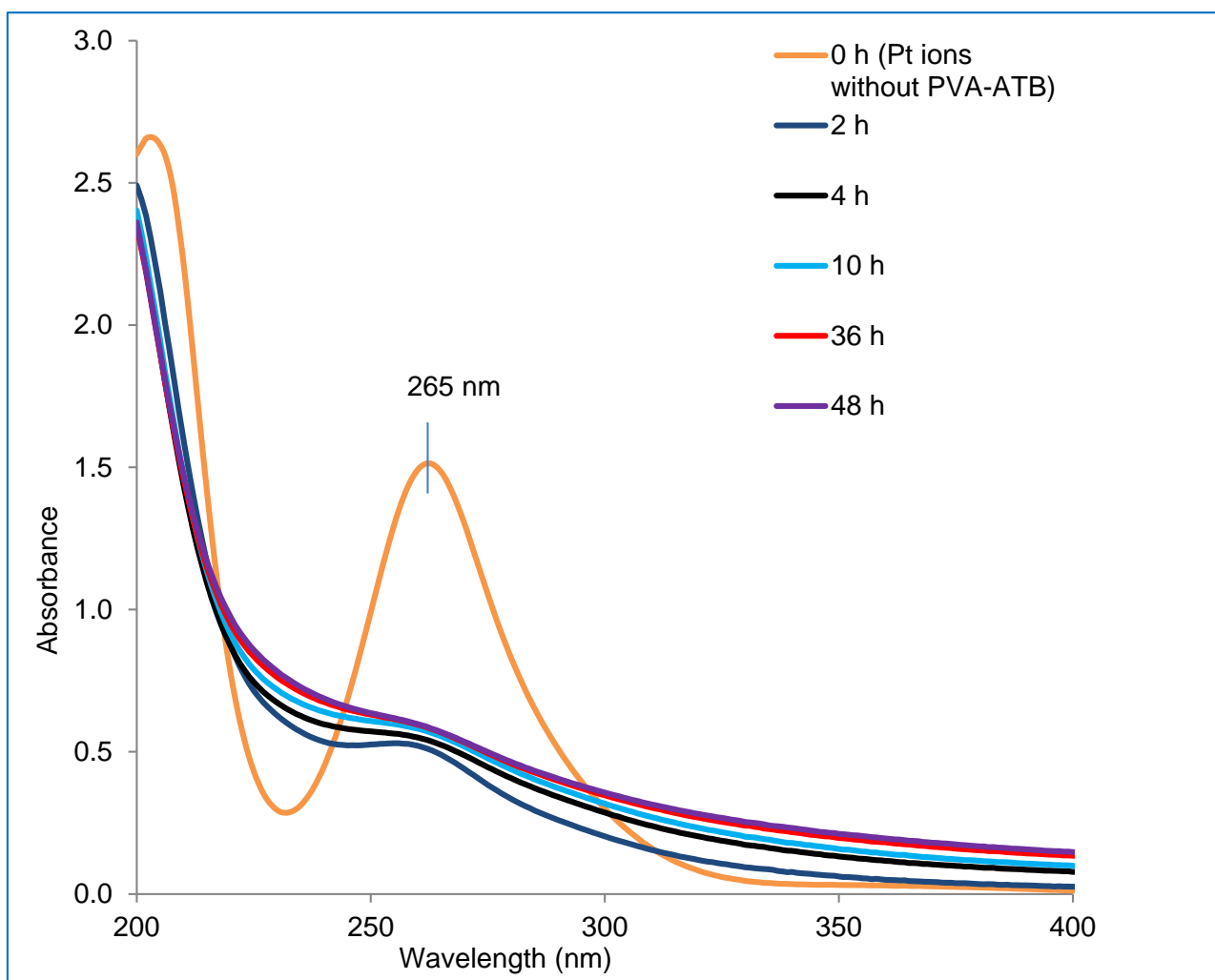


Figure 2. UV-visible spectra of the reaction mixture of **PVA-ATB** and H_2PtCl_6 at pH 8.

4.3.2.1.2: Transmission electron microscope (TEM) analysis

A TEM analysis of the **PVA–ATB–Pt NPs** was performed. The TEM images revealed that the majority of the **PVA–ATB–Pt NPs** had a spherical shape and were nearly mono-dispersed. In alkaline medium (pH 8), the diameter ranged from 10 to 15 nm and the average particle size was 12.6 ± 5.7 nm (Fig. 3a and b). In the case of an acidic medium (pH 4.5), the diameter of the particles ranged from 10 to over 30 nm with an average size of 20.3 ± 7.9 (Fig. 3c and d).

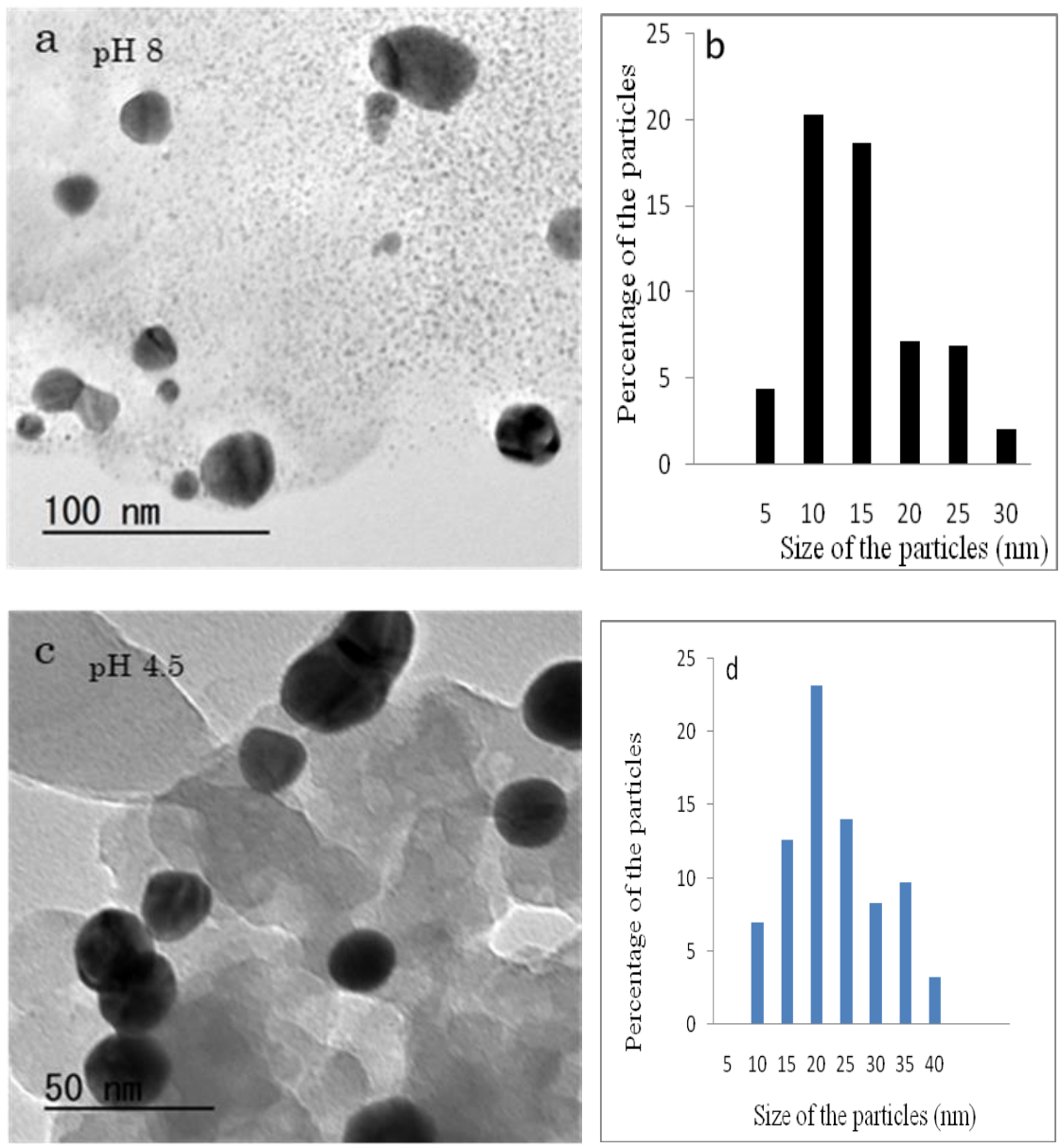


Figure 3. TEM images and histograms of **PVA-ATB-Pt NPs** at pH 8 (a & b) and pH 4.5 (c & d).

4.3.2.2: pH-dependence of the properties and peculiarities of PVA–ATB–Pt NPs

The stability and size of the **PVA–ATB–Pt NPs** were found to be dependent on the pH of the reaction mixture. Stable nanoparticles with a small size were produced at pH 8. The effect of the pH can be explained by the protonation of the aniline moieties of **PVA–ATB**, since the pKa of aniline is 5.2.³⁵ Under alkaline conditions (pH 8), the amino groups are free and can coordinate the surface of the particles leading to highly stable nanoparticles. The free (unprotonated) polymer remained coordinated to the surface of the nanoparticles; the growth stopped and small stable nanoparticles were formed.

In contrast, under acidic conditions (pH 4.5) there are more protonated amino groups than free ones, thus a considerable amount of the polymer was protonated and less coordinative. This means that the polymer, to a lesser extent, can coordinate the surface of the nanoparticles. The protonated polymer was released from the surface of the Pt NPs; thus, the particles became naked, grew larger and unstable, leading to the formation of a black precipitate.

The pH also affected the rate of the reaction for the preparation of **PVA–ATB–Pt NPs**; the reaction proceeded faster under acidic conditions (pH 4.5) than alkaline (pH 8). The reaction in the alkaline solution (pH 8) required a longer time to go to completion (48 h); however, the prepared particles were stable and smaller. The reaction at pH 4.5 proceeded faster, and it was completed within 10 h, but the particles were not stable and the formation of a precipitate was observed. As shown in Fig. 4, the peaks deriving from the Pt^{4+} ions at pH 4.5 disappeared faster than at pH 8. These results indicate that the pH affects the reactivity of the Pt^{4+} ions. Pt^{4+} ions are more reactive in an acidic medium, and a similar trend has been found with Au^{3+} .³⁶⁻³⁷

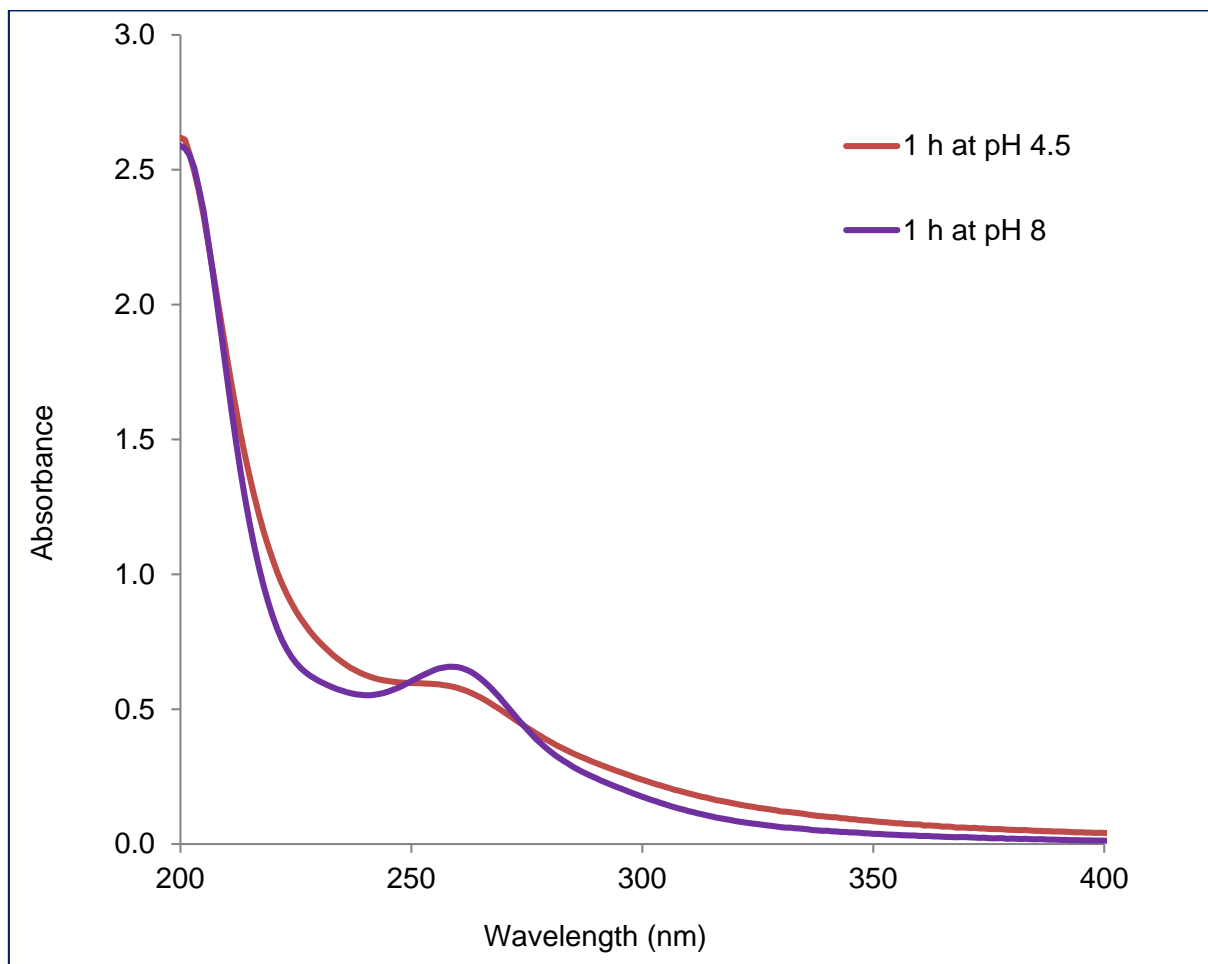


Figure 4. UV-visible spectra of the reaction mixture of H_2PtCl_6 and the PVA-ATB.

4.3.3: Application of PVA–ATB–Pt NPs as a highly efficient and broad spectrum nanocatalyst (nanocatalytic system)

4.3.3.1: Reductive hydrogenation of *p*-nitrophenol

The prepared **PVA–ATB–Pt NPs** effectively catalysed the reduction of *p*-nitrophenol in the presence of NaBH₄. The *p*-nitrophenolate, formed by the addition of NaBH₄ to *p*-nitrophenol, showed a characteristic absorption peak at 400 nm. After the addition of the **PVA–ATB–Pt NPs** to the reaction mixture as a nanocatalyst, a new peak appeared at 300 nm due to the reduction of *p*-nitrophenol to *p*-aminophenol (Fig. 5a).^{1,38} This new peak increased with time, while the peak at 400 nm, due to *p*-nitrophenolate, disappeared corresponding to the reduction of *p*-nitrophenol to *p*-aminophenol. The reaction proceeded with an obvious isosbestic point at 325 nm, indicating that no side products of the reaction were formed.³⁹⁻⁴⁰ The yellow colour of the reaction mixture due to *p*-nitrophenol completely disappeared.

The kinetic equation for the *p*-nitrophenol reduction can be expressed as Eq. (1)

$$\ln (A_t/A_0) = - k_{app} \cdot T \quad (1)$$

where A_t is the absorbance of *p*-nitrophenol at time (t), A_0 is the absorbance of *p*-nitrophenol at time (0), k_{app} is the final apparent rate constant⁴²⁻⁴⁴ that can be calculated from the decrease in the intensity of the peak at 400 nm over time. Fig. 5b shows a linear relationship between $\ln (A_t/A_0)$ and the reaction time at room temperature, thus the reaction followed pseudo first-order kinetics. In the control experiments (under the same conditions except for water being used instead of **PVA-ATB-Pt NPs**), no reduction of *p*-nitrophenol was observed (Fig. 6). Pt black (powder, WAKO chemicals) was used as a catalyst under the same reaction conditions of **PVA-ATB-Pt NPs**, however the reduction did not proceed completely even after 24 h (Fig 7). As shown in table 1, in case of using Pt black as a catalyst the conversion rate of the reaction was 54% after 24 h. By contrast, in the case of the prepared nanocatalyst, it was 100% within 10 minutes, indicating the higher activity and effectiveness of the nanocatalyst. The polymer coating made the nanoparticles stable, viable, and conserved their activity after

catalysis; therefore, they could be reused for several cycles without further treatment (Fig. 8).

As shown in Scheme 3, the **PVA-ATB-Pt NPs** served as a bridge for the hydride transfer from BH_4^- to *p*-nitrophenol, while BH_4^- was oxidised to BO_2^- . The catalytic reaction followed the Langmuir-Hinshelwood model.⁴¹ According to this model, the reduction occurred on the surface of the **PVA-ATB-Pt NPs** where both reactants were adsorbed. The hydrides were transferred from BH_4^- to *p*-nitrophenol through the **PVA-ATB-Pt NPs**, which resulted in the formation of *p*-aminophenol. Then, the *p*-aminophenol dissociated from the surface of the **PVA-ATB-Pt NPs**. The nanoparticles catalysed the conversion of *p*-nitrophenol to *p*-aminophenol successively in the presence of a high concentration of *p*-nitrophenol and a low catalyst mol%, suggesting that they possess a higher catalytic efficiency compared to other nanocatalysts (Table 2). The k_{app} of the reaction was calculated to be $7.9 \times 10^{-3} \text{ s}^{-1}$ for the basic reaction, which was found to be higher than that of other nanocatalysts (Table 3). After six catalytic cycles, the k_{app} was found to be $5.7 \times 10^{-3} \text{ s}^{-1}$.

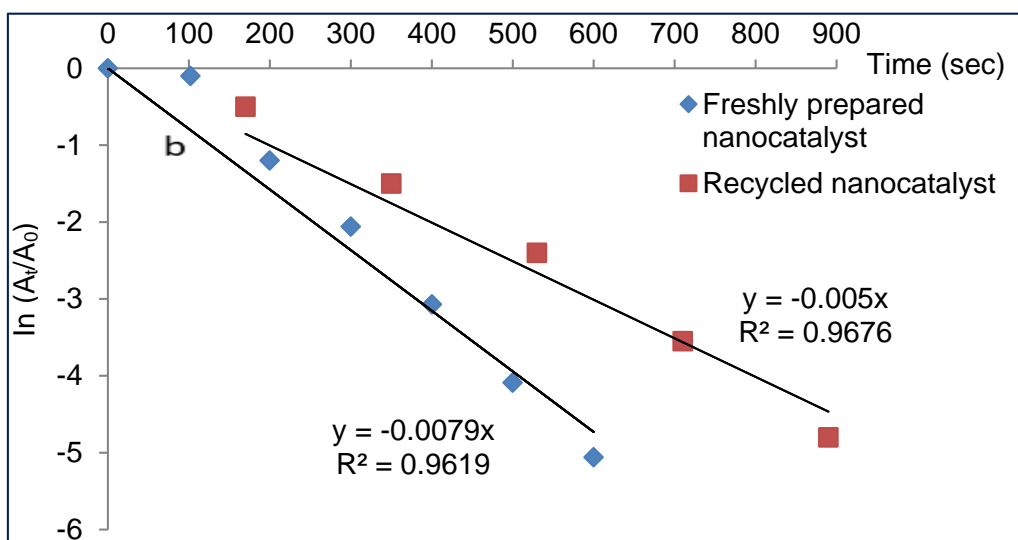
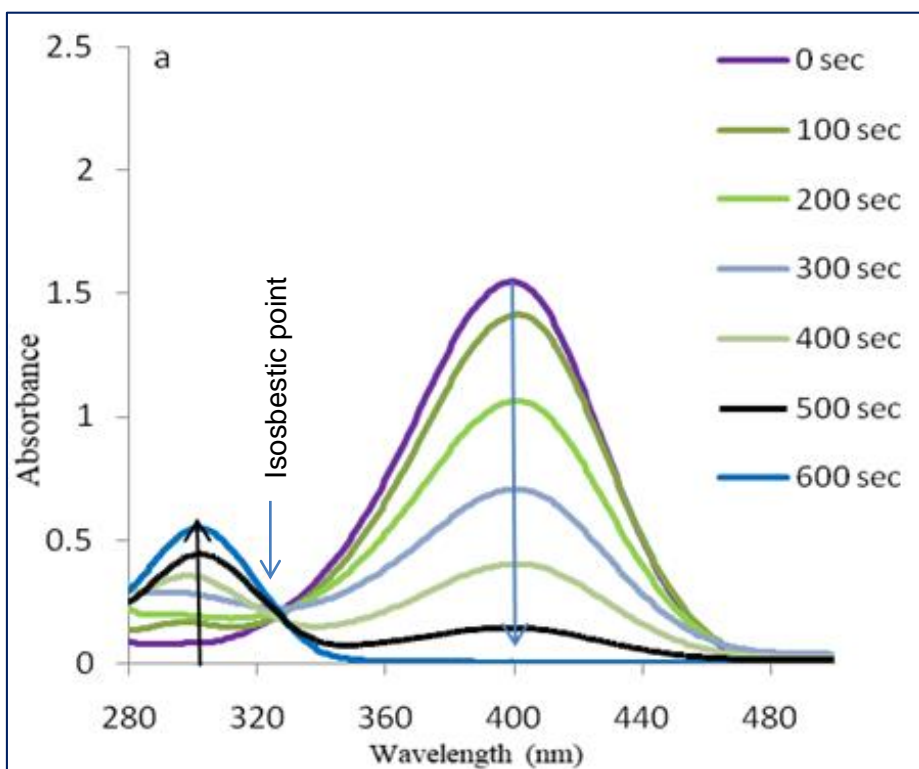


Figure 5. (a) UV-visible spectra showing the catalytic reduction of *p*-nitrophenol to *p*-aminophenol and (b) Plot of $\ln (A_t/A_0)$ vs time for the reaction using freshly prepared nanocatalyst and recycled (6th) nanocatalyst of **PVA-ATB-Pt NPs** for catalysis of *p*-nitrophenol reduction.

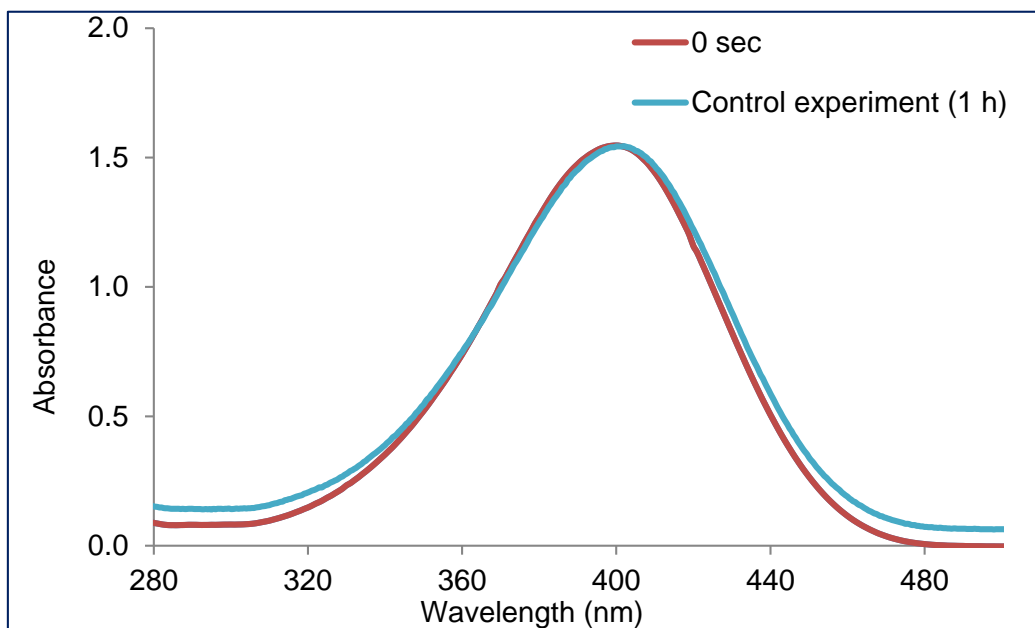


Figure 6. UV-visible spectra of the control experiment employed NaBH_4 only without involvement of the nanocatalyst.

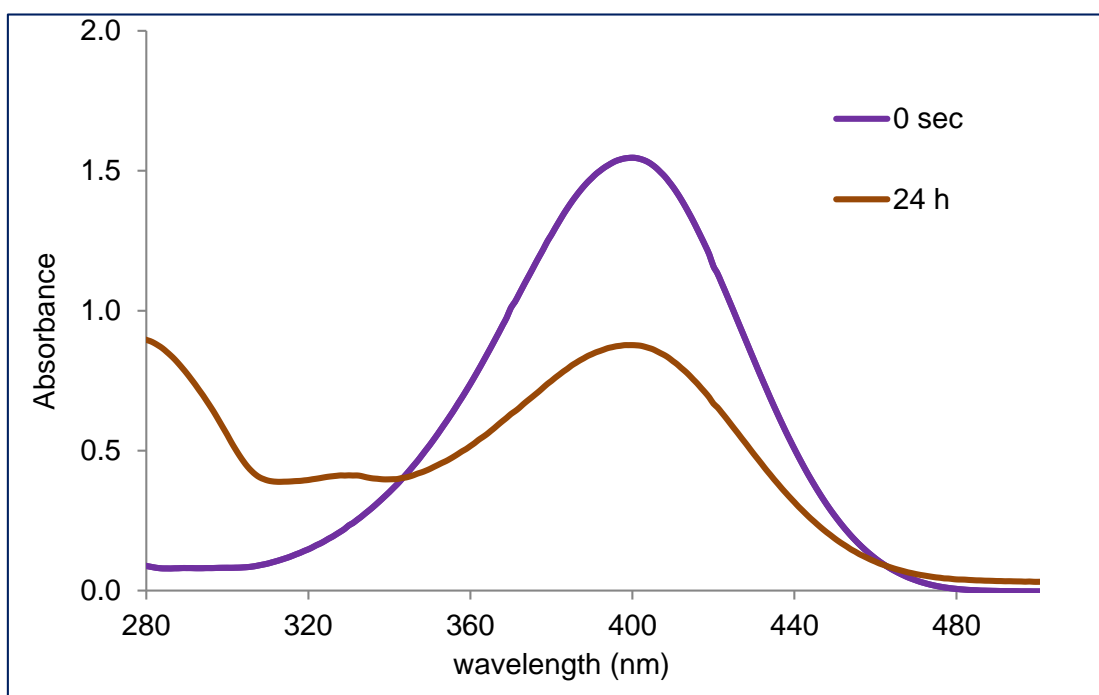


Figure 7. UV-visible spectra of catalytic reduction of *p*-nitrophenol used Pt salts.

Table 1. The conversion rate of *p*-nitrophenol to *p*-aminophenol by **PVA-ATB-Pt NPs** and Pt black catalysts.

Catalyst	<i>p</i> -Nitrophenol conc.	Conversion rate %	Time
Pt NPs	0.03 M	100%	10 min
Pt black	0.03 M	53.6%	24 h
Water (control experiment)	0.03 M	0%	1 h

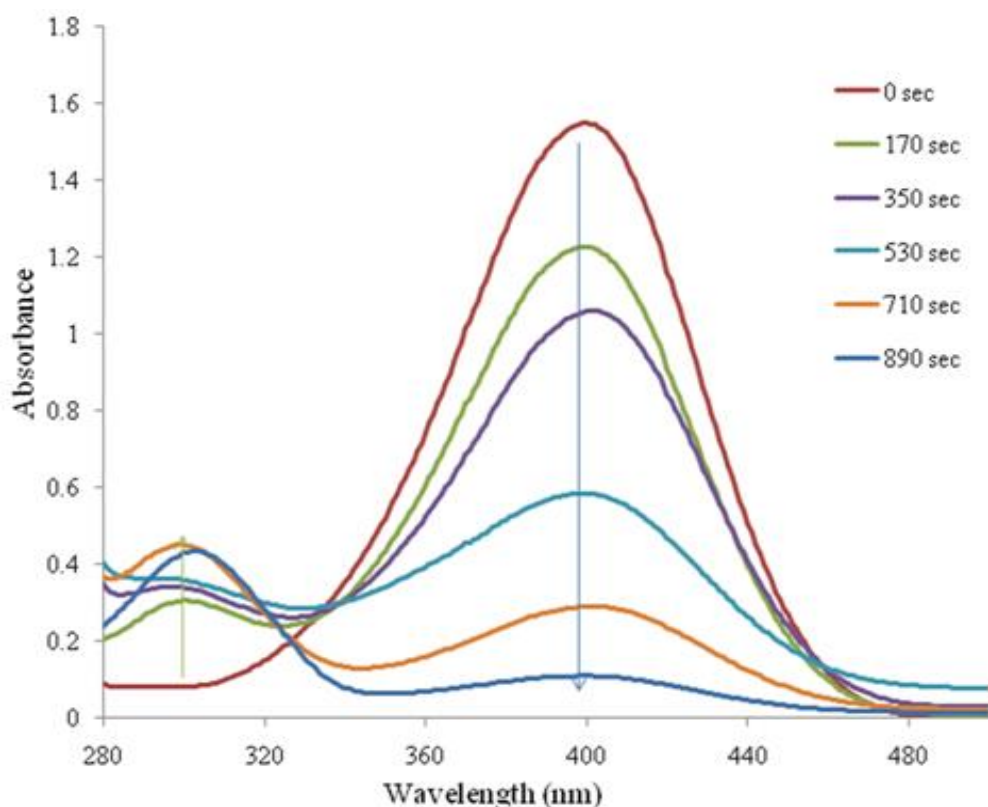
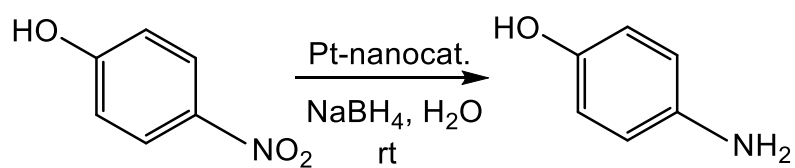


Figure 8. UV-visible spectra showing the catalytic reduction of *p*-nitrophenol to *p*-aminophenol for the 6th recycling of **PVA-ATB-Pt NPs**.



Scheme 3. The mechanism of hydride transfer for catalytic reduction of *p*-nitrophenol by **PVA-ATB-Pt NPs** as a nanocatalyst.

Table 2. Nanocatalytic reduction activity of the **PVA-ATB-Pt NPs** in comparison with literature.

Entry	Catalyst	<i>p</i> -Nitrophenol (mol)	Nanocatalyst (mol %)	Turnover number	Recycling	Reference
1	Pt NPs	3.0×10^{-5}	0.0030	310	Successive recycling	This work
2	Pt NPs	2.0×10^{-7}	0.94	1.1	No recycling	[45]
3	Pt NPs	1.0×10^{-7}	1.25	0.80	No recycling	[46]
4	Ag NPs	2.8×10^{-7}	0.18	5.6	No recycling	[47]
5	Ni NPs	0.10×10^{-3}	0.019	53	No recycling	[48]
6	Pt-amino clay thin film	3.4×10^{-7}	0.013	79	No recycling	[49]
7	Pt NPs	0.10×10^{-3}	0.0070	150	No recycling	[44]

Table 3. Comparison of the k_{app} of the **PVA-ATB-Pt NPs** with different nanocatalytic systems using *p*-nitrophenol as a substrate.

The catalyst	K_{app} (s^{-1})	Reference
Polymer stabilized Pt NPs	7.90×10^{-3} (first)	This work
	5.70×10^{-3} (6 th recycling)	
Fe ₃ O ₄ @SiO ₂ -Ag	7.67×10^{-3}	[43]
GG-s-Pt NPs	7.00×10^{-3}	[46]
Au NPs@MWCNT	0.110×10^{-3}	[42]
PAMAM dendrimer(G4)-Pd NPs	1.79×10^{-3}	[50]
Pt-aminoclay thin film	3.84×10^{-3}	[49]
Pt-PVP thin film	2.14×10^{-3}	[49]
Pt-no stabilizer thin film	1.98×10^{-3}	[49]
Bimetallic Ni-Pt nanoparticles (64:36)	0.49×10^{-3}	[51]
Ni-Pt (96:4)	1.93×10^{-3}	[51]
Au NPs-glucan bioconjugates	0.33×10^{-3}	[52]
Au NPs	0.83×10^{-3}	[53]
γ -Alumina Films supported Pt NPs	0.53×10^{-3} (first)	[54]
	0.36×10^{-3} (4 th recycling)	
Carbon nitride (C ₃ N ₄) supported Pd-Pt NPs	2.33×10^{-3} (first)	[55]
	1.45×10^{-3} (4 th recycling)	

Table 3. Comparison of the k_{app} of the **PVA-ATB-Pt NPs** with different nanocatalytic systems using *p*-nitrophenol as a substrate (continue).

The catalyst	K_{app} (s^{-1})	Reference
TAC-Ag-1.0	5.19×10^{-3}	[56]
AuNP/CeO ₂ (Au: 0.031 mg)	2.25×10^{-3}	[57]
RGO/PtNi (25:75)	1.12×10^{-3}	[58]
Dendritic Pt NPs	0.75×10^{-3}	[59]
230 nm Ni/SiO ₂ MHMs (Ni: 14.6 wt %)	4.50×10^{-3}	[60]

4.3.3.2: Chemo-selective reduction of *p*-bromonitrobenzene to *p*-bromoaniline

The experimental conditions used for the reduction of 4-bromonitrobenzene were similar to those employed for *p*-nitrophenol, with the exception that 4-bromonitrobenzene was dissolved in MeOH. The catalytic reduction of *p*-bromonitrobenzene to *p*-bromoaniline was monitored by the UV-visible spectroscopy and (GCMS). *p*-Bromonitrobenzene exhibited a characteristic absorbance peak at 277 nm, which disappeared within 15 min of the reaction after reduction with NaBH₄ in the presence of **PVA-ATB-Pt NPs** as a nanocatalyst. At the same time, a new absorbance peak appeared at 238 nm, which is characteristic for *p*-bromoaniline as compared with the absorption spectra of a standard solution of *p*-bromoaniline. These spectral changes confirmed the reduction of *p*-bromonitrobenzene to *p*-bromoaniline (Fig. 9).

The control experiment employed the same reaction conditions of the nanocatalytic experiment without the use of the nanocatalyst and it was performed to evaluate the catalytic efficiency in the absence of the

nanocatalyst. It is obvious that the reaction did not proceed without the nanocatalyst incorporation and the absorption peak of 4-bromonitrobenzene at 277 nm did not display any changes due to the lack of the mediator for electron transfer from the donor to the acceptor (Fig. 10). This signifies the crucial role of the nanocatalyst for concurrent occurrence of the reduction process as shown in scheme 4. GCMS was also utilised to confirm the successive nanocatalytic reduction of *p*-bromonitrobenzene to *p*-bromoaniline without hydrodebromination reaction. The signal of *p*-bromonitrobenzene appeared with a retention time of 11.61 min (Fig. 11a). This signal completely disappeared after the nanocatalytic reduction catalysed by **PVA-ATB-Pt NPs** together with the appearance of a new signal with a retention time of 11.40 min, which could be attributed to the highly chemo-selective formation of *p*-bromoaniline (Fig. 11b). Mass spectrometry results confirmed the molecular weight of the product coming from the peak at a retention time of 11.40 min. It is noteworthy that, no peak coming from debrominated product by mass spectroscopy, only one clear peak coming from *p*-bromoaniline (Fig. 11c). Therefore, the successful transformation of *p*-bromonitrobenzene to *p*-bromoaniline using

PVA–ATB–Pt NPs as the nanocatalyst has been achieved. Table 4 displays the start and end retention time of the signals. From the integration of the signal of the product (*p*-bromoaniline), the conversion rate of *p*-bromonitrobenzene to *p*-bromoaniline was found to be > 99%.

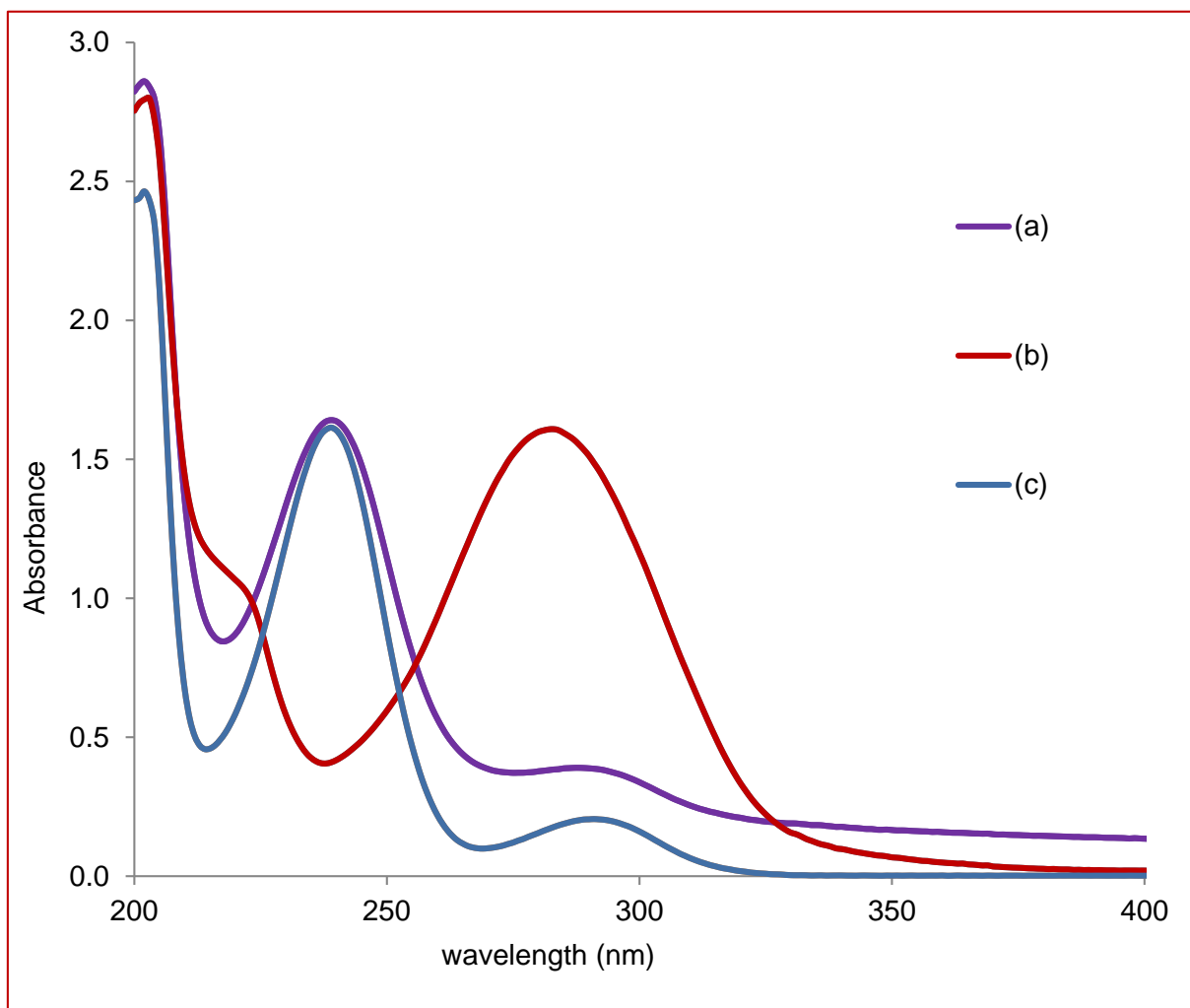


Figure 9. UV-vis absorption spectra show the reduction of *p*-bromonitrobenzene to *p*-bromoaniline with **PVA-ATB-Pt NPs** as a catalyst (a) 15 minutes reduction, (b) absorbance of *p*-bromonitrobenzene before reduction, and (c) absorbance of *p*-bromoaniline solution.

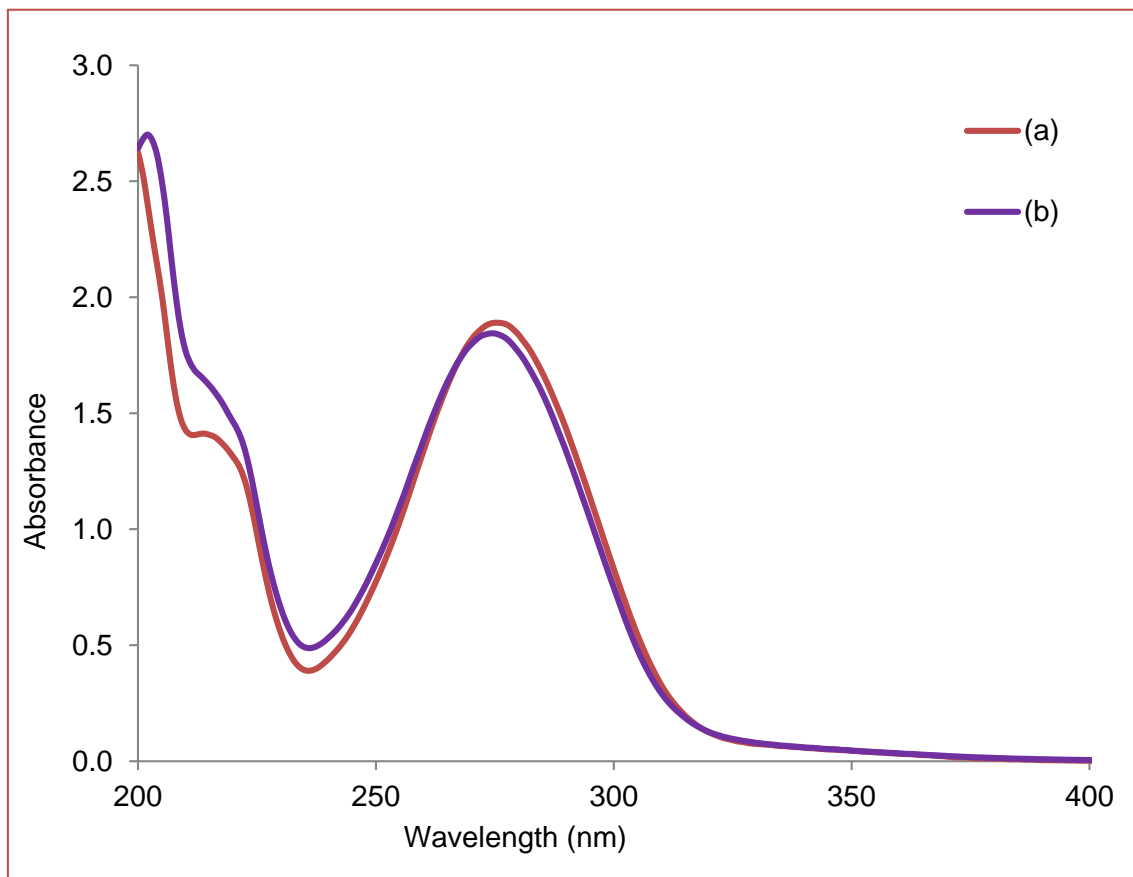
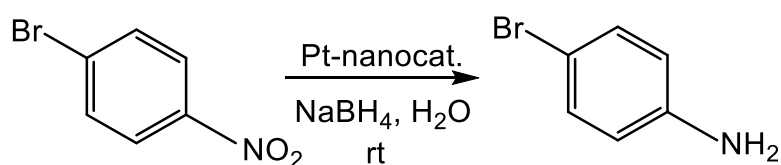


Figure 10. UV-visible spectra of the control experiment of *p*-bromonitrobenzene, no reduction was performed; (a) absorbance of *p*-bromonitrobenzene before reduction, and (b) absorbance of *p*-bromonitrobenzene after 40 min of performing the control experiment.



Scheme 4. The mechanism of hydride transfer for catalytic reduction of *p*-bromonitrobenzene by **PVA-ATB-Pt NPs** as a nanocatalyst.

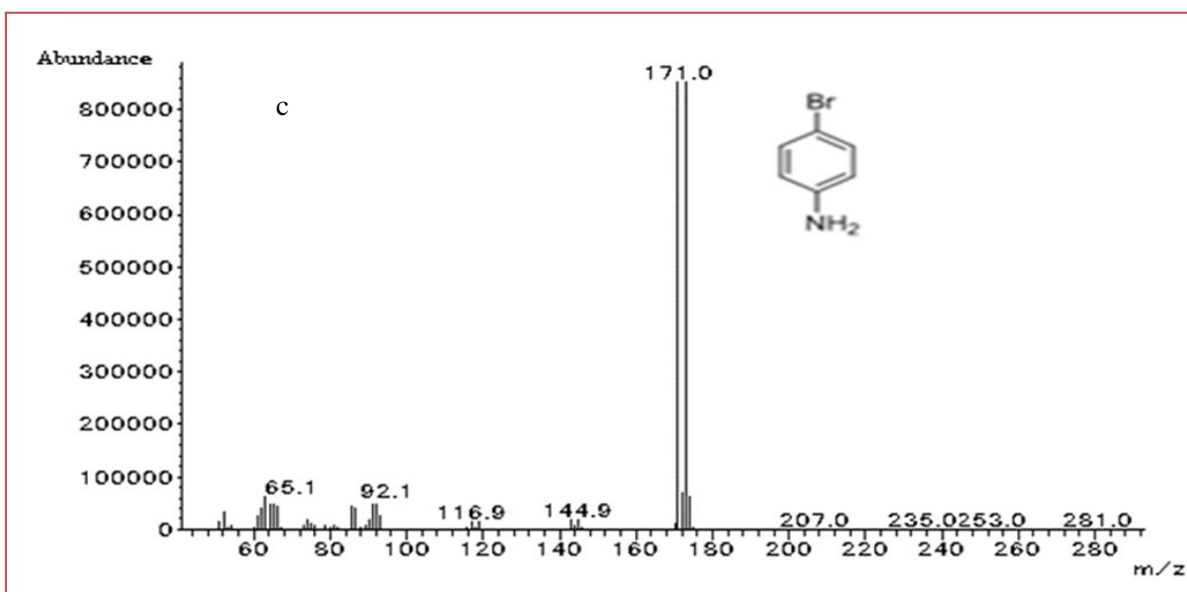
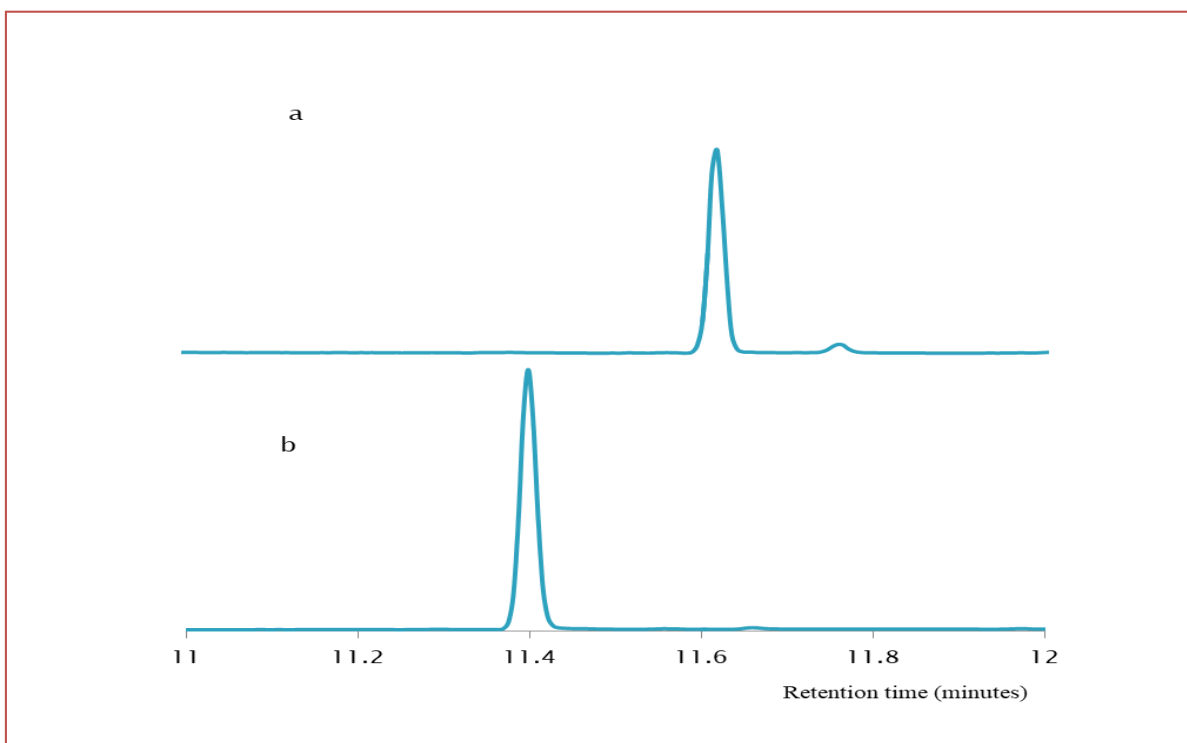


Figure 11. GCMS chromatographs after the catalytic reduction of *p*-bromonitrobenzene to *p*-bromoaniline by **PVA-ATB-Pt NPs**. (a) Chromatogram of *p*-bromonitrobenzene, (b) Chromatogram of the resulting product of the reaction (*p*-bromoaniline), and (c) Mass spectrometry of the peak at 11.4 min in (b).

Table 4. Displays the start and end retention time of the signals.

Molecules	Retention time (min)	Start time of the signal (min)	End time of the signal (min)
4-Bromonitrobenzene	11.61	11.58	11.69
4-Bromoaniline (the product)	11.40	11.36	11.44

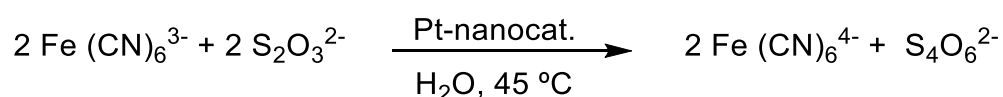
Little efforts have been paid to the reduction of *p*-bromonitrobenzene to *p*-bromoaniline, partly due to the difficulty to suppress the hydrodebromination reaction since the Br—C bond is more sensitive to reduction than the Cl—C bond.⁶¹⁻⁶⁴ In practice, some additives, either inhibitors or promoters, are added to the reaction in order to inhibit the hydrodehalogenation reaction.^{22,65-68} The prepared Pt NPs could catalyse the reduction of 4-bromonitrobenzene to *p*-bromoaniline without any additives. To the best of our knowledge, this is a rare example of the successive hydrogenation of *p*-bromonitrobenzene to *p*-bromoaniline with no concurrent hydrodebromination reaction (chemo-selective nanocatalyst) and without using any additives. This catalytic transformation of *p*-bromonitrobenzene to *p*-bromoaniline could be very beneficial in

pharmaceutical preparations. *p*-Bromoaniline is an essential compound for the preparation of biologically and medicinally active compounds such as anti-tumour, antimicrobial, and antimalarial agents as well as antihypertensive drugs.⁶⁹⁻⁷²

4.3.3.3: Nanocatalytic reduction of hexacyanoferrate (oxidation-reduction reaction, redox reaction)

The catalytic efficiency of the polymer stabilised Pt NP was also examined for inorganic nanocatalytic performance. The redox reaction between $\text{Na}_2 \text{S}_2\text{O}_3$ and $\text{K}_3 [\text{Fe} (\text{CN})_6]$ was successively carried out using the prepared Pt NPs as a nanocatalytic system. The thiosulphate was oxidised and hexacyanoferrate was reduced by the transfer of electrons from $\text{S}_2\text{O}_3^{2-}$ to $\text{Fe} (\text{CN})_6^{3-}$ in the presence of **PVA-ATB-Pt NPs** as a nanocatalyst for the mediation of this transfer as shown in scheme 5. From the results in Fig. 12, it is obvious that, the characteristic absorption peaks coming from $\text{K}_3 [\text{Fe}(\text{CN})_6]$ at 420 nm and 303 nm depleted with time due to reduction of $\text{K}_3 [\text{Fe}(\text{CN})_6]$ by accepting the electrons from $\text{S}_2\text{O}_3^{2-}$. The Pt NPs, which was used as a nanocatalyst, catalysed the transfer of electrons from $\text{S}_2\text{O}_3^{2-}$ to $\text{Fe} (\text{CN})_6^{3-}$. In the control experiment, the same experimental conditions were

utilised except instead of Pt NPs, water was used and almost no concurrent change was observed for the characteristic absorption peaks of $K_3 [Fe(CN)_6]$ at 420 nm and 303 nm (Fig. 13). The depletion of the characteristic absorbance peak at 420 nm was used to study the k_{app} of this redox reaction. The plot of $\ln (A_t/A_0)$ versus the reaction time was shown in the Fig. 14 and it was a linear relationship, which indicates that the reaction followed pseudo-first order kinetic. The k_{app} for this catalysed reaction was determined from the slope of the linear relationship between $\ln (A_t/A_0)$ and time. To the best of our knowledge, this is the second study for using of Pt NPs in catalysis of this oxidation-reduction reaction.⁵⁴ The K_{app} is $8.0 \times 10^{-4} s^{-1}$. This K_{app} is more than 4 folds than that of first study employed Pt NPs loaded on mesoporous alumina films with a $K_{app} = 1.4 \times 10^{-4} s^{-1}$.⁵⁴ It is noteworthy that our prepared nanocatalyst is more active and effective than Pt NPs loaded on mesoporous alumina films in the term of this catalysed redox reaction:



Scheme 5. The redox reaction between $Na_2 S_2O_3$ and $K_3 [Fe (CN)_6]$ PVA-ATB-Pt NPs as a nanocatalyst.

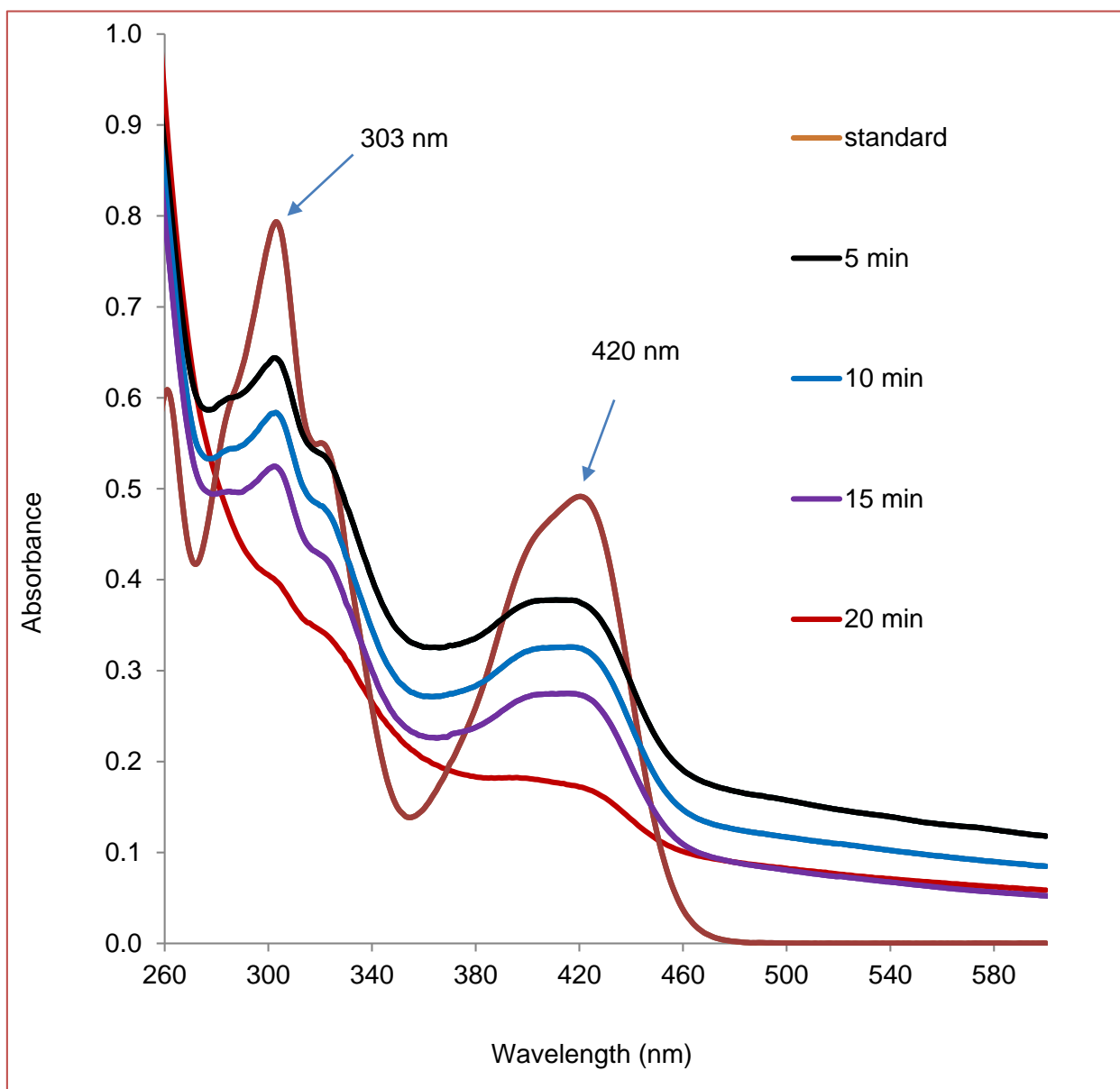


Figure 12. UV-visible spectra of the redox reaction display the depletion of the characteristic absorbance peaks of $K_3 [Fe (CN)_6]$ due to the reduction of $Fe (CN)_6^{3-}$ to $Fe (CN)_6^{4-}$ by the nanocatalyst.

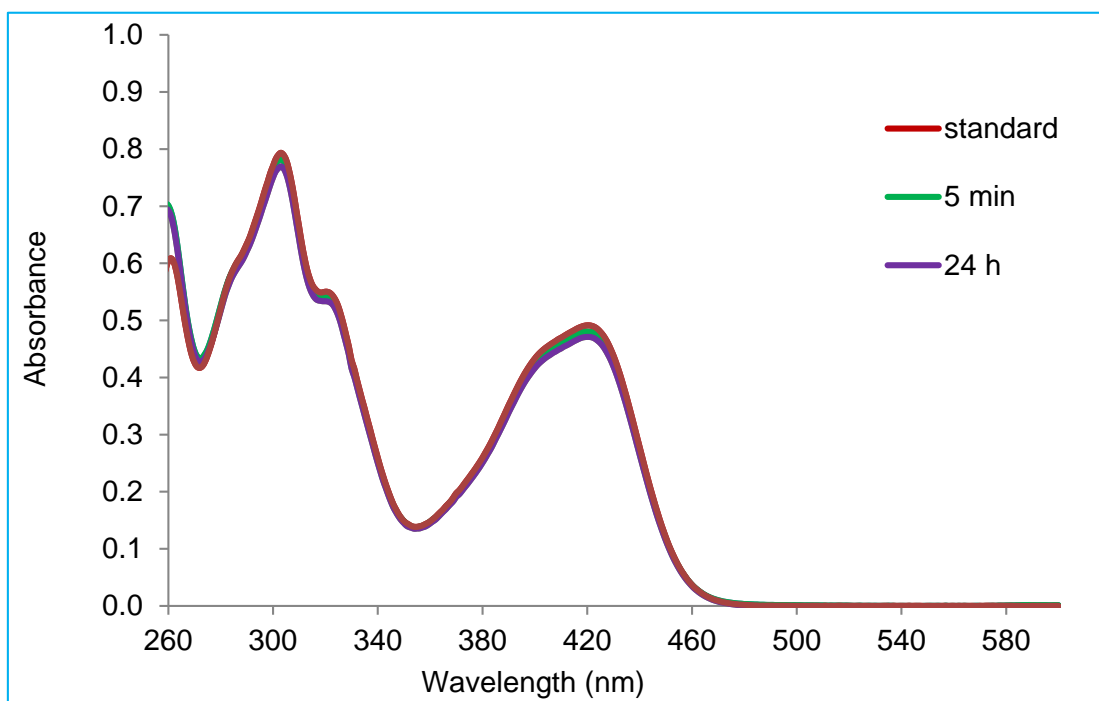


Figure 13. UV-visible spectra display the characteristic absorption peaks coming from $K_3 [Fe (CN)_6]$ at 420 nm and 303 nm. These peaks did not change in the control experiment (same conditions except water was used instead of Pt NPs).

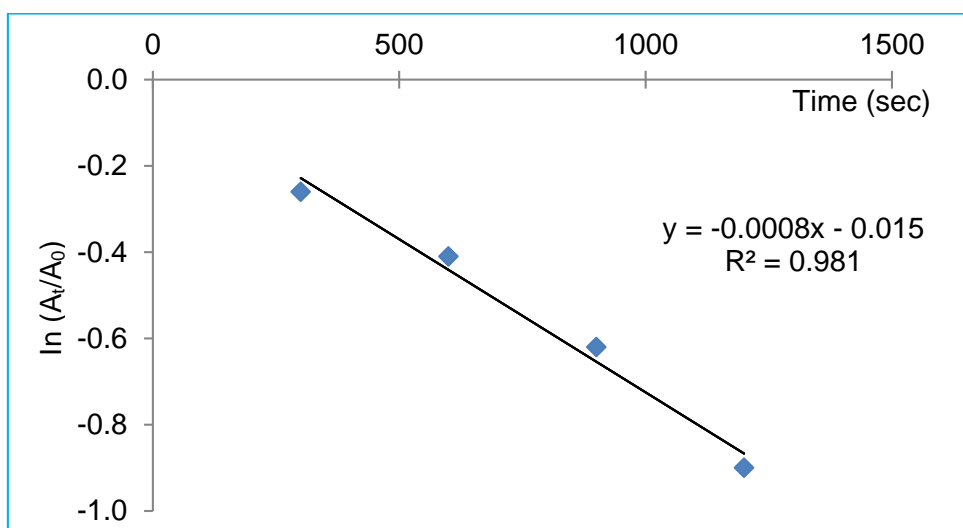


Figure 14. The plot of $\ln (A_t/A_0)$ at 420 nm versus the reaction time.

4.3.3.4: Carbon-carbon double bond reduction

4.3.3.4.1: Reduction of cinnamyl alcohol to hydrocinnamyl alcohol

GCMS was used to evaluate the hydrogenation of unsaturated cinnamyl alcohol to hydrocinnamyl alcohol. As shown in Fig. 15a, the signal coming from unsaturated cinnamyl alcohol appeared with a retention time of 12.1 min. Fig. 15b displays the appearance of a new signal with a retention time of 11.1 min, which is attributed to the hydrocinnamyl alcohol (reduced cinnamyl alcohol), at the same time, the signal coming from cinnamyl alcohol completely disappeared. These GCMS spectral changes attributed to the addition of hydrogen to carbon-carbon double bond of unsaturated cinnamyl alcohol by NaBH_4 , which is mediated by the nanocatalyst, and finally gave hydrocinnamyl alcohol. These GCMS results imply the successive reduction of cinnamyl alcohol to hydrocinnamyl alcohol. Fig. 16 shows mass spectroscopy of the resulted reduced cinnamyl alcohol, which confirms its molecular weight. To the best of our knowledge, this is the only work that uses monometallic nanoparticles (Pt NPs only), without alloy nanoparticles complex as a nanocatalyst, and successively hydrogenates cinnamyl alcohol to hydrocinnamyl alcohol. This confirms

the broad spectrum of activity the prepared nanocatalyst.

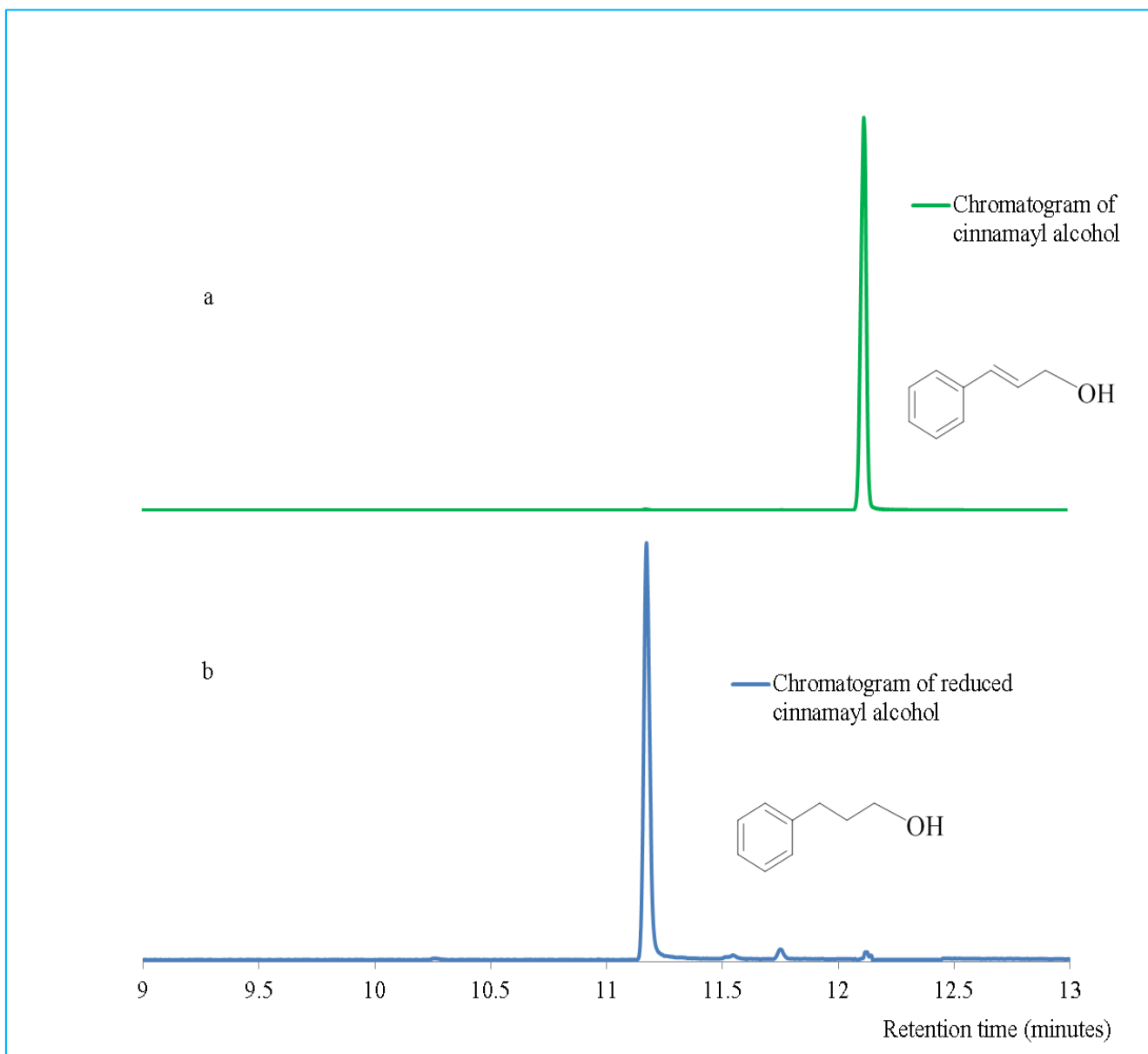


Figure 15. (a) Chromatogram of cinnamyl alcohol displays the retention time at 12.11min. (b) Chromatogram of reduced cinnamyl alcohol (the product) displays the retention time at 11.17 min.

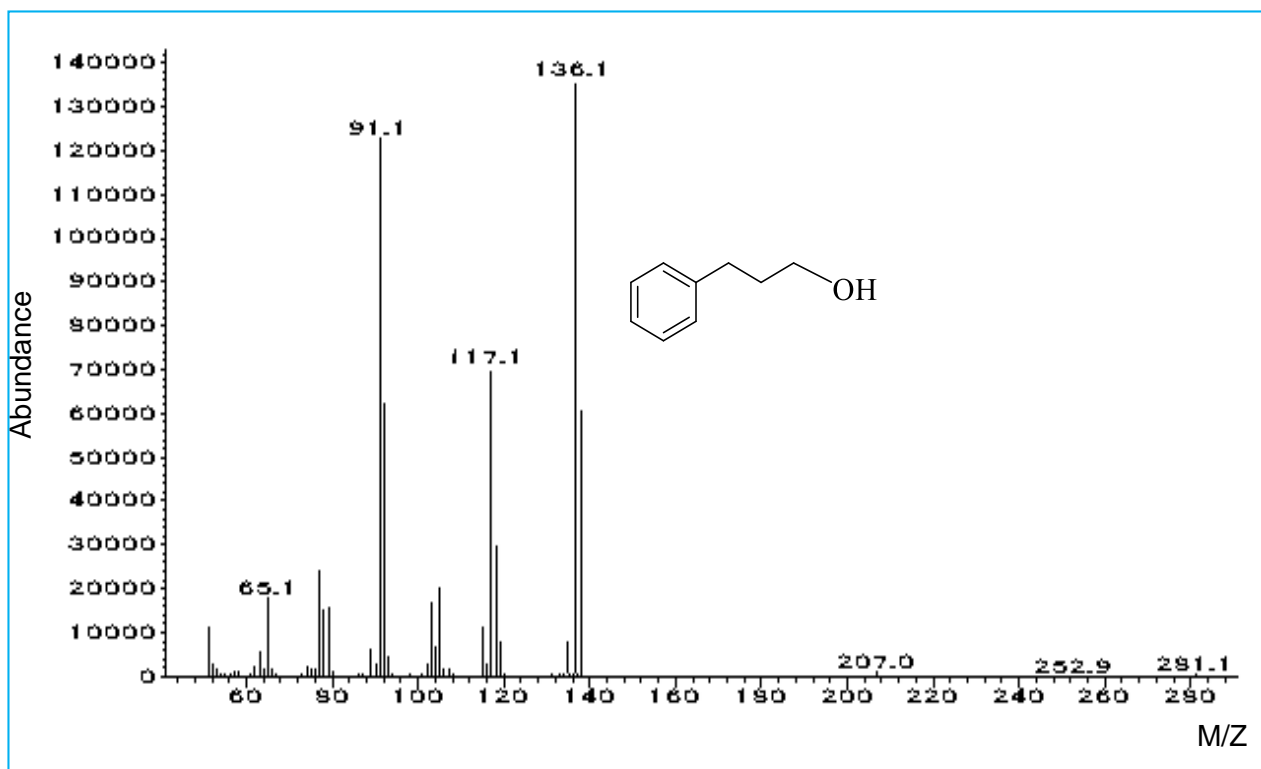


Figure 16. The mass spectroscopy of the resulted reduced cinnamyl alcohol which confirms its molecular weight.

4.3.3.4.2: Reductions of polyaromatic hydrocarbons (PAHS)

The evaluation of the nanocatalytic activity of Pt NPs for hydrogenation of anthracene as an example of PAHS was monitored by UV-visible spectroscopy. The anthracene solution has 3 characteristic absorbance peaks at 375 nm, 356 nm, and 339 nm, which completely depleted with time owing to the reduction of anthracene to its partially hydrogenated products where the absorbencies decreased gradually with time (Fig. 17). Fig. 18 indicates the time dependent absorbance of anthracene at 375 nm.

Fig. 19 displays the absence of any change in the anthracene peaks even after 30 min in the control experiments, which employed the same experimental conditions except that water was used instead of the nanocatalyst. It is noteworthy that the nanocatalyst was active under harsh reaction conditions. The nanocatalyst is not supported by other nanocomposites, as it comprises of only Pt NPs. The nanocatalyst could catalyse the nanocatalytic reduction of anthracene in a high amount (2.25 mmol, 1.50 M×1.50 mL) with the nanocatalyst amount of 0.47 mg and the

reaction completed within 30 min at 50 °C. Our results are in agreement with the results obtained by Jacinto *et al*⁷³ where they utilized Pt NPs supported by 12 nm magnetite nanocomposites coated with silica ($\text{Fe}_3\text{O}_4@\text{SiO}_2\text{-Pt}$) for the reduction of anthracene. However, they used a lower amount of anthracene (0.028 mmol, 0.0056 M \times 5.00 mL) compared with ours, catalyst amount was 100 mg, which is much higher than our prepared nanocatalyst and the reaction completed within 4 h at 75 °C. It is obvious that, our prepared nanocatalyst is more active and effective than the catalyst obtained by Jacinto *et al*.

PAHs are highly resistant to hydrogenation under mild experimental conditions same as the most of fused aromatic rings. Therefore, this nanocatalytic hydrogenation done by Pt NPs, as a nanocatalyst is very crucial for important conversion of toxic and carcinogenic PAHs into safe and less toxic materials, which can be used in pharmaceutical preparations.

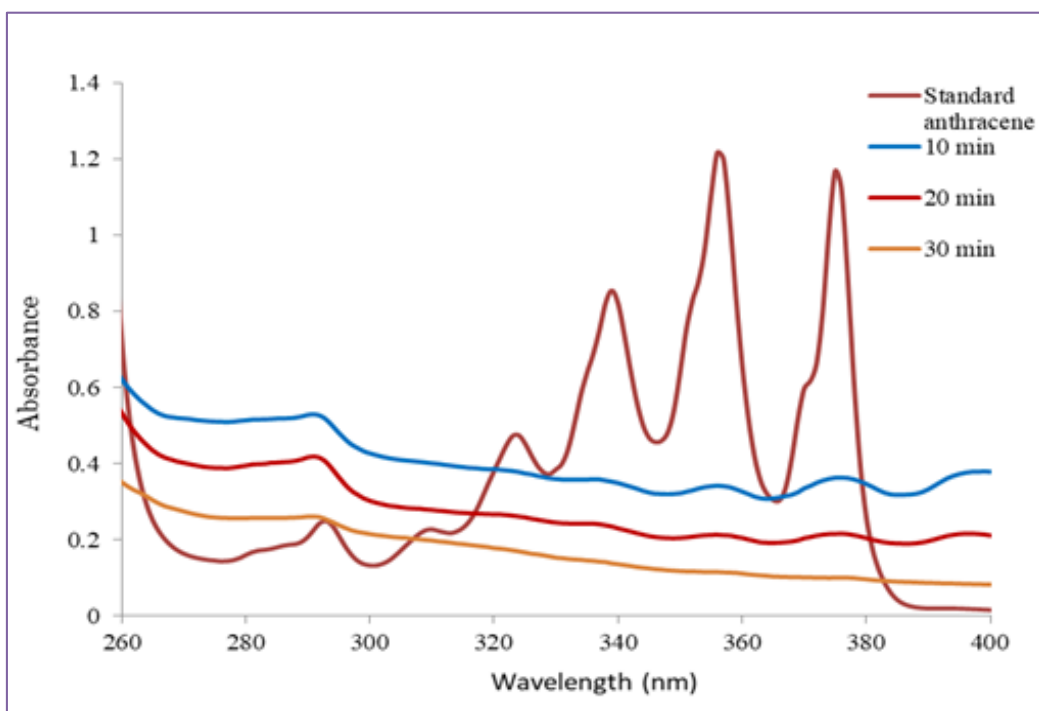


Figure 17. UV-visible spectra display the successive depletion of characteristic absorbance peaks of anthracene by using the prepared nanocatalyst.

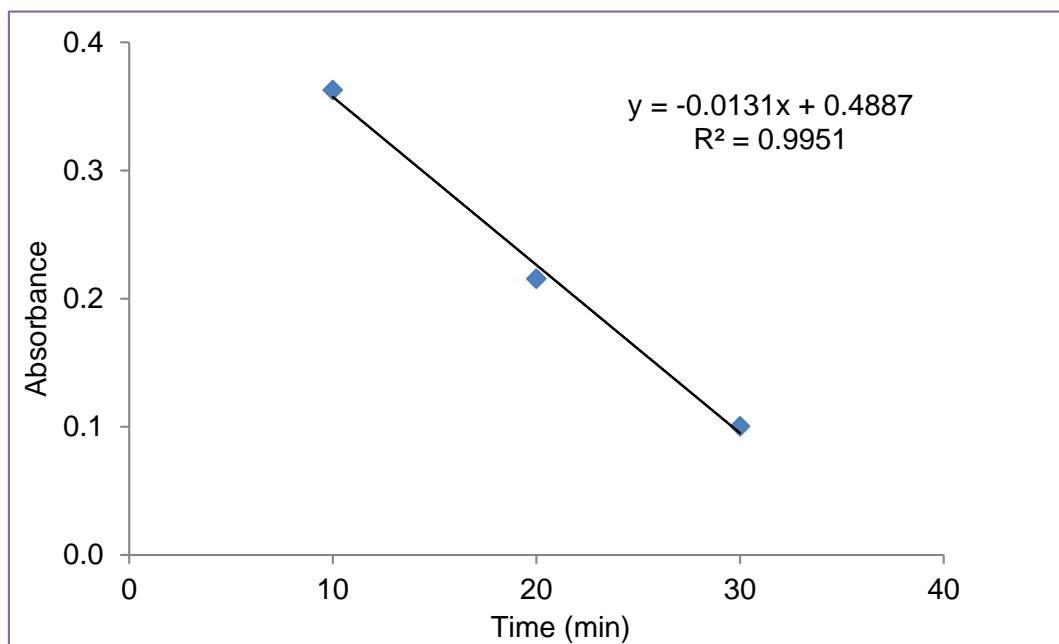


Figure 18. Time dependent absorbance of anthracene at 375 nm.

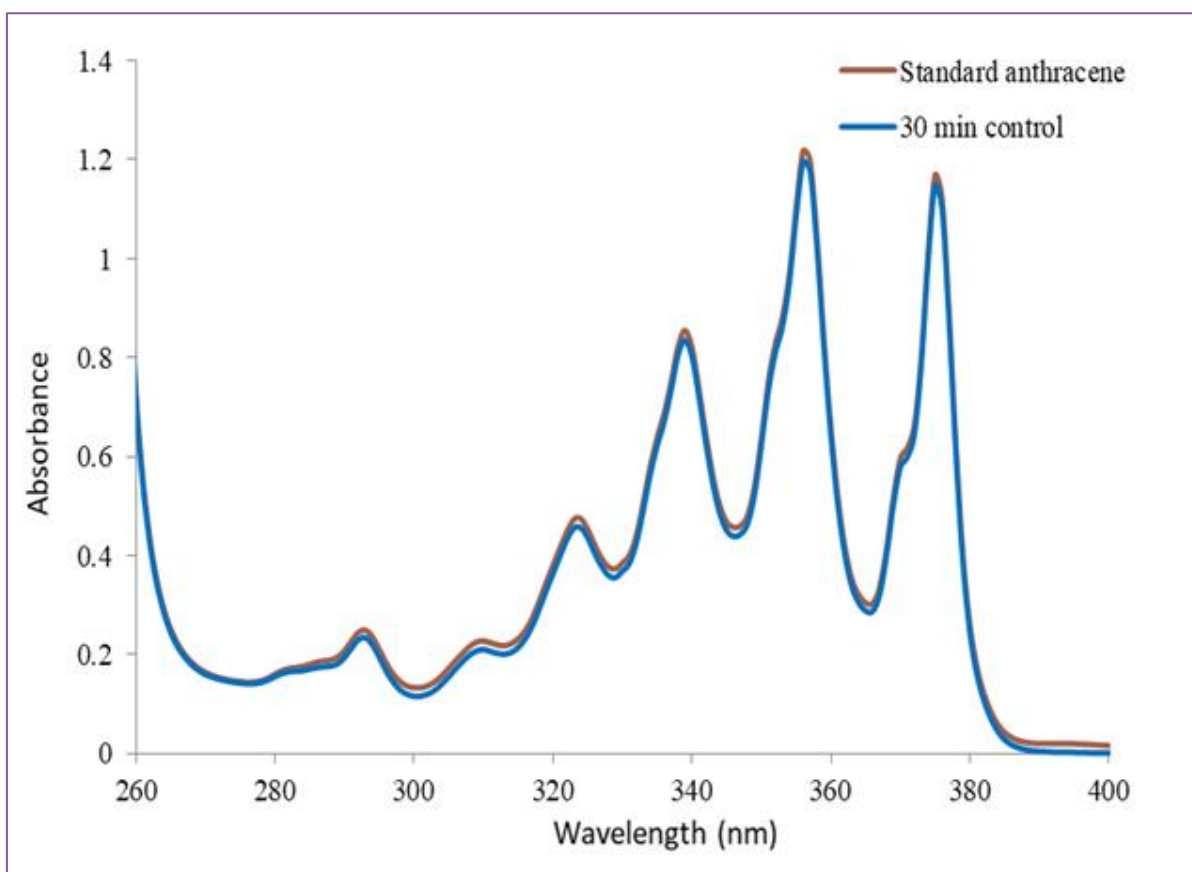


Figure 19. UV-visible spectra display the control experiment of anthracene reduction.

4.3.3.5: Nanocatalytic reduction of organic dyes

a. Methyl orange (MO)

The reduction of dyes is a purely irreversible catalytic process, and it was used to highlight the broad-spectrum catalytic activity of the prepared nanocatalyst. The reduction of MO was monitored by UV-visible spectroscopy. The aqueous solution of methyl orange dye has a characteristic absorbance peak at 464 nm. This peak completely disappeared after reaction of MO with NaBH₄ in the presence of Pt NPs as a nanocatalytic system, together with the disappearance of the orange colour of MO due to the reduction of azo group of methyl orange. Concurrently, a new peak appeared at 248 nm, which could be attributed to sulfanilic acid as a result of the breakdown of the azo bond. Therefore, we expected that sulfanilic acid is surely one of the resulting products of methyl orange reduction⁷⁴⁻⁷⁵ as it matched with the absorption spectrum of a standard solution sulfanilic acid (Fig. 20a). The control experiment was carried out to evaluate the reducing ability of NaBH₄ alone. Subsequently, the characteristic absorbance peak of MO at 464 nm had no absolute concurrent change. This was attributed to the fact the reduction did not

proceed without involvement of the nanocatalyst (control experiment used the same conditions, except water was used instead of the nanocatalyst) as indicated in Fig. 20b. The nanocatalytic process occurred on the surface of the Pt NPs, where both reactants are adsorbed and the electron transferred from the donor (NaBH_4) to the acceptor (MO) mediated by the nanoparticles, suggesting the reduction of azo group ($-\text{N}=\text{N}-$) of MO as shown in scheme 6. Therefore, the effective catalyst as platinum, silver, or gold nanoparticles should have a redox potential value located in between the electron donor and electron acceptor values to mediate the electron transfer. Thereby, the electron relay system will be facilitated by overcoming the kinetic barrier.⁷⁶

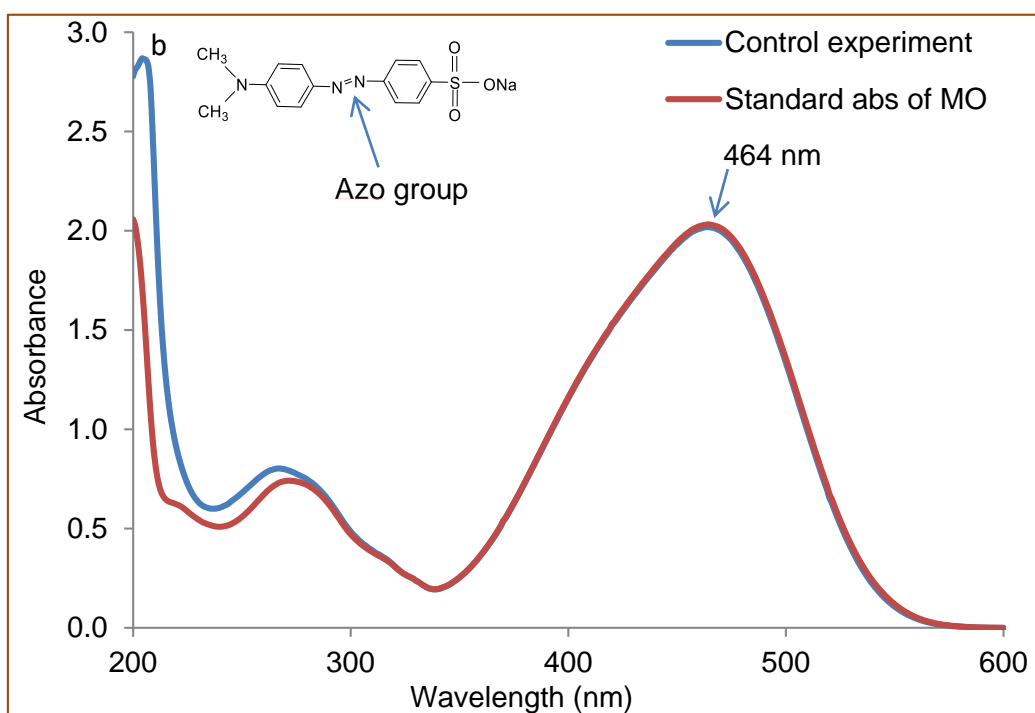
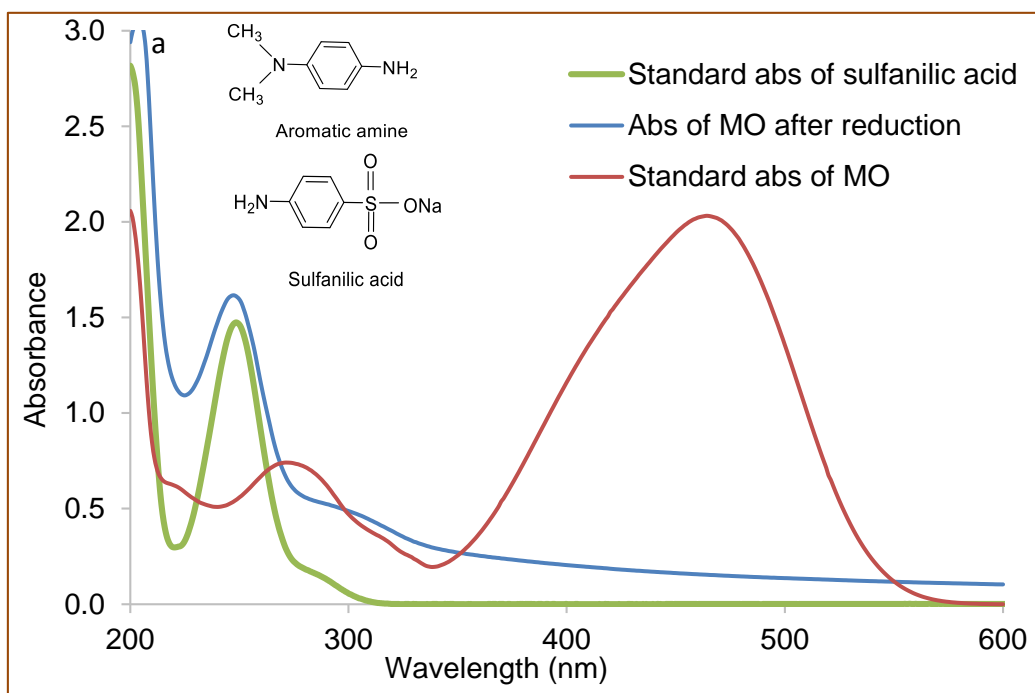
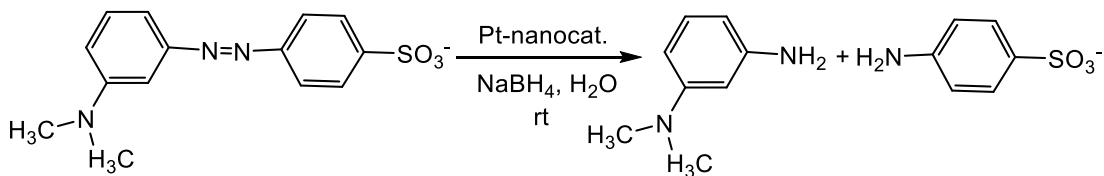


Figure 20. UV-visible spectra of organic dyes (MO) reduction, a: Degradation of the dye (nanocatalyst incorporation), b: No degradation of the dye without using the nanocatalyst (control experiment).



Scheme 6. Mechanism of catalytic reduction of methyl orange by

PVA-ATB-Pt NPs as a nanocatalyst.

As known, the organic dyes are soluble in water, organic solvent and it was revealed to be potentially toxic, carcinogenic with mutagenic effects.^{77,78} The organic dyes induce serious problems for the environment, ecosystem and aquatic organisms by interfering with the entrance of sunlight into the water^{79,80} due to its presence in the waste water of pharmaceutical plants. Therefore, there is a need to remove these dyes by introducing efficient, green and inexpensive methods to get rid of their serious effects. Waste water treatment includes physical-chemical, adsorption, and biological methods, however these methods are not green, and are ineffective because of aromatic structural stability of the dyes, and are expensive and time consuming as well.^{81,82} Recently, the breakdown of organic dyes by metal-based nanoparticles as a nanocatalyst has attracted attention. The metal nanoparticles catalyse the reduction by enhancing the

electron relaying system from the electron donor (NaBH_4) to the electron acceptor (organic dyes).⁸³ This method is an efficient degradation method, which is a green, rapid method for degradation of the pollutants and it gives degradable products such as aromatic amines, which are easily breakdown by microorganisms.^{84,85}

b. Methylene blue (MB)

Methylene blue is an aromatic heterocyclic chemical compound (3,7-bis(dimethylamino)-phenothiazin-5-iumchloride). The nanocatalytic experiment was monitored by the UV-visible spectroscopy. A freshly prepared aqueous solution of methylene blue (MB) has two characteristic absorbance peaks, the first peak appeared at 664 nm with a shoulder at 614 nm and the second peak appeared at 292 nm.⁸⁶ It is noteworthy that, in the absence of the nanocatalyst (control experiment), almost no concurrent changes occurred to the characteristic absorbance peaks of MB even after 3 h (Fig. 21) and it maintained its blue colour without change. These signs indicate that no concurrent reduction of MB occurred by utilising NaBH_4 only, without involvement of the nanocatalyst (control experiment). By the

contrast, after incorporation of the nanocatalyst in the reduction process as a nanocatalytic experiment, the two characteristic absorbance peaks completely depleted within 1 min after addition of the nanocatalyst as demonstrated by the UV-visible spectroscopy (Fig. 22) and visual notice of fading the characteristic blue colour of MB. These observations were suggesting the reduction of MB to leuco-methylene blue (LMB)^{87,88} and indicate the ability of the prepared nanocatalyst to catalyse the reduction of MB successively and effectively. The nanocatalyst acted as electron transport mediator from NaBH₄ to MB where the redox potential of the nanocatalyst was allocated in between the electron donor (NaBH₄) and electron acceptor (MB). Additionally, the nanocatalyst has decreased the activation energy of the reaction and thus, facilitate the transformation process.⁸⁹ This catalytic reduction of MB is a very crucial process as MB has harmful health hazards such as nausea, vomiting, diarrhoea, and breathing insufficiency,⁹⁰ therefore, it should be degraded by its reduction to avoid these hazards during the manipulation of the dye in pharmaceutical preparation. Table 5 indicates the comparative study of nanocatalytic efficiency between the as-prepared nanocatalyst and other nanocatalysts in

the reported literature in terms of the reductive hydrogenation of MO and MB organic molecules. This nanocatalytic difference indicates the high activity and affectivity of our prepared nanocatalyst.

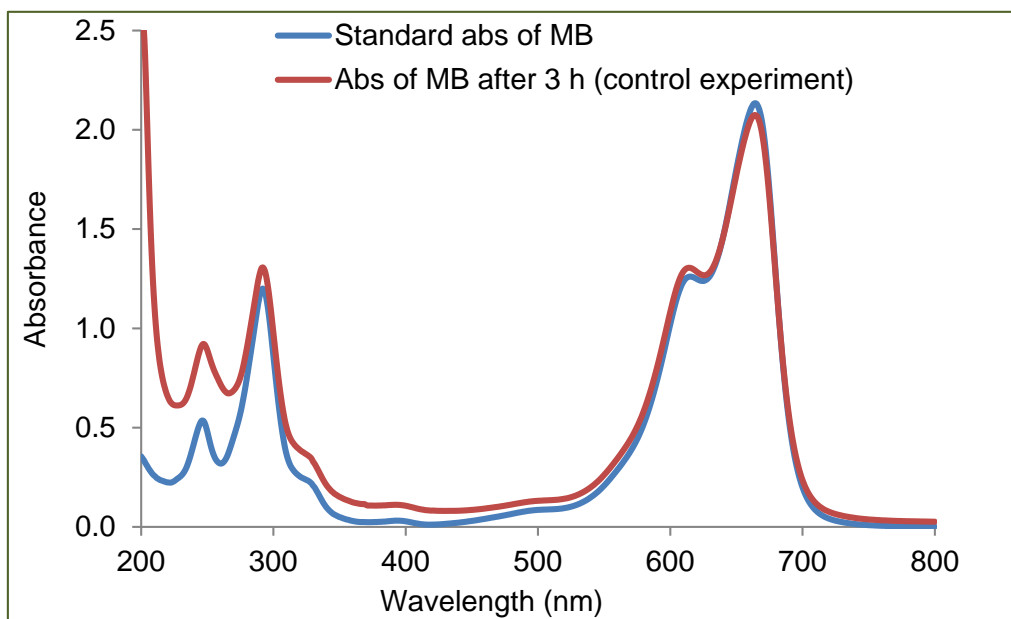


Figure 21. UV-vis absorption spectra of control experiment of MB reduction indicate no concurrent reduction in the absence of the nanocatalyst.

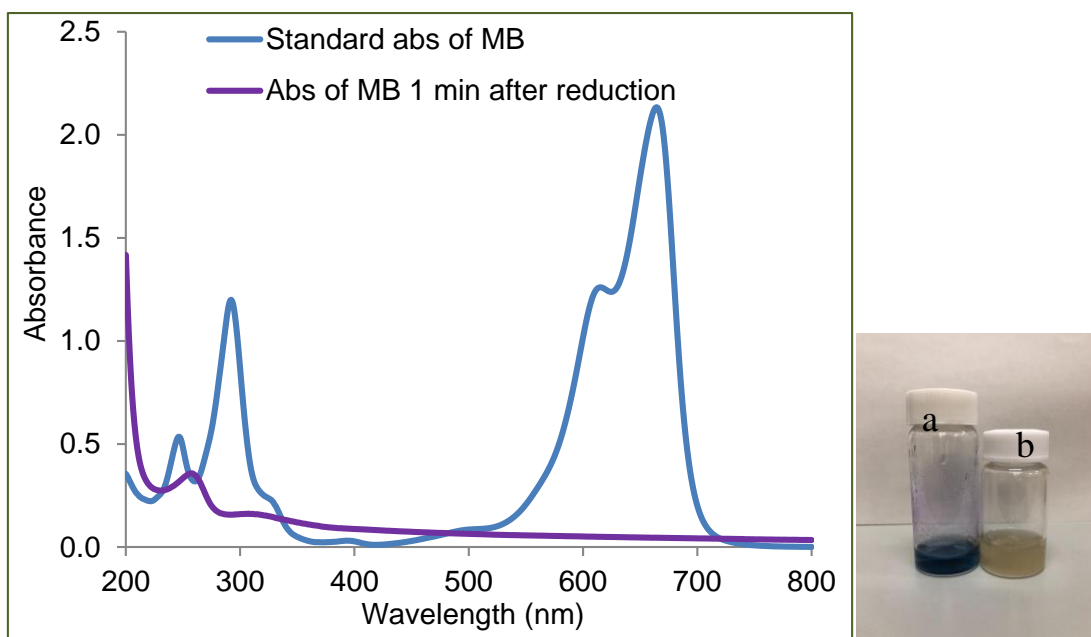


Figure 22. UV-vis absorption spectra of MB indicate successful reduction after addition of the nanocatalyst. The color of MB did not change in control experiment (a), while it faded in nanocatalytic experiment (b).

Table 5 indicates the comparative study of nanocatalytic efficiency between the as-prepared nanocatalyst and other nanocatalysts in the reported literature in terms of reductive hydrogenation of MO and MB organic molecules

Nanocatalyst	Substrate	Conc. (mM)	Moles of substrate	Moles of nanocatalyst	Nanocat. mole%	Turnover number (TON)	Time of reduction	Reference
Ag NPs	Methyl orange	3.05×10^{-2}	3.05×10^{-7}	5.88×10^{-6}	0.192	0.0518	24 h	91
Ag NPs	Methylene blue	3.12×10^{-2}	3.12×10^{-7}	5.88×10^{-6}	0.188	0.0530	24 h	91
Pt NPs	Methyl orange	3.00	3.00×10^{-6}	0.190×10^{-6}	0.000633	15.7	5 min	This work
Pt NPs	Methylene blue	10.0	10.0×10^{-6}	0.152×10^{-6}	0.000152	65.7	1 min	This work
Ag NPs	Methylene blue	10.0	10.0×10^{-5}	2.99×10^{-6}	0.000299	33.4	10 min	92

Table 5 (Continue)

Nanoatalyst	Substrate	Conc. (mM)	Moles of substrate	Moles of nanocatalyst	Nanocat. mole%	Turnover number (TON)	Time of reduction	Reference
Ag NPs and graphine oxide Ag NPs	MB	1.00×10^{-3}	1.50×10^{-9}	0.475×10^{-6}	3.16	0.00315	15 min (Ag NPs) and 30 min (GO-Ag NPs)	93
Biosynthesized Ag NPs	MO, MB	1.00	1.00×10^{-6}	5.81×10^{-7}	0.00581	1.72	7 min (MO) and 9 min (MB)	94
Ag NPs	MB	0.100	1.00×10^{-6}	1.71×10^{-6}	0.0171	0.583	20 min	95
β -Cyclodextrin coated Au nanochains	MB	3.00×10^{-2}	7.50×10^{-8}	1.20×10^{-7}	0.0160	0.625	12 min	96
Cu NPs loaded mesoporous silica SBA-15 (Cu@SBA-15)	MO	2.8×10^{-2}	63.0×10^{-8}	5.86×10^{-6}	0.0930	0.107	5.0 min	97
Cu@SBA-15	MB	9.00×10^{-2}	202×10^{-8}	5.86×10^{-6}	0.0290	0.344	8 min	97

4.4: Conclusion

In this study, an efficient, robust, chemo-selective, broad-spectrum, and recyclable Pt NPs catalyst was prepared. The **PVA–ATB** polymer was synthesised from acrylated PVA modified with *p*-aminothiobenzene. This polymer was used as a reductive stabiliser for the synthesis of the Pt NPs. This nanocatalyst was synthesised by a chemical reduction method formed of an organic (**PVA–ATB** polymer)-inorganic hybrid (Pt) system with an average particle size of 12.6 ± 5.7 nm. The nanocatalytic activity of the prepared nanocatalyst was evaluated in various experiments for nanocatalytic performance of these experiments and all of them returned with positive achievements with high efficiency and chemo-selectivity. All of the catalysed experiments are of great importance in pharmaceutical preparations, which indicates the potentiality and the promising applicability of the prepared nanocatalyst.

4.5: References

1. N. Pradhan, A. Pal, T. Pal, Silver nanoparticle catalyzed reduction of aromatic nitro compounds, *Colloids Surf. A*, **196** (2002) 247–257.
2. P. Zhao, X. Feng, D. Huang, G. Yang, D. Astruc, Basic concepts and recent advances in nitrophenol reduction by gold-and other transition metal nanoparticles, *Coord. Chem. Rev.*, **287** (2015) 114–136.
3. S. Wunder, Y. Lu, M. Albrecht, M. Ballauff, Catalytic activity of faceted gold nanoparticles studied by a model reaction: evidence for substrate-induced surface restructuring, *ACS Catal.*, **1** (2011) 908–916.
4. S. Panigrahi, S. Basu, S. Praharaj, S. Pande, S. Jana, A. Pal, S. Kumar Ghosh, T. Pal, Synthesis and Size-Selective Catalysis by Supported Gold Nanoparticles: Study on Heterogeneous and Homogeneous Catalytic Process, *J. Phys. Chem. C*, **111** (2007) 4596–4605.
5. J. J. Lv, A. J. Wang, X. Ma, R.Y. Xiang, J. R. Chen, J. J. Feng, One-pot synthesis of porous Pt–Au nanodendrites supported on reduced graphene oxide nanosheets toward catalytic reduction of 4-nitrophenol, *J. Mater. Chem., A*, **3** (2015) 290–296.
6. X. Q. Huang, Y. J. Li, H. L. Zhou, X. Zhong, X. F. Duan, Y. Huang, Simplifying the creation of dumbbell-like Cu-Ag nanostructures and their enhanced catalytic activity, *Chemistry-A European Journal*, **18** (2012) 9505–9510.

-
7. F. Bonet, V. Delmas, S. Grugeon, R. H. Urbina, P. Y. Silvert, K. T. Elhsissen, Synthesis of monodisperse Au, Pt, Pd, Ru and Ir nanoparticles in ethylene glycol, *Nanostruct. Mater.*, **11** (1999) 1277–1284.
 8. V. Vetere, A. B. Merlo, M. L. Casella, Chemoselective hydrogenation of aromatic ketones with Pt-based heterogeneous catalysts. Substituent effects, *Appl. Catal., A*, **491** (2015) 70–77.
 9. A. Corma, H. Garcia, Supported gold nanoparticles as catalysts for organic reactions, *Chemical Society Reviews*, **37** (2008) 2096–2126.
 10. J. A. LopezSanchez, N. Dimitritos, C. Hammond, G. L. Brett, L. Kesavan, S. White, P. Miedziak, R. Tiruvalam, R. L. Jenkins, A. F. Carley, D. Knight, C. J. Kiely, J. Hutchings, Facile removal of stabilizer-ligands from supported gold nanoparticles, *Nature Chemistry*, **3** (2011) 551–556.
 11. N. Zheng, G. D. Stucky, A General Synthetic Strategy for Oxide-Supported Metal Nanoparticle Catalysts, *Journal of the American Chemical Society*, **128** (2006) 14278–14280.
 12. Y. Zhu, H. Qian, B. A. Drake, R. Jin, Atomically precise Au₂₅(SR)₁₈ nanoparticles as catalysts for the selective hydrogenation of alpha,beta-unsaturated ketones and aldehydes, *Angewandte Chemie International Edition*, **49** (2010) 1295–1298.
 13. A. Abad, P. Concepcion, A. Corma, H. Garcia, A Collaborative Effect between Gold and a Support Induces the Selective Oxidation of Alcohols, *Angewandte Chemie International Edition*, **44** (2005) 4066–4069.

-
14. C. G. Long, J. D. Gilbertson, G. Vijayaraghavan, K. J. Stevenson, C. J. Pursell, B. D. Chandler, Kinetic Evaluation of Highly Active Supported Gold Catalysts Prepared from Monolayer-Protected Clusters: An Experimental Michaelis–Menten Approach for Determining the Oxygen Binding Constant during CO Oxidation Catalysis, *Journal of the American Chemical Society*, **130** (2008) 1010–1015.
15. M. Comotti, W-C. Li, B. Spliethoff, F. Schuth, Support Effect in High Activity Gold Catalysts for CO Oxidation, *Journal of the American Chemical Society*, **128** (2006) 917–924.
16. X. Zhang, H. Shi, B-Q. Xu, Catalysis by Gold: Isolated Surface Au³⁺ Ions are Active Sites for Selective Hydrogenation of 1,3 - Butadiene over Au/ZrO₂ Catalysts, *Angewandte Chemie International Edition*, **44** (2005) 7132–7135.
17. Z-P. Liu, C-M. Wang, K-N. Fan, Single Gold Atoms in Heterogeneous Catalysis: Selective 1,3 - Butadiene Hydrogenation over Au/ZrO₂, *Angewandte Chemie International Edition*, **45** (2006) 6865–6868.
18. A. Horvath, A. Beck, G. Stefler, T. Benko, G. Safran, Z. Varga, J. Gubicza, L. Gucci, Silica-Supported Au Nanoparticles Decorated by CeO₂: Formation, Morphology, and CO Oxidation Activity, *Journal of Physical Chemistry C*, **115** (2011) 20388–20398.
19. A. Horvath, A. Beck, A. Sarkany, G. Stefler, Z. Varga, O. Geszti, L.

Toth, L. Guzzi, Silica-Supported Au Nanoparticles Decorated by TiO₂: Formation, Morphology, and CO Oxidation Activity, *Journal of Physical Chemistry B*, **110** (2006) 15417–15425.

20. F. Xiao, F. Wang, X. Fu, Y. Zheng, A green and facile self-assembly preparation of gold nanoparticles/ZnO nanocomposite for photocatalytic and photoelectrochemical applications, *Journal of Materials Chemistry*, **22** (2012) 2868–2877.

21. Y. Y. Chen, C. Wang, H. Y. Liu, J. S. Qiu, X. H. Bao, Ag/SiO₂: a novel catalyst with high activity and selectivity for hydrogenation of chloronitrobenzenes, *Chem. Commun.*, **42** (2005) 5298–5300.

22. X. H. Yan, J. Q. Sun, Y. W. Wang, J. F. Yang, A Fe-promoted Ni–P amorphous alloy catalyst (Ni–Fe–P) for liquid phase hydrogenation of *m*- and *p*-chloronitrobenzene, *J. Mol. Catal. A*, **252** (2006) 17–22.

23. X. X. Han, R. X. Zhou, G. H. Lai, X. M. Zheng, Influence of support and transition metal (Cr, Mn, Fe, Co, Ni and Cu) on the hydrogenation of *p*-chloronitrobenzene over supported platinum catalysts, *Catal. Today*, **93–95** (2004) 433–437.

24. X. X. Han, R. X. Zhou, G. H. Lai, X. M. Zheng, Influence of alloying platinum for the hydrogenation of chloronitrobenzene over PtM/ZrO₂ catalysts with M=Cr, Mn, Fe, Co, Ni, Cu, *React. Kinet. Catal. Lett.*, **83** (2004) 55–61.

25. W. W. Yu, H. F. Liu, Singular modification effects of metal cations and

metal complex ions on the catalytic properties of metal colloidal nanocatalysts, *J. Mol. Catal. A*, **243** (2006) 120–141.

26. M. H. Liu, B. L. He, H. F. Liu, X. P. Yan, Unexpected effects of trace impurities on the properties of polymer-stabilized ruthenium colloids from different sources of ruthenium(III) chloride hydrate, *J. Colloid Interf. Sci.*, **263** (2003) 461–466.

27. J. Wiss, A. Zilian, Online Spectroscopic Investigations (FTIR/Raman) of Industrial Reactions: Synthesis of TributyltinAzide and Hydrogenation of Chloronitrobenzene, *Org. Process Res. Dev.*, **7** (2003) 1059–1066.

28. M. Benz, A.M. Draan, R. Prins, Reduction of aromatic nitrocompounds with hydrazine hydrate in the presence of an iron oxide hydroxide catalyst: II. Activity, X-ray diffraction and Mössbauer study of the iron oxide hydroxide catalyst, *Appl. Catal. A*, **172** (1998) 149–157.

29. S. Saha, A. Pal, S. Kundu, S. Basu, T. Pal, Photochemical green synthesis of calcium-alginate-stabilized Ag and Au nanoparticles and their catalytic application to 4-nitrophenol reduction, *Langmuir*, **26** (2010) 2885–2893.

30. H. Cheng, C. Xi, X. Meng, Y. Hao, Y. Yu, F. Zhao, Polyethylene glycol-stabilized platinum nanoparticles: The efficient and recyclable catalysts for selective hydrogenation of o-chloronitrobenzene to o-chloroaniline, *Journal of Colloid and Interface Science*, **336** (2009) 675–678.

-
31. Z. Liu, X. Y. Ling, J. Y. Lee, X. Su, L. M. Gan, Nanosized Pt and Pt Ru colloids as precursors for direct methanol fuel cell catalysts, *J. Mater. Chem.*, **13** (2003) 3049–3052.
32. G. De, C. N. R. Rao, Au–Pt alloy nanocrystals incorporated in silica films, *J. Mater. Chem.*, **15** (2005) 891–894.
33. W. Siriwatcharapiboon, N. Tinnarat, P. Supaphol, Preparation and characterization of electrospun poly(vinyl alcohol) nanofibers containing platinum or platinum-ruthenium nanoparticles, *J Polym Res*, **40** (2013) 1–8.
34. R. M. Crooks, M. Zhao, L. Sun, V. Chechik, L. K. Yeung, Dendrimer-Encapsulated Metal Nanoparticles: Synthesis, Characterization, and Applications to Catalysis, *Acc. Chem. Res.*, **34** (2001) 181–190.
35. J. J. Elliott, S. F. Mason, The heats and entropies of ionization of of some aromatic and N-heteroaromatic amines, *J. Chem. Soc.*, (1959) 2352–2359.
36. X. Ji, X. Song, J. Li, Y. Bai, W. Yang, X. Peng, Size Control of Gold Nanocrystals in Citrate Reduction: The third role of citrate, *J. Am. Chem. Soc.*, **129** (2007) 13939–13948.
37. D. V. Goia, E. Matijevic, Tailoring the particle size of monodispersed colloidal gold, *Colloids Surf. A*, **146** (1999) 139–152.
38. K. Hayakawa, T. Yoshimura, K. Esumi, Preparation of gold dendrimer nanocomposites by laser irradiation and their catalytic reduction of 4-nitrophenol, *Langmuir*, **19** (2003) 5517–5521.

-
39. B. J. Lee, J. C. Park, H. Song, A nanoreactor framework of a Au@SiO₂ yolk/shell structure for catalytic reduction of p-nitrophenol, *Adv. Mater.*, **20** (2008) 1523–1528.
40. S. K. Ghosh, M. Mandal, S. Kundu, S. Nath, T. Pal, Bimetallic Pt–Ni nanoparticles can catalyze reduction of aromatic nitro compounds by sodium borohydride in aqueous solution, *Appl. Catal. A*, **268** (2004) 61–66.
41. J. M. Thomas, W. J. Thomas, Introduction to the principles of heterogenous catalysis, Academic Press, London (1967).
42. T. M. Abdel-fattah, A. Wixtrom, Catalytic reduction of 4-nitrophenol using gold nanoparticles supported on carbon nanotubes, *ECS journal of Solid State Science and Technology*, **3** (2014) 18–20.
43. Y. Chi, Q. Yuan, Y. Li, J. Tu, L. Zaho, N. Li, X. Li, Synthesis of Fe₃O₄@SiO₂-Agmagnetic nanocomposite based on small-sized and highly dispersed silver nanoparticles for catalytic reduction of 4-nitrophenol, *J. Colloid and Interface science*, **383** (2012) 96–102.
44. Y. Mei, G. Sharma, Y. Lu, M. Ballauff, High Catalytic Activity of Platinum Nanoparticles Immobilized on Spherical Polyelectrolyte Brushes, *Langmuir*, **21** (2005) 12229–12234.
45. K. Xiang, C. Hongliang, L. Chang, C. Xin, One step photochemical synthesis of clean surfaced sponge-like porous platinum with high catalytic performances, *Journal of Colloid and Interface Science*, **487** (2017) 60–67.
46. P. Sadanand, B. M. Shivani, Catalytic reduction of p-nitrophenol by

using platinum nanoparticles stabilized by guar gum, *Carbohydrate Polymer*, **113** (2014) 525–531.

47. J. Deli, X. Jimin, C. Min, L. Di, Z. Jianjun, Q. Huiru, Facile route to silver submicron-sized particles and their catalytic activity towards 4-nitrophenol reduction, *J. alloys Compd.*, **509** (2011) 1975–1979.

48. C. Rizhi, W. Qinqin, D. Yan, X. Weihong, X. Nanping, Effect of initial solution apparent pH on nano-sized nickel catalysts in p-nitrophenol hydrogenation, *Chem. Eng. Journal*, **145** (2009) 371–376.

49. H. Jafar, R. Mehdi, B. Mehrangiz, Platinum nanostructures at the liquid-liquid interface: catalytic reduction of *p*-nitrophenol to *p*-aminophenol, *J. Mater. Chem.*, **21** (2011) 16170–16176.

50. K. Esumi, R. Isono, T. Yoshimura, Preparation of PAMAM-and PPI metal (silver, platinum and palladium) nanocomposites and their catalytic activities for reduction of 4-nitrophenol, *Langmuir*, **20** (2004) 237–243.

51. S. K. Ghosh, M. Mandal, S. Kundu, S. Nath, T. Pal, Bimetallic Pt–Ni nanoparticles can catalyze reduction of aromatic nitro compounds by sodium borohydride in aqueous solution, *Appl. Catal., A*, **268** (2004) 61–66.

52. I. K. Sen, K. Maity, S. S. Islam, Green synthesis of gold nanoparticles using a glucan of an edible mushroom and study of catalytic activity, *Carbohydrate Polymers*, **91** (2013) 518–528.

-
53. F. Agata, R. Jacek, K. Oleksandr, S. Magdalena, Kinetic studies of catalytic reduction of 4-nitrophenol with NaBH_4 by means of Au nanoparticles dispersed in a conducting polymer matrix, *J. Solid State Electrochem.*, **19** (2015) 2849–2858.
54. A. Dandapat, D. Jana, G. De, Synthesis of thick mesoporous γ -alumina films, loading of Pt nanoparticles and use of the composite film as a reusable catalyst, *ACS Appl. Mater. Interfaces*, **1** (2009) 833–840.
55. R. Nazir, P. Fageria, M. Basu, S. Gangopadhyay, S. Pande, Decoration of Pd and Pt nanoparticles on a carbon nitride (C_3N_4) surface for nitro-compounds reduction and hydrogen evolution reaction, *New J. Chem.*, **41** (2017) 9658–9667.
56. M. H. Rashid, T. K. Mandal, Synthesis and catalytic application of nanostructured silver dendrites, *J. Phys. Chem. C*, **111** (2007) 16750–16760.
57. J. Zhang, G. Chen, M. Chaker, F. Rosei, D. Ma, Gold nanoparticle decorated ceria nanotubes with significantly high catalytic activity for the reduction of nitrophenol and mechanism study, *Appl. Catal. B*, **132** (2013) 107–115.
58. P. K. Sahoo, B. Panigrahy, D. Bahadur, Facile synthesis of reduced graphene oxide/Pt–Ni nanocatalysts: Their magnetic and catalytic properties, *RSC Adv.*, **4** (2014) 48563–48571.
59. J. Wang, X-B. Zhang, Z-L. Wang, L-M. Wang, W. Xing, X. Liu,

One-step and rapid synthesis of “clean” and monodisperse dendritic Pt nanoparticles and their high performance toward methanol oxidation and p-nitrophenol reduction, *Nanoscale*, **4** (2012) 1549–1552.

60. Niu, Z., Zhang, S., Sun, Y., Gai, S.; He, F.; Dai, Y.; Li, L.; Yang, P. Controllable synthesis of Ni/SiO₂ hollow spheres and their excellent catalytic performance in 4-nitrophenol reduction, *Dalton Trans.*, **43** (2014) 16911–16918.

61. R. Baltzly, A. P. Phillips, The Catalytic Hydrogenolysis of Halogen Compounds, *J. Am. Chem. Soc.*, **68** (1946) 261–265.

62. A. M. Stratz, J.R. Kosak (Ed.), *Catalysis of Organic Reactions*, Dekker, New York, 1984, 335–375.

63. W. Pascoe, P. N. Rylander (Ed.), *Catalysis of Organic Reactions*, Dekker, New York, 1988, 121–134.

64. H. Greenfield, F. S. Dovell, Metal sulfide catalysts for hydrogenation of halonitrobenzenes to haloanilines, *J. Org. Chem.*, **32** (1967) 3670–3671.

65. J. R. Kosak, Catalytic Hydrogenation of Aromatic Halo nitro Compounds, *Acad. Sci. Ann.*, **172** (1970) 175–185.

66. X. X. Han, R. X. Zhou, X. M. Zheng, H. Jiang, Effect of rare earths on the hydrogenation properties of p-chloronitrobenzene over polymer-anchored platinum catalysts, *J. Mol. Catal. A*, **193** (2003) 103–108.

-
67. X. X. Han, R. X. Zhou, G. h. Lai, B. h. Yue, X. M. Zheng, Effect of transition metal (Cr, Mn, Fe, Co, Ni and Cu) on the hydrogenation properties of chloronitrobenzene over Pt/TiO₂ catalysts, *J. Mol. Catal. A*, **209** (2004) 83–87.
68. P. Kapa, T. L. George, C. Apurva, J. G. Michael, W. S. James, R. Oljan, Design of New Reaction Conditions for the Sugasawa Reaction Based on Mechanistic Insights, *Org. Process Res. Dev.*, **7** (2003) 723–732.
69. F. Ralf, W. K. R. M. Wemer, A Convenient Synthetic Route to Spiro [indole-3,4'-piperidin]-2-ones, *Helv. Chim. Acta*, **83** (2000) 1247–1255.
70. G. Aleem, Y. Jie, A. I. Michael, K. Shekhar, Antiangiogenic and antitumor agents: Design, synthesis, and evaluation of novel 2-amino-4-(3-bromoanilino)-6-benzyl substituted pyrrolo[2,3-*d*] pyrimidines as inhibitors of receptor tyrosine kinases, *Bioorg. Med. Chem.*, **11** (2003) 5155–5170.
71. D. H. Beata, M. Katrien, E. Oliver, K. Laszlo, T. Pal, U. W. M. Bert, R. Zsuzsanna, H. Gyorgy, A. D. Roger, L. F. L. Guy, K. Janez, M. Peter, Synthesis of 5*H*-pyridazino[4,5-*b*]indoles and their benzofurane analogues utilizing an intramolecular Heck-type reaction, *Tetrahedron*, **60** (2004) 2283–2291.
72. H. Steven, U. W. M. Bert, P. Luc, L. F. L. Guy, M. Peter, H. Gyorgy, A. D. Roger, Synthesis of the benzo- β -carbolineisoneocryptolepine: the missing indoloquinoline isomer in the alkaloid series cryptolepine,

neocryptolepine and isocryptolepine, *Tetrahedron*, **61** (2005) 1571–1577.

73. M. J. Jacinto, M. Wizbiki, L. C. Justino, V. C. Silva, Platinum-supported mesoporous silica of facile recovery as a catalyst for hydrogenation of polyaromatic hydrocarbons under ultra-mild conditions, *J. Sol-Gel Sci Technol.*, **77** (2016) 298–305.

74. J. Fan, Y. Guo, J. Wang, M. Fan, Rapid decolorization of azo dye methyl orange in aqueous solution by nanoscale zerovalent iron particles, *J. Hazard. Mater.*, **166** (2009) 904–910.

75. A. K. Ilunga, T. Khoza, E. Tjabadi, R. Meijboom, Effective Catalytic Reduction of Methyl Orange Catalyzed by the Encapsulated Random Alloy Palladium-Gold Nanoparticles Dendrimer, *Chemistry Select*, **2** (2017) 9803–9809.

76. K. Mallick, M. Witcomb, M. Scurrall, Silver nanoparticle catalysed redox reaction: An electron relay effect, *Mater. Chem. Phys.*, **97** (2006) 283–287.

77. G. A. Umbuzeiro, H. S. Freeman, S. H. Warren, D. P. D. Oliveira, Y. Terao, T. Watanabe, L. D. Claxton, The contribution of azo dyes to the mutagenic activity of the Cristais River, *Chemosphere*, **60** (2005) 55–64.

78. R. O. A. Lima, A. P. Bazo, D. M. F. Salvadori, C. M. Rech, D. P. D. Oliveira, G. A. Umbuzeiro, Mutagenic and carcinogenic potential of a textile azo dye processing plant effluent that impacts a drinking water source, *Mutat. Res. Toxicol. Environ. Mutagen*, **626** (2007) 53–60.

-
79. V. K. Gupta, S. Khamparia, I. Tyagi, D. Jaspal, A. Malviya, Decolorization of mixture of dyes: A critical review, *Glob. J. Environ. Sci. Manag.*, **1** (2015) 71–94.
80. M. Faisal, M. A. Tariq, M. Muneer, Photocatalysed degradation of two selected dyes in UV-irradiated aqueous suspensions of titania, *Dyes and Pigm.*, **72** (2007) 233–239
81. D. Wesenberg, I. Kyriakides, S. N. Agathos, White-rot fungi and their enzymes for the treatment of industrial dye effluents, *Biotechnol. Adv.*, **22** (2003) 161–187.
82. W. Z. Tang, H. An, UV/TiO₂ photocatalytic oxidation of commercial dyes in aqueous solutions, *Chemosphere*, **31** (1995) 4157–4170.
83. B. Khodadadi, M. Bordbar, M. Nasrollahzadeh, Green synthesis of Pd nanoparticles at Apricot kernel shell substrate using *Salvia hydrangea* extract: Catalytic activity for reduction of organic dyes, *J. Colloid Interface Sci.*, **490** (2017) 1–10.
84. N. Sobana, M. Muruganadham, M. Swaminathan, Nano-Ag particles doped TiO₂ for efficient photodegradation of direct azo dyes. *J Mol Catal A*, **258** (2006) 124–132.
85. E. L. Appleton, A nickel-iron wall against contaminated groundwater, *Environmental Science and Technology*, **30** (1996) 536A–539A.
86. T. Shahwan, S. AbuSirriah, M. Nairat, E. Boyaci, A. E. Eroglu, T.

B. Scott, K. R. Hallman, Green synthesis of iron nanoparticles and their application as a Fenton-like catalyst for the degradation of aqueous cationic and anionic dyes, *Chem. Eng. J.*, **172** (2011) 258–266.

87. B. Khodadadi, M. Bordbar, M. Nasrollahzadeh, Achillea millefolium L. extract mediated green synthesis of waste peach kernel shell supported silver nanoparticles: Application of the nanoparticles for catalytic reduction of a variety of dyes in water, *Journal of Colloid and Interface Science*, **493** (2017) 85–93.

88. K. B. A. Ahmed, S. Subramanian, A. Sivasubramanian, G. Veerappan, V. Veerappan, Preparation of gold nanoparticles using Salicornia brachiata plant extract and evaluation of catalytic and antibacterial activity, *Spectrochim Acta A Mol. Biomol. Spectrosc.*, **130** (2014) 54–58.

89. B. Ajitha, Y. A. K. Reddy, P. S. Reddy, Y. Suneetha, H-J. Jeon, C. W. Ahn, Instant biosynthesis of silver nanoparticles using Lawsonia inermis leaf extract: Innate catalytic, antimicrobial and antioxidant activities, *Journal of Molecular Liquids*, **219** (2016) 474–481.

90. D. Kavitha, C. Namasivayam, Experimental and kinetic studies on methylene blue adsorption by coir pith carbon, *Bioresour. Technol.*, **98** (2007) 14–21.

91. J. Kumari, S. Ajeet, Green synthesis of nanostructured silver particles and their catalytic application in dye degradation, *Journal of Genetic Engineering and Biotechnology*, **14** (2016) 311–317.

-
92. J. Saha, A. Begum, A. Mukherjee, S. Kumar, A novel green synthesis of silver nanoparticles and their catalytic action in reduction of Methylene Blue dye, *Sustainable Environment Research*, **27** (2017) 245–250.
93. T. V. M. Sreekanth, M-J. Jung, I-Y. Eom, Green synthesis of silver nanoparticles, decorated on graphene oxide nanosheets and their catalytic activity, *Applied Surface Science*, **361** (2016) 102–106.
94. V. K. Vidhu, D. Philip, Catalytic degradation of organic dyes using biosynthesized silver nanoparticles, *Micron*, **56** (2014) 54–62.
95. S. Hamed, S. Abbas, S. sadati, A. Mohammadi, Evaluation of the catalytic, antibacterial and anti-biofilm activities of the *Convolvulus arvensis* extract functionalized silver nanoparticles, *Journal of Photochemistry and Photobiology B: Biology*, **167** (2017) 36–44.
96. A. KumarSinha, M. Basu, S. Sarkar, M. Pradhan, T. Pal, Synthesis of gold nanochains via photoactivation technique and their catalytic applications, *Journal of Colloid and Interface Science*, **398** (2013) 13–21.
97. B. K. Ghosh, S. Hazra, B. Naik, N. N. Ghosh, Preparation of Cu nanoparticle loaded SBA-15 and their excellent catalytic activity in reduction of variety of dyes, *Powder Technology*, **269** (2015) 371–378.

Chapter 5: Summary of the results

In chapter 1, an overview on the historical aspects, preparation methods, characterising techniques and stabilisation of metal nanoparticles in the colloidal solutions has been discussed. Also, the principals of biomedical and chemical applications of noble metal nanoparticles have been clarified.

In chapter 2, new reductive stabilisers **1** and **2** have been developed. Au NPs can be synthesised and stabilised by ω -Sulfonylated Alkylsulfanylaniline **1** and **2** by the spontaneous reaction of HAuCl_4 and **1** or **2** in an aqueous solution of pH 8. The reaction yielded spherical **1-Au NPs** with an average size of 11.2 ± 5.9 . The **1-Au NP**, which have been prepared by this method, are stable in adverse conditions such as highly acidic conditions, highly basic conditions and in high salt concentrations such as PBS, which is commonly used in biological media. The **1-Au NP** were successfully re-dispersed after the dryness-redispersion cycle either directly after dryness or after keeping in air at room temperature for at least 2 weeks, which confirms the stability of the particles. Surface modification

of the **1-Au NP** can occur through ligand exchange reaction with thiol molecules. Ligand exchange was monitored by the strong absorbance peak of thiol molecule rather than that of ω -sulfonylated alkylsulfanylaniline, which is very faint. These advantages suggested that **1-Au NP** can be an attractive alternative for citrate- or ascorbate-stabilised Au NPs, particularly in biological and biomedical applications

In Chapter 3, we synthesised and characterised a novel paclitaxel-DNA-Au NPs bio-conjugate for targeted drug delivery of paclitaxel. Paclitaxel was modified by succinic anhydride to give succinyltaxol terminated with carboxylic group. Then, succinyltaxol was loaded on the surface of ω -sulfonylated alkylsulfanylaniline Au NPs through DNA oligonucleotides linker. The synthesis of the bio-conjugate was characterised by a LCMS and UV-visible spectroscopy. The drug-loaded NPs showed a significant anticancer activity against SK-BR3 breast cancer cells and neuro 2a brain tumour cells. Therefore, this drug delivery strategy suggested enhanced cellular uptake in comparison with the free drug and subsequently, efficient antineoplastic action. Our results imply that the paclitaxel-DNA-Au NPs bio-conjugate could have high

potentials to be used for targeted chemotherapy for treating neoplastic diseases.

In chapter 4, a stable PVA–ATB–Pt NPs with an efficient catalytic reduction activity, recyclability, and chemo-selectivity were prepared. The **PVA–ATB** polymer was synthesised from acrylated PVA modified with *p*-aminothiobenzene. This polymer was used as a reductive stabiliser to form **PVA–ATB–Pt NPs** (organic-inorganic hybrid system) in a one-step reaction. The Pt NPs solution was obtained by the reaction of H_2PtCl_6 with the polymer in boiling water under stirring. The colour of the solution changed from faint yellow to dark brown owing to the formation of the Pt NPs. The formation of the Pt NPs was pH dependent; small and stable nanoparticles were formed at pH 8. The as-prepared Pt NPs were characterised by UV-visible spectra and TEM. The average particle size of the prepared Pt NPs was 12.6 ± 5.7 nm. The synthesised nanoparticles showed a good catalytic reduction activity as demonstrated by the standard hydrogenation of *p*-nitrophenol. It was found that the **PVA–ATB–Pt NPs** exhibited a higher turnover number and apparent rate constant when compared to other nanocatalysts in the literature. Furthermore, the

nanocatalyst could be reused for at least six successive catalytic cycles. The **PVA-ATB-Pt NPs** also possessed the ability to catalyse the conversion of *p*-bromonitrobenzene to *p*-bromoaniline with high chemo-selectivity and no concurrent hydrodebromination reaction without using any additives. In addition, the nanocatalyst possessed a broad spectrum and wide scope nanocatalytic activity where it could catalyse the reduction of hexacyanoferrate (oxidation reduction reaction). Moreover, the wide scope nanocatalytic activity includes the hydrogenation of carbon-carbon double bond; where it could catalyse the reduction of cinnamyl alcohol to hydrocinnamyl alcohol and anthracene reduction to its partially hydrogenated products as well. Furthermore, the nanocatalyst could catalyse organic dyes degradation to less toxic and beneficial compounds.

Curriculum Vitae

Name: Mahmoud Ibrahiem Mohieeldin Darwish

Place of birth: Sharkia prefecture, Egypt

Educaional history:

Elementary school: kafr hasan attallah elementary school

Junior high school: shobra elsalam junior high school

High school: Gamal abdelnaser high school

University level: Faculty of Veterinary Medicine, Zagazig University, Egypt

Master degree: Nanomedicine and its application as anticancer, Department of Biochemistry and Molecular biology, Faculty of Veterinary Medicine, Zagazig University, Egypt

Occupation:

Assistant lecturer, Department of Biochemistry and Molecular biology, Faculty of Veterinary Medicine, Zagazig University, Egypt